

Phase diagram of QCD in a magnetic field: A review

Jens O. Andersen and William R. Naylor

*Department of Physics,
Norwegian University of Science and Technology,
Høgskoleringen 5,
N-7491 Trondheim,
Norway*

Anders Tranberg

*Faculty of Science and Technology,
University of Stavanger,
N-4036 Stavanger,
Norway*

(Dated: December 24, 2014)

Abstract

We review in detail recent advances in our understanding of the phase structure and the phase transitions of hadronic matter in strong magnetic fields B and zero quark chemical potentials μ_f . Many aspects of QCD are described using low-energy effective theories and models such as the MIT bag model, the hadron resonance gas model, chiral perturbation theory, the Nambu-Jona-Lasinio (NJL) model, the quark-meson (QM) model and Polyakov-loop extended versions of the NJL and QM models. We critically examine their properties and applications. This includes mean-field calculations as well as approaches beyond the mean-field approximation such as the functional renormalization group (FRG). Renormalization issues are discussed and the influence of the vacuum fluctuations on the chiral phase transition is pointed out. Magnetic catalysis at $T = 0$ is covered as well. We discuss recent lattice results for the thermodynamics of nonabelian gauge theories with emphasis on $SU(2)_c$ and $SU(3)_c$. In particular, we focus on inverse magnetic catalysis around the transition temperature T_c as a competition between contributions from valence quarks and sea quarks resulting in a decrease of T_c as a function of B . Finally, we discuss recent efforts to modify models in order to reproduce the behavior observed on the lattice.

CONTENTS

I. Introduction	2	D. Quark-meson model	24
II. Energy spectra for charged particles in a constant magnetic field and their propagators	4	E. Hadron resonance gas model	29
III. One-loop free energy densities	7	VI. Polyakov-loop extended models	30
IV. Schwinger's results	10	A. Coupling to the Polyakov loop	30
V. Effective theories and models	11	B. Two-color QCD	34
A. MIT bag model	11	VII. Functional renormalization group	35
B. Chiral perturbation theory	14	A. Local-potential approximation	36
1. Quark condensate, pion mass, and pion decay constant	17	B. Beyond the LPA	39
C. Nambu-Jona-Lasinio model	19	VIII. Magnetic catalysis	41
1. Quark condensates	21	IX. Lattice simulations and inverse magnetic catalysis	46
2. Other condensates	22	A. $SU(3)_c$	47
		B. $SU(2)_c$	50
		X. Model calculations revisited	51

A. B -dependent transition temperature T_0	51
B. B -dependent coupling constant	52
XI. Anisotropic pressure and magnetization	55
XII. Conclusions and outlook	57
Acknowledgments	59
A. Notation and conventions	59
B. Sum-integrals	59
C. Small and large- B expansions	61
D. Propagators in a magnetic background	61
References	63

I. INTRODUCTION

The phase structure of QCD is usually drawn in a phase diagram spanned by the temperature T and the baryon chemical potential μ_B . The first phase diagram was conjectured already in the 1970s suggesting a confined low-temperature phase of hadrons and a deconfined high-temperature phase of quarks and gluons. Since the appearance of this phase diagram, huge efforts have been made to map it out in detail. It turns out that the phase diagram of QCD is surprisingly rich, for example there may be several color superconducting phases at low temperature depending on the baryon chemical potential μ_B (Alford *et al.*, 2000, 2008; Fukushima and Hatsuda, 2011; Hsu and Schwetz, 2000; Rajagopal and Wilczek, 2001). Furthermore, the phase diagram can be generalized in a variety of ways. For example, instead of using a baryon chemical potential μ_B , i.e. the same chemical potential for each quark flavor, one can introduce an independent chemical potential μ_f for each flavor. Equivalently (for two quark flavors), one can use a baryon chemical potential $\mu_B = \frac{1}{2}(\mu_u + \mu_d)$ and an isospin chemical potential $\mu_I = \frac{1}{2}(\mu_u - \mu_d)$. A nonzero isospin chemical potential allows for new phases with pion condensation once it exceeds the pion mass, $\mu_I \geq m_\pi$ (Son and Stephanov, 2001). One can also add one new axis for each quark mass m_f in the system. It turns out that the nature of the chiral transition de-

pends on the number of flavors and on their masses (Pisarski and Wilczek, 1984; Stephanov, 2006), and this information has been conveniently displayed in the so called Columbia plot. Finally, there are external parameters, such as an external magnetic field B , that can be varied and are of phenomenological interest.

There are at least three areas of high-energy physics where strong magnetic fields play an important role:

- (1) Noncentral heavy-ion collisions
- (2) Compact stars
- (3) The early universe

In noncentral heavy-ion collisions, very strong and time-dependent magnetic fields are created. The basic mechanism is simple. In the center-of-mass frame, the two nuclei represent electric currents in opposite directions and according to Maxwell's equations, they produce a magnetic field B . The magnetic field depends on the energy of the ions, the impact parameter b , position as well as time. Detailed calculations of these magnetic fields depend on a number of assumptions. For example, it is common to ignore the contribution to the magnetic field from the particles produced in the collision as the expansion of these is almost spherical. It is then sufficient to take into account only the colliding particles. (Kharzeev *et al.*, 2008). The strength of these short-lived fields have been estimated to be up to the order of $B \sim 10^{19}$ Gauss or $|qB| \sim 6m_\pi^2$, where q is the electric charge of the pion. Detailed calculations have been carried out by Bzdak and Skokov (2012); Kharzeev *et al.* (2008); and Skokov *et al.* (2009). The result of such a calculation is displayed in Fig. 1, where the curves show the magnetic field as a function of proper time τ for three different impact parameters.

There is a certain class of neutron stars, called magnetars, that is characterized by very high magnetic fields and relatively low rotation frequencies as compared to a typical neutron star (Duncan and Thompson, 1992). The strength of the magnetic fields on the surface of such stars are believed to be on the order of

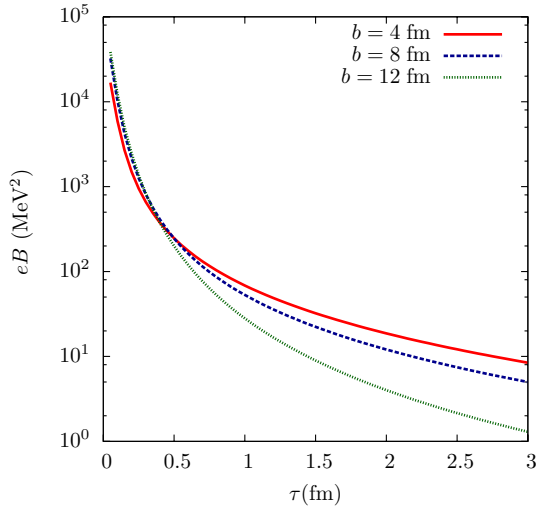


FIG. 1 Magnetic field as a function of proper time τ for three different values of the impact parameter b . Figure taken from Kharzeev *et al.* (2008).

$10^{14} - 10^{15}$ Gauss. The magnetic field strength depends on the density and is highest in the core of the star. In the interior one expects magnetic fields on the order of $10^{16} - 10^{19}$ Gauss. This implies that in order to calculate the mass-radius relation for magnetars, a detailed knowledge of the equation of state of strongly interacting matter in a large range of magnetic field strengths is required. If the density in the core of the star is sufficiently large to allow for quark matter, one must match the equation of state for hadronic matter to that of deconfined quark matter. The latter may again be color superconducting and perhaps even inhomogeneous depending on the values of the relevant parameters (Ferrer and de la Incera, 2007; Ferrer *et al.*, 2005, 2006; Fukushima and Warringa, 2008; Noronha and Shovkovy, 2007, 2012).

The situation is further complicated by the fact that the star is (globally) electrically neutral as well as the fact that the magnetic field breaks spherical symmetry. The magnetic field then gives rise to an anisotropic pressure \mathcal{P} whose components \mathcal{P}_{ij} can be expressed in terms of the components of the energy-momentum tensor \mathcal{T}_{ij} , that enter on the right-hand side of Einstein's field equations (Strickland *et al.*, 2012).

In the absence of a magnetic field, the Minimal Standard Model has a first-order transition

for low Higgs masses m_H (Kajantie *et al.*, 1998). With increasing m_H the first-order transition becomes weaker (Kajantie *et al.*, 1996) and the first-order line eventually ends at a second-order point for a critical value $m_H^c \approx 72$ GeV (Rummukainen *et al.*, 1998). The universality class of the critical end point is that of the three-dimensional Ising model. For larger Higgs masses, there is only a crossover. In the presence of a (hyper)magnetic field, the transition becomes somewhat stronger (Giovanni and Shaposhnikov, 1998). Allowing for a primordial hypermagnetic field of arbitrary magnitude, it is possible that even at the physical Higgs mass, the electroweak phase transition may be first order. If the magnetic fields are generated from bubble collisions during the electroweak transition, they will typically be of order $B/T^2 \lesssim 0.5$ (Baym *et al.*, 1996), in which case non-perturbative numerical simulations suggest that the transition is still not first order at the physical Higgs mass (Kajantie *et al.*, 1998). Moreover, such magnetic fields could have other implications relevant for baryogenesis, for instance through its effect on sphaleron processes (De Simone *et al.*, 2011). In the Minimal Supersymmetric Standard Model, the transition is stronger than in the Standard Model, and even moderate magnetic fields may allow for a first order transition even at the physical Higgs mass.

There is now a large body of literature on QCD in a magnetic background and we think that a review on the subject is timely. In order to restrict the topics covered, we will focus on zero quark chemical potentials, $\mu_f = 0$. Even with this restriction, we have to make a selection of topics and papers that we consider in detail. Such a selection is debatable, but hopefully we have covered the field in a balanced way. Finally, a word of caution. Writing a review is a challenge in terms of notation. We have tried to consistently use the same notation for a given quantity, but once in a while we have changed the notation so as not to be in conflict with the notation for other quantities. Hopefully, it is clear from the context which is which.

The review is organized as follows. In Sec. II,

we briefly discuss the solutions to the Dirac equation in a constant magnetic field and explain that there is no sign problem in lattice QCD in a finite magnetic field. In Sec. III, we calculate the one-loop free energy densities for fermions and bosons in a constant magnetic field using dimensional regularization and ζ -function regularization. In Sec. IV, we discuss Schwinger's classic results for the vacuum energy of bosons and fermions in a constant magnetic background B . In Sec. V, we discuss various low-energy models and theories that are being used to study the behavior of hadronic systems at finite T and B . These include the MIT bag model, chiral perturbation theory (Chpt), the Nambu-Jona-Lasinio (NJL) model, and the quark-meson (QM) model. The Polyakov extended versions of the NJL and QM models (PNJL and PQM models) are discussed in Sec. VI. In Sec. VII, we review the functional renormalization group and its application to hadronic matter at finite B . In Sec. VIII, we discuss magnetic catalysis at zero temperature and compare model - Dyson-Schwinger (DS), and lattice calculations. In Sec. IX, lattice results for $SU(2)_c$ and $SU(3)_c$ at finite temperature are reviewed, focussing on the mechanism behind magnetic catalysis. In Sec. X, we analyze recent efforts to incorporate inverse magnetic catalysis in model calculations. Finally, we discuss anisotropic pressure and magnetization in Sec. XI. The appendices provide the reader with our conventions and notation, list of sum-integrals needed in the calculations, expansions of some special functions, and some explicit calculations.

II. ENERGY SPECTRA FOR CHARGED PARTICLES IN A CONSTANT MAGNETIC FIELD AND THEIR PROPAGATORS

In this section, we briefly discuss the spectra of fermions and bosons in a constant magnetic background B . We first consider fermions. The Dirac equation for a single fermion of mass m_f in a background gauge field A_μ is given by

$$(i\mathcal{D} - m_f)\psi = 0, \quad (1)$$

where $\mathcal{D} = \gamma^\mu D_\mu$, γ^μ are the γ -matrices in Minkowski space, $D_\mu = \partial_\mu - iq_f A_\mu$ is the covariant derivative, and q_f is the electric charge. In the case where the zeroth component of the gauge field vanishes, $A_0 = 0$, the stationary solutions can be written as

$$\psi = e^{-iEt} \begin{pmatrix} \phi \\ \chi \end{pmatrix}, \quad (2)$$

where ϕ and χ are two-component spinors. Inserting Eq. (2) into Eq. (1) and using the Dirac representation of the γ -matrices, we obtain the coupled equations

$$(E - m_f)\phi = -i(\boldsymbol{\sigma} \cdot \mathbf{D})\chi, \quad (3)$$

$$(E + m_f)\chi = -i(\boldsymbol{\sigma} \cdot \mathbf{D})\phi. \quad (4)$$

Eliminating χ from the Eqs. (3)–(4), we find an equation for ϕ

$$(E^2 - m_f^2)\phi = -(\boldsymbol{\sigma} \cdot \mathbf{D})^2 \phi. \quad (5)$$

Specializing to a constant magnetic field, we choose the Landau gauge, $A_\mu = (0, 0, -Bx, 0)$.¹ Eq. (5) then reads

$$\left[E^2 - m_f^2 + \frac{\partial^2}{\partial x^2} + \left(\frac{\partial}{\partial y} + iq_f Bx \right)^2 + \frac{\partial^2}{\partial z^2} + \sigma_z q_f B \right] \phi = 0. \quad (6)$$

The solution is now written as $\phi = e^{is_\perp(q_f B)p_y y + ip_z z} f(x)$, where $s_\perp(q_f B) = \text{sign}(q_f B)$. The equation for $f(x)$ then becomes

$$\left[-\frac{d^2}{dx^2} + (s_\perp p_y + q_f Bx)^2 - \sigma_z q_f B \right] f(x) = [E^2 - m_f^2 - p_z^2] f(x). \quad (7)$$

¹ Another common choice is the symmetric gauge, $A_\mu = \frac{1}{2}(0, By, -Bx, 0)$.

This is a 2×2 matrix equation. However, the two equations decouple and the solutions can then be written as

$$f(x) = \begin{pmatrix} f_+(x) \\ 0 \end{pmatrix} \quad \text{and} \quad f(x) = \begin{pmatrix} 0 \\ f_-(x) \end{pmatrix}, \quad (8)$$

where the subscript \pm indicates that the solutions are eigenvectors of σ_z with eigenvalues ± 1 , respectively. The equation for $f_{\pm}(x)$ finally becomes

$$\left[-\frac{d^2}{dx^2} + (s_{\perp} p_y + q_f B x)^2 \right] f_{\pm}(x) = [E^2 - m_f^2 - p_z^2 \pm q_f B] f_{\pm}(x). \quad (9)$$

This is the equation for a harmonic oscillator with known solutions involving the Hermite polynomials $H_k(x)$. The solutions are

$$\phi = c e^{-\frac{1}{2}(\frac{x}{l} + p_y l)^2} H_k\left(\frac{x}{l} + p_y l\right) \times e^{i(s_{\perp} p_y y + p_z z)}, \quad (10)$$

where c is a normalization constant and $l = 1/\sqrt{|q_f B|}$. The spectrum is

$$E_k^2 = m_f^2 + p_z^2 + |q_f B|(2k + 1 - s), \quad (11)$$

where $k = 0, 1, 2, \dots$ and $s = \pm 1$. We note that there is a two-fold degeneracy due to the spin variable s for all values of k except for $k = 0$. Moreover, the energy is independent of p_y and the energy levels are therefore degenerate in this variable. The degeneracy is associated with the position of the center of the Landau levels. Assume that we use a quantization volume $V = L^3$, where L is the length of the side of the box. Since the characteristic size of a Landau level is $1/\sqrt{|q_f B|}$, the degeneracy N associated with the quantum number p_y is $N = \frac{|q_f B|}{2\pi} L^2$. The sum over states in the quantization volume V is then given by a sum over spin s , Landau levels k , and

the z -component of the momentum p_z multiplied by N :

$$\frac{1}{V} \frac{|q_f B|}{2\pi} L^2 \sum_{s=\pm 1} \sum_{k=0}^{\infty} \sum_{p_z}. \quad (12)$$

In the thermodynamic limit, the sum over p_z is replaced by an integral such that the expression in Eq. (12) is replaced by

$$\frac{|q_f B|}{2\pi} \sum_{s=\pm 1} \sum_{k=0}^{\infty} \int_{-\infty}^{\infty} \frac{dp_z}{2\pi}. \quad (13)$$

In the thermodynamic limit and for $B = 0$, the sum over three-momenta \mathbf{p} is replaced by an integral in the usual way

$$\frac{1}{V} \sum_{\mathbf{p}} \rightarrow \int \frac{d^3 p}{(2\pi)^3}. \quad (14)$$

Once we have found a complete set of eigenstates, we can calculate the fermion propagator. We then need the expression for the two-component spinor χ as well. The fermion propagator at $T = 0$ for a fermion with electric charge q_f in Minkowski space is given by the expression (Gusynin *et al.*, 1996)

$$S(x, x') = e^{i\Phi(\mathbf{x}_{\perp}, \mathbf{x}'_{\perp})} \int \frac{d^4 p}{(2\pi)^4} e^{-ip(x-x')} \tilde{S}(\mathbf{p}_{\perp}, \mathbf{p}_{\parallel}), \quad (15)$$

where $x = (t, \mathbf{x})$, $\mathbf{x}_{\perp} = (x^1, x^2)$, $p = (p_0, \mathbf{p})$, $\mathbf{p}_{\perp} = (p_1, p_2)$, $\mathbf{p}_{\parallel} = (p_0, p_3)$ and with $\Phi(\mathbf{x}_{\perp}, \mathbf{x}'_{\perp})$ and $\tilde{S}(\mathbf{p}_{\perp}, \mathbf{p}_{\parallel})$ given by

$$\Phi(\mathbf{x}_{\perp}, \mathbf{x}'_{\perp}) = s_{\perp} \frac{(x^1 + x'^1)(x^2 - x'^2)}{2l^2}, \quad (16)$$

$$\begin{aligned} \tilde{S}(\mathbf{p}_\perp, \mathbf{p}_\parallel) = & \int_0^\infty ds \exp \left\{ is \left[p_\parallel^2 - m_f^2 \right] - i \frac{p_\perp^2}{|q_f B|} \tan(|q_f B|s) \right\} \\ & \times \left[(\gamma^0 p_0 - \gamma^3 p_3 + m)(1 + \gamma^1 \gamma^2 \tan(q_f B s)) - \boldsymbol{\gamma}_\perp \cdot \mathbf{p}_\perp (1 + \tan^2(q_f B s)) \right] \end{aligned} \quad (17)$$

The prefactor $\Phi(\mathbf{x}_\perp, \mathbf{x}'_\perp)$ is the so-called Schwinger phase and the term $\tilde{S}(p_\perp, p_\parallel)$ is translationally invariant. The translationally invariant part can be decomposed into contributions from the different Landau levels

$$\tilde{S}(\mathbf{p}_\perp, \mathbf{p}_\parallel) = ie^{-\frac{p_\perp^2}{|q_f B|}} \sum_{k=0}^\infty \frac{(-1)^k D_k(\mathbf{p}_\perp, \mathbf{p}_\parallel)}{p_\parallel^2 - m_f^2 - 2|q_f B|k}, \quad (18)$$

where

$$\begin{aligned} D_k(\mathbf{p}_\perp, \mathbf{p}_\parallel) = & (\gamma^0 p_0 - \gamma^3 p_3 + m) \left[(1 - i\gamma^1 \gamma^2 s_\perp) L_k \left(2 \frac{p_\perp^2}{|q_f B|} \right) - (1 + i\gamma^1 \gamma^2 s_\perp) L_{k-1} \left(2 \frac{p_\perp^2}{|q_f B|} \right) \right] \\ & + 4(\boldsymbol{\gamma}_\perp \cdot \mathbf{p}_\perp) L_{k-1}^1 \left(2 \frac{p_\perp^2}{|q_f B|} \right), \end{aligned} \quad (19)$$

and $L_k^a(x)$ are the generalized Laguerre polynomials. Note that $L_{-1}^a(x) = 0$.

The spectrum for bosons with mass m and charge q can be found using the same techniques. In this case, the differential operator does not involve the term $|q_f B| \sigma_z$ and so the resulting eigenvalue equation is easier to solve. The spectrum is obtained immediately by setting $s = 0$:

$$E_k^2 = m^2 + p_z^2 + |qB|(2k+1), \quad (20)$$

where $k = 0, 1, 2, \dots$. The eigenfunction are again given by Eq. (10). Once we have a complete set of eigenfunctions, we can derive the propagator. We derive the bosonic propagator in Appendix D and at $T = 0$ it reads

$$\Delta(x, x') = e^{i\Phi(\mathbf{x}_\perp, \mathbf{x}'_\perp)} \int \frac{d^4 p}{(2\pi)^4} e^{-ip(x-y)} \Delta_B(p_\perp, p_\parallel), \quad (21)$$

where the translationally invariant part is

$$\Delta_B(\mathbf{p}_\perp, \mathbf{p}_\parallel) = \int_0^\infty \frac{ds}{\cos(|qB|s)} \exp \left\{ is \left[p_\parallel^2 - m^2 \right] - ip_\perp^2 \frac{\tan(|qB|s)}{|qB|} \right\}. \quad (22)$$

We close this section with briefly commenting on the sign problem of QCD. It is straightforward to show that there is no sign problem in QCD in an external Abelian gauge field A_μ . In order to show this, we go to Euclidean space. The partition function of QCD can be written as

$$\mathcal{Z} = \int \mathcal{D}\bar{\psi} \mathcal{D}\psi \mathcal{D}A_\mu e^{-\int d^3x \int_0^\beta d\tau \bar{\psi}[(\not{D} + m_f)]\psi} e^{-S_g}$$

$$= \int \mathcal{D}A_\mu e^{-S_g} \det(\not{D} + m_f), \quad (23)$$

where $\beta = 1/T$ and S_g is the Euclidean action for the gluons,

$$S_g = \frac{1}{4} \int_0^\beta d\tau \int d^3x \text{Tr} [G_{\mu\nu} G_{\mu\nu}]. \quad (24)$$

$S_g > 0$ and the exponent can be regarded as a positive probability weight. We also have to

check the sign of the fermion determinant. It is convenient to use the chiral representation of the γ -matrices. The matrix \mathcal{D} can then be written as

$$\mathcal{D} = \begin{pmatrix} 0 & iX \\ iX^\dagger & 0 \end{pmatrix}, \quad (25)$$

where $iX = D_0 + i\boldsymbol{\sigma} \cdot \mathbf{D}$. The fermion determinant then takes the form

$$\det(\mathcal{D} + m_f) = \det[XX^\dagger + m_f^2], \quad (26)$$

which shows that it is manifestly positive. QCD in a magnetic field is therefore free of the sign problem and one can use standard lattice techniques based on importance sampling.

III. ONE-LOOP FREE ENERGY DENSITIES

In this review, we are often concerned with Euclidean Lagrangian densities of the form

$$\mathcal{L} = \bar{\psi}_f \gamma_\mu D_\mu \psi_f + m_f \bar{\psi}_f \psi_f + (D_\mu \Phi)^\dagger (D_\mu \Phi) + m^2 \Phi^\dagger \Phi + \mathcal{L}_{\text{int}}, \quad (27)$$

where ψ_f is a fermion field of flavor f and Φ is a complex scalar field. Unless otherwise stated, we consider two flavors, $N_f = 2$ and $f = u, d$. Moreover, $D_\mu = \partial_\mu - iqA_\mu$ is the covariant derivative for bosons and $D_\mu = \partial_\mu - iq_f A_\mu$ is the covariant derivative for fermions. Here $q = \pm e$ is the electric charge for the charged scalars, $q_u = 2/3e$ and $q_d = -1/3e$ are the electric charges for u -quarks and d -quarks, respectively. m and m_f are the tree-level masses of the bosons and fermions. \mathcal{L}_{int} is the interacting part of the Lagrangian. It may contain bosonic and fermionic four-point interactions as well as Yukawa-type couplings between the bosons and fermions.

In the functional approach to the imaginary-time formalism, the partition function \mathcal{Z} is given by a path integral

$$\mathcal{Z} = \int \mathcal{D}\Phi^\dagger \mathcal{D}\Phi \mathcal{D}\bar{\psi} \mathcal{D}\psi e^{-S[\Phi^\dagger, \Phi, \bar{\psi}, \psi]}, \quad (28)$$

where the action is given by

$$S[\Phi^\dagger, \Phi, \bar{\psi}, \psi] = \int_0^\beta d\tau \int d^d x \mathcal{L}, \quad (29)$$

and d is the number of spatial dimensions. In many cases, we approximate the free energy density $\mathcal{F} = -\frac{T}{V} \log \mathcal{Z}$ (where V is the spatial volume) of the system by a one-loop calculation. We therefore need to perform Gaussian integrals over bosonic or fermionic fields. These are given by the standard expressions. The one-loop free energy density \mathcal{F}_1 for a boson is

$$\mathcal{F}_1 = \frac{1}{\beta V} \frac{1}{2} \text{Tr} \ln D_0^{-1}, \quad (30)$$

and for a fermion

$$\mathcal{F}_1 = -\frac{1}{\beta V} \text{Tr} \ln D_0^{-1}, \quad (31)$$

where D_0^{-1} is the free inverse propagator. Here the trace is over spacetime, field indices, and Dirac indices in the case of fermions. These expressions are general as they apply whether or not the particle couples to an external magnetic field. Of course, the explicit expressions after evaluating the traces and making the substitutions, (13) or (14), are different. For example, the one-loop free energy density for a neutral boson with mass m reads

$$\mathcal{F}_1 = \frac{1}{2} \sum_P' \ln [P_0^2 + p^2 + m^2], \quad (32)$$

where the sum-integral is defined in Eq. (B1) and involves a sum over Matsubara frequencies P_0 and an integral over three-momenta \mathbf{p} . The explicit expression for this sum-integral as well as others needed are listed in Appendix B. The one-loop free energy density for a boson with electric charge q and for a fermion with electric charge q_f as a function of B are given by the sum-integrals

$$\mathcal{F}_1 = \frac{1}{2} \sum_P' \ln [P_0^2 + p_z^2 + m^2 + |qB|(2k+1)], \quad (33)$$

$$\mathcal{F}_1 = -\sum_{\{P\}}^B \ln \left[P_0^2 + p_z^2 + m_f^2 + |q_f B|(2k+1-s) \right], \quad (34)$$

where the sum-integrals are defined in Eqs. (B4) and (B5), and involves a sum over spin s , Landau levels k and Matsubara frequencies P_0 , as well as an integral over p_z . We next evaluate the sum-integral (34) in some detail. We first sum over the Matsubara frequencies using Eq. (B19). This yields

$$\mathcal{F}_1 = -\frac{|q_f B|}{2\pi} \sum_{s=\pm 1} \sum_{k=0}^{\infty} \int_{p_z} \left\{ \sqrt{p_z^2 + M_B^2} + 2T \ln \left[1 + e^{-\beta \sqrt{p_z^2 + M_B^2}} \right] \right\}, \quad (35)$$

where $M_B^2 = m_f^2 + |q_f B|(2k+1-s)$. Let us first consider the temperature-independent term. Using dimensional regularization in $d-2 = 1-2\epsilon$ dimensions to regulate the ultraviolet divergences, we obtain

$$\int_{p_z} \sqrt{p_z^2 + M_B^2} = -\frac{M_B^2}{4\pi} \left(\frac{e^{\gamma_E} \Lambda^2}{M_B^2} \right)^{\epsilon} \Gamma(-1+\epsilon), \quad (36)$$

where Λ is the renormalization scale associated with the modified minimal subtraction scheme $\overline{\text{MS}}$. The sum over Landau levels k involves the term $M_B^{2-2\epsilon}$ and is divergent for $\epsilon = 0$. We will regularize the sum using ζ -function regularization. The sum over spin s and Landau levels k can then be written as

$$\begin{aligned} \sum_{s=\pm 1} \sum_{k=0}^{\infty} M_B^{2-2\epsilon} &= 2(2|q_f B|)^{1-\epsilon} \sum_{k=0}^{\infty} \left[k + \frac{m_f^2}{2|q_f B|} \right]^{1-\epsilon} - m_f^{2-2\epsilon} \\ &= 2(2|q_f B|)^{1-\epsilon} \zeta(-1+\epsilon, x_f) - m_f^{2-2\epsilon}, \end{aligned} \quad (37)$$

where we have defined $x_f = \frac{m_f^2}{2|q_f B|}$ and the Hurwitz ζ -function $\zeta(s, q)$ is defined by

$$\zeta(s, q) = \sum_{k=0}^{\infty} (q+k)^{-s}. \quad (38)$$

Inserting Eq. (37) into Eq. (35), the temperature-independent part of the free energy density, $\mathcal{F}_1^{T=0}$, becomes

$$\mathcal{F}_1^{T=0} = \frac{(q_f B)^2}{2\pi^2} \left(\frac{e^{\gamma_E} \Lambda^2}{2|q_f B|} \right)^{\epsilon} \Gamma(-1+\epsilon) \left[\zeta(-1+\epsilon, x_f) - \frac{1}{2} x_f^{1-\epsilon} \right]. \quad (39)$$

Expanding Eq. (39) in powers of ϵ through order ϵ^0 gives

$$\begin{aligned} \mathcal{F}_1^{T=0} &= \frac{1}{(4\pi)^2} \left(\frac{\Lambda^2}{2|q_f B|} \right)^{\epsilon} \left[\left(\frac{2(q_f B)^2}{3} + m_f^4 \right) \left(\frac{1}{\epsilon} + 1 \right) - 8(q_f B)^2 \zeta^{(1,0)}(-1, x_f) \right. \\ &\quad \left. - 2|q_f B| m_f^2 \ln x_f + \mathcal{O}(\epsilon) \right], \end{aligned} \quad (40)$$

where we have defined

$$\zeta^{(1,0)}(-a, x) = \left. \frac{\partial \zeta(-a+\epsilon, x)}{\partial \epsilon} \right|_{\epsilon=0}. \quad (41)$$

The expression (40) has simple poles in ϵ . One of the divergences is proportional to $(q_f B)^2$ while the other is proportional to m_f^4 . Later we will

show how one can eliminate these divergences by renormalization.

The temperature-dependent part of the free energy density in Eq. (35), \mathcal{F}_1^T , can be integrated by parts and this gives

$$\begin{aligned}\mathcal{F}_1^T &= -\frac{|q_f B|}{\pi} T \sum_{s=\pm 1} \sum_{k=0}^{\infty} \int_{p_z} \ln \left[1 + e^{-\beta \sqrt{p_z^2 + M_B^2}} \right] \\ &= -\frac{|q_f B|}{2\pi^2} \left(e^{\gamma_E} \Lambda^2 \right)^\epsilon \frac{\Gamma(\frac{1}{2})}{\Gamma(\frac{3}{2} - \epsilon)} \sum_{s=\pm 1} \sum_{k=0}^{\infty} \int_0^\infty \frac{p_z^{2-2\epsilon} dp_z}{\sqrt{p_z^2 + M_B^2}} \frac{1}{e^{\beta \sqrt{p_z^2 + M_B^2}} + 1} . \\ &= -\frac{2}{(4\pi)^2} \left(\frac{e^{\gamma_E} \Lambda^2}{2|q_f B|} \right)^\epsilon K_0^B(\beta m_f) |q_f B| T^2 ,\end{aligned}\tag{42}$$

where $K_0^B(\beta m_f)$ is defined in Eq. (B18). The sum of Eqs. (40) and (42) is then Eq. (B10). The other sum-integrals needed can be calculated using the same techniques. They are listed in Appendix B.

We close this section with some comments on regulators. By changing variables $p_\perp^2 = 2k|q_f B|$, summing over s and taking the limit $B \rightarrow 0$ in Eq. (35), the first term reduces to

$$\mathcal{F}_1^{T=0} = -2 \int_p \sqrt{p^2 + m_f^2} ,\tag{43}$$

where $p^2 = p_\perp^2 + p_z^2$. Using dimensional regularization, this becomes

ization, this becomes

$$\mathcal{F}_1^{T=0} = \frac{1}{(4\pi)^2} \left(\frac{\Lambda^2}{m_f^2} \right)^\epsilon \left[\left(\frac{1}{\epsilon} + \frac{3}{2} \right) m_f^4 + \mathcal{O}(\epsilon) \right] .\tag{44}$$

This is the same result one finds if one takes the limit $B \rightarrow 0$ in Eq. (40) and uses the large- x_f expansion of $\zeta^{(1,0)}(-1, x_f)$ given by Eq. (C5). Using a sharp three-dimensional cutoff Λ , one obtains

$$\mathcal{F}_{T=0} = \frac{1}{(4\pi)^2} \left\{ -2\Lambda \sqrt{\Lambda^2 + m_f^2} (2\Lambda^2 + m_f^2) + 2m_f^4 \ln \left[\frac{\Lambda}{m_f} + \sqrt{1 + \frac{\Lambda^2}{m_f^2}} \right] \right\} .\tag{45}$$

If the starting point is the expression for the free energy density as a four-dimensional Euclidean integral, one finds by imposing a four-dimensional cutoff Λ ,

$$\begin{aligned}\mathcal{F}_{T=0} &= -2 \int \frac{d^4 p}{(2\pi)^4} \ln [p^2 + m_f^2] \\ &= \frac{1}{(4\pi)^2} \left\{ \frac{1}{2} \Lambda^4 - \Lambda^4 \ln \left[1 + \frac{m_f^2}{\Lambda^2} \right] - \Lambda^2 m_f^2 + m_f^4 \ln \left[1 + \frac{\Lambda^2}{m_f^2} \right] \right\} .\end{aligned}\tag{46}$$

We notice that the coefficient of the logarithmic term is independent of the regulator, while the power divergences (for $\Lambda \rightarrow \infty$) depend on the regulator. In particular, they are all set to

zero in dimensional regularization while the logarithmic divergence in the cutoff scheme corresponds to a pole in ϵ in dimensional regularization.

IV. SCHWINGER'S RESULTS

In this section, we rederive Schwinger's classic results (Schwinger, 1951) for the vacuum energy of a boson and a fermion in a constant magnetic field B . In the original derivation, the result was given for an arbitrary constant electromagnetic field. Not only is the calculation useful to see the connection with the derivation in the previous section, but the one-loop expression for the vacuum energy also takes form such that it is straightforward to use a simple ultraviolet cutoff Λ instead of dimensional regularization and zeta-function regularization. This will be useful when we consider Nambu-Jona-Lasinio models in which the ultraviolet divergences often are regulated by a simple UV cutoff.

The starting point is the zero-temperature expression for the one-loop free energy density for a charged boson with mass m and charge q , and its antiparticle with mass m and charge $-q$. In the limit $T \rightarrow 0$, the sum over Matsubara frequencies approaches an integral over the continuous variable p_0 . The free energy density reads

$$\mathcal{F}_1 = \frac{|qB|}{2\pi} \sum_{k=0}^{\infty} \int_{-\infty}^{\infty} \frac{dp_0}{2\pi} \int_{p_z} \ln [p_0^2 + p_z^2 + M_B^2] . \quad (47)$$

where $M_B^2 = m^2 + |qB|(2k+1)$. The derivative of \mathcal{F}_1 with respect to M^2 is

$$\frac{\partial \mathcal{F}_1}{\partial m^2} = \frac{|qB|}{2\pi} \sum_{k=0}^{\infty} \int_{-\infty}^{\infty} \frac{dp_0}{2\pi} \int_{p_z} \frac{1}{p_0^2 + p_z^2 + M_B^2} . \quad (48)$$

The effective propagator in momentum space $1/(p_0^2 + p_z^2 + M_B^2)$ has the integral representation

$$\frac{1}{p_0^2 + p_z^2 + M_B^2} = \int_0^{\infty} e^{-s(p_0^2 + p_z^2 + M_B^2)} ds . \quad (49)$$

Inserting Eq. (49) into Eq. (48), we obtain

$$\begin{aligned} \frac{\partial \mathcal{F}_1}{\partial m^2} &= \frac{|qB|}{2\pi} \sum_{k=0}^{\infty} \int_{-\infty}^{\infty} \frac{dp_0}{2\pi} \\ &\times \int_{p_z} \int_0^{\infty} e^{-s(p_0^2 + p_z^2 + M_B^2)} ds . \end{aligned} \quad (50)$$

The integral over p_z is finite for $\epsilon = 0$ and after integration over p_z and p_0 , Eq. (50) reduces to

$$\frac{\partial \mathcal{F}_1}{\partial m^2} = \frac{|qB|}{8\pi^2} \sum_{k=0}^{\infty} \int_0^{\infty} \frac{e^{-sM_B^2}}{s} ds . \quad (51)$$

Likewise, the sum over Landau levels is convergent and after summation over k , Eq. (51) reduces to

$$\frac{\partial \mathcal{F}_1}{\partial m^2} = \frac{1}{(4\pi)^2} \int_0^{\infty} \frac{ds}{s^2} e^{-sm^2} \frac{|qB|s}{\sinh(|qB|s)} . \quad (52)$$

Finally integrating over m^2 , we obtain the one-loop free energy density

$$\mathcal{F}_1 = -\frac{1}{(4\pi)^2} \int_0^{\infty} \frac{ds}{s^3} e^{-sm^2} \frac{|qB|s}{\sinh(|qB|s)} , \quad (53)$$

where the constant of integration has been set to zero. The result, Eq. (53), is divergent at $s = 0$. Since s has mass dimension -2 , this corresponds to an ultraviolet divergence in momentum space. It is therefore convenient to organize the result by adding and subtracting divergent terms to Eq. (53), writing it as

$$\begin{aligned} \mathcal{F}_{0+1} &= \frac{1}{2} B^2 + \frac{(qB)^2}{6(4\pi)^2} \int_0^{\infty} \frac{ds}{s} e^{-sm^2} - \frac{1}{(4\pi)^2} \int_0^{\infty} \frac{ds}{s^3} e^{-sm^2} \\ &- \frac{1}{(4\pi)^2} \int_0^{\infty} \frac{ds}{s^3} e^{-sm^2} \left[\frac{|qB|s}{\sinh(|qB|s)} - 1 + \frac{(qBs)^2}{6} \right] , \end{aligned} \quad (54)$$

where we have added the tree-level term $\frac{1}{2} B^2$. The first and second integrals are divergent at $s = 0$, while the third integral is finite. The divergent integrals are regulated by introducing an ultraviolet cutoff Λ via $s = 1/\Lambda^2$ and evaluating Eq. (54), we obtain

$$\mathcal{F}_{0+1} = \frac{1}{2} B^2 \left[1 + \frac{q^2}{3(4\pi)^2} \left(\ln \frac{\Lambda^2}{m^2} - \gamma_E \right) \right] - \frac{1}{2(4\pi)^2} \left[\Lambda^4 - 2\Lambda^2 m^2 + m^4 \left(\ln \frac{\Lambda^2}{m^2} - \gamma_E + \frac{3}{2} \right) \right]$$

$$+ \frac{4(qB)^2}{(4\pi)^2} \left[\zeta^{(1,0)}(-1, \frac{1}{2} + x) + \frac{1}{4}x^2 - \frac{1}{2}x^2 \ln x + \frac{1}{24} \ln x + \frac{1}{24} \right], \quad (55)$$

where $x = \frac{m^2}{2|qB|}$. In most applications, one omits the Λ^4 -term as it is independent of m and B .

For fermions with mass m_f and electric charge q_f , one obtains in a similar manner the result

$$\begin{aligned} \mathcal{F}_{0+1} &= \frac{1}{2}B^2 + \frac{4(q_f B)^2}{3(4\pi)^2} \int_0^\infty \frac{ds}{s} e^{-sm_f^2} + \frac{2}{(4\pi)^2} \int_0^\infty \frac{ds}{s^3} e^{-sm_f^2} \\ &\quad + \frac{2}{(4\pi)^2} \int_0^\infty \frac{ds}{s^3} e^{-sm_f^2} \left[|q_f B| s \coth(|q_f B| s) - 1 - \frac{1}{3}(q_f B s)^2 \right] \\ &= \frac{1}{2}B^2 \left[1 + \frac{4q_f^2}{3(4\pi)^2} \left(\ln \frac{\Lambda^2}{m_f^2} - \gamma_E \right) \right] + \frac{1}{(4\pi)^2} \left[\Lambda^4 - 2\Lambda^2 m_f^2 + m_f^4 \left(\ln \frac{\Lambda^2}{m_f^2} - \gamma_E + \frac{3}{2} \right) \right] \\ &\quad - \frac{8(q_f B)^2}{(4\pi)^2} \left[\zeta^{(1,0)}(-1, x_f) + \frac{1}{4}x_f^2 - \frac{1}{2}x_f^2 \ln x_f + \frac{1}{2}x_f \ln x_f - \frac{1}{12} \ln x_f - \frac{1}{12} \right]. \end{aligned} \quad (56)$$

We end this section by noting that there is alternative way of regularizing the divergent integrals over s . Instead of performing these in integrals in one dimension, we use dimensional regularization. For example, the first integral in Eq. (54) is replaced by

$$\frac{(e^{\gamma_E} \Lambda^2)^\epsilon}{(4\pi)^2} \int_0^\infty \frac{ds}{s^{3-\epsilon}} e^{-sm^2} = \frac{m^4}{(4\pi)^2} \left(\frac{e^{\gamma_E} \Lambda^2}{m^2} \right)^\epsilon \Gamma(-2 + \epsilon) = \frac{m^4}{2(4\pi)^2} \left[\frac{1}{\epsilon} + \frac{3}{2} + \ln \left(\frac{\Lambda^2}{m^2} \right) + \mathcal{O}(\epsilon) \right]. \quad (57)$$

With the extra factor of $e^{\gamma_E \epsilon}$, the result (57) is identical to that obtained in the $\overline{\text{MS}}$ scheme, cf. Eq. (B7).

V. EFFECTIVE THEORIES AND MODELS

A. MIT bag model

The MIT bag model was introduced in the 1970s as a simple phenomenological model for the confinement of quarks inside hadrons (Chodos *et al.*, 1974). The quarks are confined to a spherical cavity by requiring that the quark vector current vanishes on the boundary. The quarks inside the bag are considered non-interacting which is justified by appealing to asymptotic freedom of QCD. The idea is that the vacuum energy density of the perturbative vacuum (inside the hadron) is larger than that of the nonperturbative vacuum outside the bag. Equivalently, the vacuum pressure inside the bag is smaller than that outside the bag and the radius R of a hadron is (heurestically) given by the balance between this difference and the pressure generated by the quarks inside the bag. The bag constant B can be estimated as fol-

lows (Johnson, 1975). The pressure generated by the quarks inside a spherical cavity is, by the uncertainty relation, on the order of $1/R$. Balancing this contribution and that from the bag, which is on the order of R^3 , one finds a relation between the mass and the radius of hadron. Minimizing the total mass with respect to R gives $R \sim B^{-\frac{1}{4}}$ and using the mass of a proton gives a bag constant on the order of 100 MeV.

Chakrabarty (1996) was the first to discuss the MIT bag model in a magnetic field in the context of compact stars and the stability of strange quark matter. More recently, the deconfinement transition has been investigated using the bag model (Fraga and Palhares, 2012).

One can investigate the phase structure of QCD by calculating the pressure in the hadronic phase as well as in the deconfined phase as a function of temperature, particle masses and magnetic field B . The phase with the larger pressure wins. The transition takes place when the pressure in the two phases is equal and

the deconfinement temperature therefore satisfies $P_{\text{HHG}} = P_{\text{QGP}}$. Thus there is no order parameter for the deconfinement transition in the bag model. This is different from other models we will be discussing later, such as the Polyakov-loop extended Nambu-Jona-Lasinio model and the Polyakov-loop extended quark-meson model. In these models, we analyze the behavior of the Polyakov loop variable which is an order parameter

for confinement in pure-gluon QCD and an approximate order parameter in QCD with dynamical quarks (Yaffe and Svetitsky, 1982a,b). Finally, the MIT bag model tells us nothing about the chiral transition in QCD since this is governed by the behavior of the quark condensate as a function of T (and B).

The free energy density of the hadronic phase is approximated by that of an ideal gas of massive pions and reads

$$\mathcal{F}_{\text{HHG}} = \frac{1}{2}B^2 + \frac{1}{2}\oint_P \ln [P^2 + m_\pi^2] + \oint_P^B \ln [P_0^2 + p_z^2 + M_B^2] , \quad (58)$$

where the first term is the tree-level contribution from the constant magnetic field and the second term is from the neutral pion which does not couple to the magnetic field. The third term is the contribution from the charged pions. This expression is the same as one obtains from a one-loop approximation to the free energy density in chiral perturbation theory. We will discuss Chpt later.

Using the expressions for the bosonic sum-integrals given by Eqs. (B7) and (B8), Eq. (58) can be written as

$$\begin{aligned} \mathcal{F}_{\text{HHG}} = & \frac{1}{2}B^2 + \frac{1}{2(4\pi)^2} \left(\frac{\Lambda^2}{|2qB|} \right)^\epsilon \left[\left(\frac{(qB)^2}{3} - m_\pi^4 \right) \left(\frac{1}{\epsilon} + 1 \right) + 8(qB)^2 \zeta^{(1,0)}(-1, \frac{1}{2} + x) \right. \\ & \left. - 2J_0^B(\beta m_\pi) |qB| T^2 \right] - \frac{1}{4(4\pi)^2} \left(\frac{\Lambda^2}{m_\pi^2} \right)^\epsilon \left[m_\pi^4 \left(\frac{1}{\epsilon} + \frac{3}{2} \right) + 2J_0(\beta m_\pi) T^4 \right] , \end{aligned} \quad (59)$$

where the thermal integrals $J_n(\beta m)$ and $J_n^B(\beta m)$ are defined in Appendix B. The first divergence is proportional to $(qB)^2$ and is removed by wavefunction renormalization of the term $\frac{1}{2}B^2$ in Eq. (59). This is done by making the replacement $B^2 \rightarrow Z^2 B^2$, where Z is the wavefunction renormalization term. The second divergence, which is proportional to m_π^4 , can be removed by adding an appropriately chosen vacuum counterterm $\Delta\mathcal{E}$ to the free energy density. The counterterms are given by

$$Z^2 = 1 - \frac{q^2}{3(4\pi)^2 \epsilon} , \quad \Delta\mathcal{E} = \frac{3m_\pi^4}{4(4\pi)^2 \epsilon} . \quad (60)$$

After renormalization, the free energy density of the hot hadronic gas is

$$\begin{aligned} \mathcal{F}_{\text{HHG}} = & \frac{1}{2}B^2 \left[1 + \frac{q^2}{3(4\pi)^2} \ln \frac{\Lambda^2}{2|qB|} \right] - \frac{3m_\pi^4}{4(4\pi)^2} \left[\ln \frac{\Lambda^2}{m_\pi^2} + \frac{3}{2} \right] + \frac{4(qB)^2}{(4\pi)^2} \left[\zeta^{(1,0)}(-1, \frac{1}{2} + x) \right. \\ & \left. + \frac{1}{4}x^2 - \frac{1}{2}x^2 \ln x + \frac{1}{24} \right] - \frac{1}{2(4\pi)^2} \left[J_0(\beta m_\pi) T^4 + 2J_0^B(\beta m_\pi) |qB| T^2 \right] . \end{aligned} \quad (61)$$

Note that here and in the following, the thermal integrals $J_n(\beta m)$, $J_n^B(\beta m)$, $K_n(\beta m)$, and $K_n^B(\beta m)$ are always evaluated at $\epsilon = 0$ whenever they appear in renormalized expressions for

the free energy density and other physical quantities.

The free energy density in the quark-gluon plasma phase is

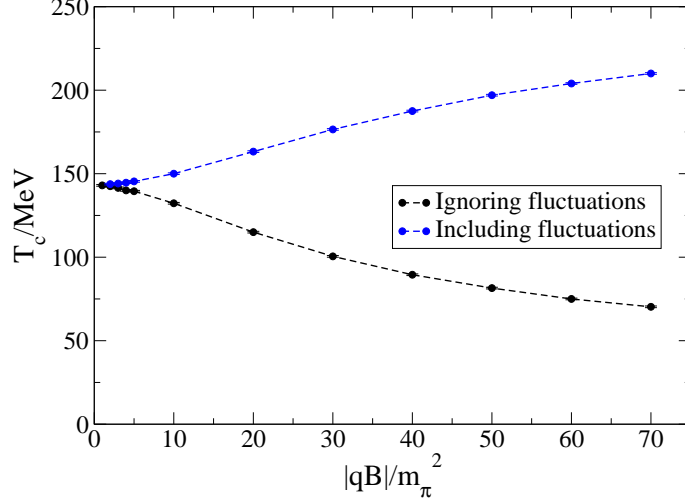


FIG. 2 Critical temperature as a function of $|qB|/m_\pi^2$ in the MIT bag model. See main text for details.

$$\mathcal{F}_{\text{QGP}} = \frac{1}{2}B^2 + (N_c^2 - 1) \sum_P \ln(P^2) - N_c \sum_f \sum_{\{P\}}^B \ln[P_0^2 + p_z^2 + M_B^2] + \mathcal{B}, \quad (62)$$

where the first term is from the constant magnetic field, the second term is from the gluons, the third term is from the quarks, and the last term \mathcal{B} is the bag constant. This term represents the difference in the vacuum energy between the two phases. Using the expressions for the bosonic and fermionic sum-integrals Eqs. (B7) and (B10), we find

$$\begin{aligned} \mathcal{F}_{\text{QGP}} = & -(N_c^2 - 1) \frac{\pi^2 T^4}{45} + \frac{1}{2}B^2 + \frac{N_c}{(4\pi)^2} \left(\frac{\Lambda^2}{|2q_f B|} \right)^\epsilon \sum_f \left[\left(\frac{2(q_f B)^2}{3} + m_f^4 \right) \left(\frac{1}{\epsilon} + 1 \right) \right. \\ & \left. - 8(q_f B)^2 \zeta^{(1,0)}(-1, x_f) - 2|q_f B| m_f^2 \ln x_f - 2K_0^B(\beta m_f) |q_f B| T^2 \right] + \mathcal{B}. \end{aligned} \quad (63)$$

Again, the ultraviolet divergences are removed by wavefunction renormalization and by adding a vacuum counterterm. This amounts to the substitutions $B^2 \rightarrow Z^2 B^2$ and $\mathcal{B} \rightarrow \mathcal{B} + \Delta\mathcal{B}$, where

$$Z^2 = 1 - N_c \sum_f \frac{4q_f^2}{3(4\pi)^2 \epsilon}, \quad \Delta\mathcal{B} = -N_c \sum_f \frac{m_f^4}{(4\pi)^2 \epsilon}. \quad (64)$$

The renormalized free energy density in the quark-gluon plasma phase then reduces to

$$\begin{aligned} \mathcal{F}_{\text{QGP}} = & -(N_c^2 - 1) \frac{\pi^2 T^4}{45} + \frac{1}{2}B^2 \left(1 + N_c \sum_f \frac{4q_f^2}{3(4\pi)^2} \ln \frac{\Lambda^2}{|2q_f B|} \right) + \frac{N_c}{(4\pi)^2} \sum_f m_f^4 \left[\ln \frac{\Lambda^2}{m_f^2} + \frac{3}{2} \right] \\ & - \frac{8N_c}{(4\pi)^2} \sum_f (q_f B)^2 \left[\zeta^{(1,0)}(-1, x_f) + \frac{1}{4}x_f^2 - \frac{1}{2}x_f^2 \ln x_f + \frac{1}{2}x_f \ln x_f - \frac{1}{12} \right] \\ & - \frac{2N_c}{(4\pi)^2} \sum_f K_0^B(\beta m_f) |q_f B| T^2 + \mathcal{B}. \end{aligned} \quad (65)$$

Fraga and Palhares (2012) take a slightly different approach to the renormalization of the MIT bag model than the one presented so far. The divergent terms $(qB)^2/\epsilon$ and $(q_f B)^2/\epsilon$ in the two phases remain after the subtraction of the vacuum energy at $T = B = 0$. These divergences can

be removed as done above, but leaves us with some finite terms. They argue that the finite terms proportional to $(qB)^2$ and $(q_f B)^2$ must be subtracted in an ad hoc fashion since the charges that generate the magnetic field are not included in the description. They therefore subtract all mass-independent terms that are proportional to $(qB)^2$ or $(q_f B)^2$, which leads to free energies densities in the two phases

$$\mathcal{F}_{\text{HHG}} = \frac{4(qB)^2}{(4\pi)^2} \left[\zeta^{(1,0)}(-1, \tfrac{1}{2} + x) - \zeta^{(1,0)}(-1, \tfrac{1}{2}) + \frac{1}{4}x^2 - \frac{1}{2}x^2 \ln x \right] - \frac{1}{2(4\pi)^2} \left[J_0(\beta m_\pi) T^4 + 2J_0^B(\beta m_\pi) |qB| T^2 \right], \quad (66)$$

$$\mathcal{F}_{\text{QGP}} = -\frac{N_c}{2\pi^2} \sum_f (q_f B)^2 \left[\zeta^{(1,0)}(-1, x_f) - \zeta^{(1,0)}(-1, 0) + \frac{1}{4}x_f^2 - \frac{1}{2}x_f^2 \ln x_f + \frac{1}{2}x_f \ln x_f \right] - (N_c^2 - 1) \frac{\pi^2 T^4}{45} - \frac{2N_c}{(4\pi)^2} \sum_f K_0^B(\beta m_f) |q_f B| T^2 + \mathcal{B}. \quad (67)$$

In Fig. 2 we show the critical temperature T_c for the phase transition as a function of $|qB|/m_\pi^2$ for $N_c = 3$ and $N_f = 2$. We have used $m_\pi = 140$ MeV, $m_u = m_d = 5$ MeV as well as $\Lambda = 600$ MeV, and $\mathcal{B} = (200 \text{ MeV})^4$. The black curve is with the $B = 0$ vacuum fluctuations and the red curve is where the $B = 0$ vacuum fluctuations have been subtracted. Clearly, the figure demonstrates the importance of how one treats the vacuum fluctuations in the model. In both cases, we have an effective B -dependent bag constant, which can be easily found by absorbing all the $T = 0$ terms into \mathcal{B} . An obvious quantity to calculate is a B -dependent effective bag constant $\mathcal{B}(B)$ that reproduces the critical temperature determined by lattice simulations.

We close this section by mentioning two related calculations (Agasian and Fedorov, 2008; Orlovsky and Simonov, 2014). Instead of a bag constant, the pressure contains another constant term arising from the gluonic condensate. The energy density term in the hadronic phase is of the form

$$\mathcal{E}_{\text{vac}} = -\frac{b}{8(4\pi)^2} \langle G^2 \rangle, \quad (68)$$

where $b = (33N_c - 2N_f)/3$ and $G^2 = (g_s G_{\mu\nu}^a)^2$. At temperatures around the transition temperature, the condensate is approximately half the value at $T = 0$. Lattice calculations at zero magnetic field give the value $\langle G^2 \rangle = 0.87 \text{ GeV}^4$ and a critical temperature of 177 MeV. Agasian and Fedorov (2008) showed that the critical temperature as well as the latent heat decrease as functions of the magnetic field B . The deconfinement transition is first order as defined by a nonzero latent heat between the two phases for magnetic fields smaller than $\sqrt{|qB|} \sim 600$ MeV. The transition is a crossover for magnetic fields larger than this value.

As pointed out by Orlovsky and Simonov (2014), the masses of the pions are strongly dependent on the magnetic field and should be taken into account. Similarly, the vacuum energy density (68) also depends on B (Ozaki, 2013). This calls for a more systematic study at finite magnetic field.

B. Chiral perturbation theory

Chiral perturbation theory is an effective low-energy theory for QCD in the hadronic phase (Gasser and Leutwyler, 1984, 1985; Weinberg, 1979). It is a model-independent framework in the sense that it only depends on the symmetries of QCD, the symmetry breaking pattern of QCD in the vacuum, and the relevant degrees of freedom. At sufficiently low energy or temperature, only the pseudo-Goldstone bosons are relevant degrees of freedom, although other degrees of freedom can be systematically added. In massless QCD with N_f flavors, the chiral Lagrangian has a

global $SU(N_f)_L \times SU(N_f)_R$ symmetry describing $N_f^2 - 1$ massless excitations. If the quarks have equal masses, this symmetry is explicitly broken to $SU(N_f)_V$. Explicit symmetry breaking in the chiral Lagrangian can be systematically included by adding terms to the Lagrangian that respect the $SU(N_f)_V$ symmetry.

In QCD, when one couples the quarks to the electromagnetic field, the flavor symmetry is broken. One can no longer freely transform a u -quark into a d -quark or an s -quark. For massless QCD with $N_f = 2$, the $SU(2)_L \times SU(2)_R$ symmetry is broken down to $U(1)_V \times U(1)_A$ by electromagnetic interactions. The $U(1)_V$ -symmetry corresponds to the invariance under a rotation of a u -quark by an angle α , $u \rightarrow e^{i\alpha}u$ and a rotation of a d -quark by the opposite angle, $d \rightarrow e^{-i\alpha}d$. The $U_A(1)$ symmetry corresponds to the invariance under a chiral rotation $u \rightarrow e^{i\gamma_5\alpha}u$ and $d \rightarrow e^{-i\gamma_5\alpha}d$.

Chiral perturbation theory is not an expansion in some small coupling constant, but is an expansion in powers of momenta p , where a derivative in the Lagrangian counts as one

power and a quark mass counts as two powers. Chpt is a nonrenormalizable quantum field theory, implying that a calculation at a given order n in momentum p , requires that one adds higher-order operators in order to cancel the divergences that arise in the calculations at order n . One needs more and more couplings as one goes to higher loop orders, and therefore more measurements to determine them. However, this poses no problem; as long as one is content with finite precision, a nonrenormalizable field theory has predictive power and is as good as any other field theory. This is the essence of effective field theory.

In this section, we restrict ourselves to two-flavor QCD. Chpt is then an effective theory for the three pions and the effective Lagrangian can be written as a power series

$$\mathcal{L}_{\text{eff}} = \mathcal{L}^{(2)} + \mathcal{L}^{(4)} + \dots \quad (69)$$

where the superscript indicates the order in momentum. In Euclidean space, the leading term is given by

$$\mathcal{L}^{(2)} = \frac{1}{4}F^2\text{Tr} \left[(D_\mu U)^\dagger (D_\mu U) - M^2(U + U^\dagger) \right], \quad (70)$$

where M and F are the tree-level values of the pion mass and pion decay constant, respectively. Moreover $U = e^{i\tau_i\pi_i/F}$ is a unitary $SU(2)$ matrix, τ_i are the Pauli matrices, π_i are the pion fields, and D_μ is the covariant derivative defined by

$$D_\mu U = \partial_\mu U - i[Q, U]A_\mu, \quad (71)$$

where Q is the charge matrix of the quarks, $Q = \text{diag}(\frac{2}{3}, -\frac{1}{3})e$. As explained earlier, a constant magnetic field B explicitly breaks the global chiral symmetry that transforms u and d quarks into each other, but leaves a residual $U(1)_A$ symmetry. Due to this reduced symmetry, there is only one true Goldstone boson namely the neutral pion $\pi^0 \equiv \pi_3$. If the magnetic field is sufficiently strong, the charged pions are very heavy and expected to decouple from the low-energy dynamics. In this regime, the low-energy field theory involves a single massless particle. The space-time symmetry is $SO(1,1) \times SO(2)$, which are Lorentz boosts in the x_0x_3 -plane as well as rotations in the x_1x_2 -plane perpendicular to B . We therefore need to consider separately the derivative operators $\partial_\perp = (\partial_1, \partial_2)$ and $\partial_\parallel = (\partial_0, \partial_3)$ and build our invariants from these. The effective Lagrangian for π^0 then reads

$$\mathcal{L}_{\text{eff}} = \frac{1}{4}F_\perp^{(1)}(\partial_\perp U_\perp)(\partial_\perp U_\perp)^\dagger + \frac{1}{4}F_\parallel^{(1)}(\partial_\parallel U_\parallel)(\partial_\parallel U_\parallel)^\dagger + \dots, \quad (72)$$

where $U_\perp = e^{i\pi^0/F_\perp}$ and $U_\parallel = e^{i\pi^0/F_\parallel}$. Note that we must allow for two different decay constants $F_\perp^{(1)}$ and $F_\parallel^{(1)}$ (Fayazbakhsh and Sadooghi, 2013; Kamikado and Kanazawa, 2014a). The

Lagrangian (72) is a special case (albeit with different notation) of the general case with N_u up quark flavors and N_d down quark flavors considered by Miransky and Shovkovy (2002). In this case the symmetry is $SU(N_u)_L \times SU(N_u)_R \times SU(N_d)_L \times SU(N_d)_R \times U(1)_A$ which is broken down to the diagonal subgroup $SU(N_u)_V \times SU(N_d)_V$. This gives rise to $N_u^2 + N_d^2 - 1$ massless Goldstone particles.

The Lagrangian $\mathcal{L}^{(2)}$, Eq. (70) can be expanded in powers of the pion fields. Through fourth order, we obtain

$$\begin{aligned} \mathcal{L}^{(2)} = & -F^2 M^2 + \frac{1}{2} (\partial_\mu \pi^0)^2 + \frac{1}{2} M^2 (\pi^0)^2 + (\partial_\mu + iqA_\mu) \pi^+ (\partial_\mu - iqA_\mu) \pi^- + M^2 \pi^+ \pi^- \\ & - \frac{M^2}{24F^2} [(\pi^0)^2 + 2\pi^+ \pi^-]^2 + \frac{1}{6F^2} \left\{ 2\pi^0 [\partial_\mu \pi^0] [\partial_\mu (\pi^+ \pi^-)] - 2\pi^+ \pi^- (\partial_\mu \pi^0)^2 \right. \\ & \left. - 2 \left[(\pi^0)^2 + 2\pi^+ \pi^- \right] (\partial_\mu \pi^+) (\partial_\mu \pi^-) + [\partial_\mu (\pi^+ \pi^-)]^2 \right\}, \end{aligned} \quad (73)$$

where we have defined the complex pion fields as $\pi_\pm = \frac{1}{\sqrt{2}}(\pi_1 \pm i\pi_2)$. In the same manner, we can expand the Lagrangian $\mathcal{L}^{(4)}$ to second order in the pion fields

$$\begin{aligned} \mathcal{L}^{(4)} = & \frac{1}{4} F_{\mu\nu}^2 + \frac{2l_5}{F^2} (qF_{\mu\nu})^2 \pi^+ \pi^- + \frac{2il_6}{F^2} qF_{\mu\nu} [(\partial_\mu \pi^-)(\partial_\nu \pi^+) + iqA_\mu \partial_\nu (\pi^+ \pi^-)] + (l_3 + l_4) \frac{M^4}{F^2} (\pi^0)^2 \\ & + 2(l_3 + l_4) \frac{M^4}{F^2} \pi^+ \pi^- + l_4 \frac{M^2}{F^2} (\partial_\mu \pi^0)^2 + 2l_4 \frac{M^2}{F^2} (\partial_\mu + iqA_\mu) \pi^+ (\partial_\mu - iqA_\mu) \pi^-. \end{aligned} \quad (74)$$

The Lagrangian $\mathcal{L}^{(6)}$ contains more than fifty terms for two flavors. However, in a two-loop calculation of the pressure at finite B only one term contributes, namely $M^2 (qF_{\mu\nu})^2$ (Agasian and Shushpanov, 2000; Cohen *et al.*, 2007; Werbos, 2008).

As mentioned above, the parameters M and F in the Lagrangian can be interpreted as the tree-level values of the pion mass m_π and pion decay constant F_π , respectively. However, these quantities receive loop corrections and they can no longer be identified with the bare parameters of the Lagrangian \mathcal{L} . The loop integrals are ultraviolet divergent and the divergences are cancelled by the renormalization of the low-energy constants l_i ($l_i = 1, 2, 3, \dots$) that appear in the Lagrangian. The relation between the bare low-energy constants l_i and their renormalized counterparts \bar{l}_i is

$$l_i = -\frac{\gamma_i}{2(4\pi)^2} \left[\frac{1}{\epsilon} + \bar{l}_i \right], \quad (75)$$

evaluated at the scale $\Lambda = M$. The coefficients γ_i are tabulated in the paper by Gasser and Leutwyler (1984). In the actual calculations, we present below, we need $\gamma_3 = \frac{1}{2}$

and $\gamma_4 = 2$. Note that our relation Eq. (75) does not involve the renormalization scale Λ as in Gasser and Leutwyler (1984) since it is a part of the definition of the sum-integrals. Moreover, our expression (73) for the truncated Lagrangian $\mathcal{L}^{(2)}$ differs from the expression found in for example the papers by Cohen *et al.* (2007) and Shushpanov and Smilga (1997) since they use a different parametrization for the unitary matrix U , namely the Weinberg parametrization. However, we obtain the same expressions for physical quantities independent of parametrization (Bochkarev and Kapusta, 1996). This simply reflects that physical quantities are independent of the coordinate system used.

To leading order in chiral perturbation theory and second order in the pion fields, the Lagrangian describes free bosons in a magnetic field. Thus a one-loop calculation of the free energy density is the same as the one we did in the hadronic phase for the MIT bag model and the renormalized result is given by Eq. (61), except that one must add the tree-level term $-M^2 F^2$ from Eq. (73), i.e. $\mathcal{F}_1^{\text{Chpt}} = -M^2 F^2 + \mathcal{F}_{\text{HHG}}$. The vacuum energy to one-

loop order at finite B was first calculated by Schwinger (1951) and generalized to two loops by Agasian and Shushpanov (2000). The two-loop result for the free energy density at finite temperature first appeared recently (Andersen, 2012a,b).

1. Quark condensate, pion mass, and pion decay constant

The zero-temperature quark condensate at one-loop in the chiral limit was first derived by Shushpanov and Smilga (1997) and later generalized to finite quark mass, i.e. finite m_π by Cohen *et al.* (2007). They also generalized their result to constant electromagnetic fields. The two-loop result for the chiral condensate in the chiral limit was calculated by Agasian and Shushpanov (2000) and generalized to finite pion mass by Werbos (2008). Agasian and Shushpanov also calculated the

finite-temperature quark condensate at one-loop (Agasian and Shushpanov, 2001), which was extended to two loops by Andersen (2012a).

Let us write the free energy density through n loops as $\mathcal{F}_n = \mathcal{F}_n^{\text{vac}} + \mathcal{F}_n^T + \mathcal{F}_n^B$, where $\mathcal{F}_n^{\text{vac}}$ is the contribution in the vacuum, i.e. for $B = T = 0$, \mathcal{F}_n^B is the zero-temperature contribution due to a finite magnetic field, and \mathcal{F}_n^T is the finite-temperature contribution. The chiral condensate is given by (Gerber and Leutwyler, 1989)

$$\langle \bar{q}q \rangle_B = \langle \bar{q}q \rangle_0 \left[1 - \frac{c}{F^2} \frac{\partial(\mathcal{F}_n^B + \mathcal{F}_n^T)}{\partial m_\pi^2} \right], \quad (76)$$

where $\langle \bar{q}q \rangle_0$ denotes the quark condensate at $T = B = 0$, $c = -F^2 \frac{\partial m_\pi^2}{\partial m} \langle \bar{q}q \rangle_0^{-1}$. Using $\mathcal{F}_1^B + \mathcal{F}_1^T = -M^2 F^2 + \mathcal{F}_{\text{HHG}} - \mathcal{F}_{\text{HHG}}(B = 0)$ and the fact that $c = 1$ in the chiral limit (Gerber and Leutwyler, 1989), one obtains the one-loop result for the quark condensate

$$\langle \bar{q}q \rangle_B = \langle \bar{q}q \rangle_0 \left[1 + \frac{1}{(4\pi)^2 F^2} \left(I_B(B) - J_1(\beta M) T^2 - 2J_1^B(\beta M) |qB| \right) \right], \quad (77)$$

where the function $I_B(M)$ is defined by

$$I_B(M) = M^2 \ln \frac{M^2}{2|qB|} - M^2 - 2|qB| \zeta^{(1,0)}(0, \frac{1}{2} + x). \quad (78)$$

Using the first term of the small- x expansion (C4), one finds that at $T = 0$, the condensate grows linearly with the field in the chiral limit (Shushpanov and Smilga, 1997), $\langle \bar{q}q \rangle_B = \langle \bar{q}q \rangle_0 \left[1 + \frac{|qB| \ln 2}{(4\pi)^2 F^2} \right]$.

In Fig. 3, we show the one- and two-loop results for the normalized quark condensate $\langle \bar{q}q \rangle_B / \langle \bar{q}q \rangle_0$ in the chiral limit as a function of T for $|qB| = 5(140 \text{ MeV})^2$ and for $B = 0$ for comparison. The vacuum contribution has been included and amounts to an increase of the chiral condensate of about 5% in this case. The effects are large due to the very strong magnetic field,

and for weaker fields, the difference between the two sets of curves is smaller. The curves suggest that the critical temperature for the chiral transition is increasing as a function of B , but since Chpt breaks down at perhaps $T \sim 150$ MeV, one should be careful making quantitative statements. For temperatures where Chpt can be trusted the curves suggest that perturbation theory in a magnetic field converges at least as well as for $B = 0$.

We next consider the correction to the neutral pion mass m_{π^0} due to a magnetic field. The Feynman diagrams contributing to the one-loop self-energy $\Pi(P_0, \mathbf{p})$ are shown in Fig. 4. The inverse propagator can be written as

$$\Gamma^{(2)}(P_0, \mathbf{p}) = P^2 + M^2 + \Pi(P_0, \mathbf{p}), \quad (79)$$

where the one-loop self-energy is given by the expression

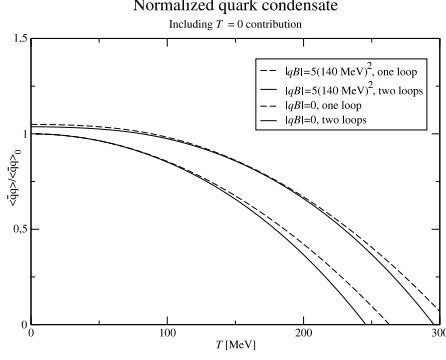


FIG. 3 Normalized quark condensate at one and two loops in the chiral limit as a function of T for $B = 0$ and $|qB| = 5(140 \text{ MeV})^2$. Figure taken from Andersen (2012a).

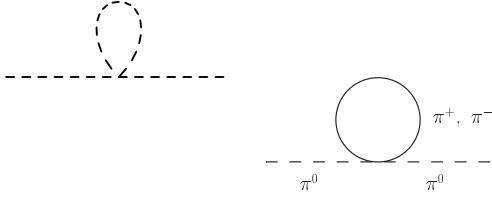


FIG. 4 One-loop graphs contributing to the self-energy of the neutral pion.

$$\begin{aligned} \Pi(P_0, \mathbf{p}) = & -\frac{2}{3F^2} P^2 \oint_K^B \frac{1}{K_0^2 + k_z^2 + M_B^2} + \frac{1}{6F^2} M^2 \left[2 \oint_K^B \frac{1}{K_0^2 + k_z^2 + M_B^2} - 3 \oint_P \frac{1}{K^2 + M^2} \right] \\ & + 2l_4 P^2 \frac{M^2}{F^2} + 2(l_3 + l_4) \frac{M^4}{F^2}, \end{aligned} \quad (80)$$

where the terms in the second line are counterterms coming from $\mathcal{L}^{(4)}$. Collecting all terms proportional to P^2 , we redefine the field π^0 such that the coefficient of P^2 in Eq. (79) equals unity (Loewe and Villavicencio, 2003). This yields

$$\Gamma^{(2)}(P_0, \mathbf{p}) = P^2 + m_{\pi^0}^2, \quad (81)$$

where the physical pion mass squared $m_{\pi^0}^2$ is

$$\begin{aligned} m_{\pi^0}^2 = & M^2 + \frac{M^2}{F^2} \oint_P^B \frac{1}{P_0^2 + p_z^2 + M_B^2} - \frac{1}{2} \frac{M^2}{F^2} \oint_P \frac{1}{P^2 + M^2} + 2l_3 \frac{M^4}{F^2} \\ = & M^2 \left[1 - \frac{1}{(4\pi)^2 F^2} \left(I_B(M) + \frac{1}{2} J_1(\beta M) T^2 - J_1^B(\beta M) |qB| \right) \right]. \end{aligned} \quad (82)$$

This result was first obtained at zero temperature by Shushpanov and Smilga (1997) and later generalized to finite temperature by Agasian and Shushpanov (2000). We note that m_{π^0} vanishes in the chiral limit $M \rightarrow 0$, as it must since the neutral pion is a Goldstone boson.

We next consider the pion decay constant for the neutral pion, F_{π^0} . The components of the axial current \mathcal{A}_μ^0 are given by

$$\mathcal{A}_\mu^0 = -F\partial_\mu\pi^0 + \frac{2}{3F} \left[2\pi^+\pi^-\partial_\mu\pi^0 - \pi^0\partial_\mu(\pi^+\pi^-) - 2M^2l_4\partial_\mu\pi^0 \right]. \quad (83)$$

In order to calculate the pion decay constant, we need to evaluate the matrix element $F_{\pi^0} = \langle 0 | \mathcal{A}_\mu^0 | \pi^0 \rangle$. In a consistent one-loop calculation, one needs to take into account wavefunction renormalization of the tree-level term $-F\partial_\mu\pi^0$.² Calculating the matrix element, one finds

$$F_{\pi^0} = F \left[1 - \frac{1}{F^2} \not\!\!\!\int_P^B \frac{1}{P_0^2 + p_z^2 + M_B^2} + \frac{M^2}{F^2} l_4 \right]. \quad (84)$$

After renormalization, we find

$$F_{\pi^0} = F \left[1 + \frac{1}{(4\pi)^2 F^2} (I_B(M) - J_1^B(\beta M) |qB|) \right], \quad (85)$$

Using Eqs. (82) and (85), we see that

$$m_{\pi^0}^2 F_{\pi^0}^2 = m \langle \bar{q}q \rangle_B, \quad (86)$$

which is the Oakes-Gell-Mann-Renner relation in a magnetic field. This relation was first shown by Agasian and Shushpanov (2001).

C. Nambu-Jona-Lasinio model

The Nambu-Jona-Lasinio (NJL) model was originally proposed as a theory for interacting nucleons and pions in the 1960s before the discovery of quarks (Nambu and Jona-Lasinio, 1961a,b). After the discovery of quarks and the formulation of QCD as the theory of the strong interactions, the fermion fields in the Lagrangian were reinterpreted as quark fields and the NJL model as an effective low-energy model for QCD. We will make a few remarks on the NJL model below, but for a detailed discussion of its properties, we refer to the reviews

by Klevansky (1992) and Buballa (2005). In the NJL model, one-gluon exchange between the quarks is replaced by local four-point quark interactions. Thus there are no gauge fields in the model and the local $SU(N_c)$ gauge symmetry of QCD is replaced by a global $SU(N_c)$ symmetry. As a result, two of the most prominent features of QCD - asymptotic freedom and confinement - are lost. The latter can be seen by the fact that the polarization function for pions, $\Pi_M(p^2)$, develops an imaginary part for $p^2 > 4M^2$ where M is the quark mass and the pions become unstable against decay to their constituent parts (Buballa, 2005).

Another important aspect of QCD, namely that of chiral symmetry breaking in the vacuum, is taken into account by the NJL model. The spontaneous breaking of chiral symmetry guarantees via the Goldstone theorem the appearance of massless, or light if chiral symmetry is explicitly broken, bosonic excitations in the spectrum. For $N_f = 2$, these particles are the (light) pions and the explanation of the low pion mass was a success of the NJL model. We note in passing that in Lorentz invariant theories, the number of Goldstone bosons equals the number of broken generators. When Lorentz invariance is broken, for example at finite density, the number of massless excitations maybe strictly smaller than the number of broken generators (Brauner, 2010; Nielsen and Chadha, 1976) and some of them have a quadratic dispersion relation $E \sim p^2$ instead of a linear one.

However, chiral symmetry breaking is not seen at any finite order in perturbation theory and one needs to sum an infinite number of a certain class of diagrams to obtain a nonzero chiral condensate. This is done by introducing a set of collective bosonic or auxiliary fields such that the Lagrangian becomes bilinear in the quark fields. One can then integrate out exactly the fermions in the path integral and afterwards expand the

² This wavefunction renormalization counterterm is the same we used to obtain Eq. (82).

resulting functional determinant in powers of the collective fields and their derivatives. This expansion is an expansion in $1/N_c$. To leading order in $1/N_c$, i.e. in the large- N_c limit, this gives rise to a gap equation for the chiral condensate. This is also referred to as the mean-field approximation, since the collective fields are replaced by their expectation values. At next-to-leading order, this expansion generates kinetic terms for the bosonic fields and so they become propagating quantum fields. At next-to-next-to-leading order, the expansion generates interaction terms among the bosons (Boomsma and Boer, 2009; Eguchi, 1976; Klevansky, 1992).

The NJL model is nonrenormalizable in the sense that loop diagrams generate divergences that cannot be cancelled by local counterterms of the same type as those appearing in the original Lagrangian. One therefore needs to add new operators to cancel these divergences. The operators that are induced this way are suppressed by some power of some (large) mass scale Λ . This mass scale signals new physics that is not captured by the model, but as long as we stay well below this scale, this is not a problem. At finite precision, only a finite number of operators contribute to a given physical quantity. One way of dealing with the ultraviolet divergences in the momentum integrals is by cutting them off using a sharp three-dimensional cutoff Λ or a smooth ultraviolet cutoff. In the case of a sharp cutoff, the momentum scale Λ can be interpreted as an upper scale below which the model or theory is valid. A soft cutoff is often referred to as a form factor and denoted by $F(p)$, where p is the three-momentum. A form factor that mimics asymptotic freedom is

$$F(p) = \frac{\Lambda^2}{\Lambda^2 + p^2}, \quad (87)$$

where Λ is a mass scale. The function $F(p)$ guarantees that loop integrals converge for large momentum p . A three-dimensional cutoff breaks Lorentz invariance, but this may be less severe at finite temperature, where it is broken anyway. There are other form factors that are tailored to the problem of a magnetic background and we will briefly discuss them below.

The Minkowski space Lagrangian of the NJL model with $N_f = 2$ can be written as

$$\mathcal{L} = \mathcal{L}_0 + \mathcal{L}_{\bar{q}q} + \mathcal{L}_{\text{det}}, \quad (88)$$

where the various terms are

$$\mathcal{L}_0 = i\bar{\psi}\not{D}\psi - m_0\bar{\psi}\psi, \quad (89)$$

$$\mathcal{L}_{\bar{q}q} = G_1 \left[(\bar{\psi}\psi)^2 + (\bar{\psi}\boldsymbol{\tau}\psi)^2 + (\bar{\psi}i\gamma_5\psi)^2 + (\bar{\psi}i\gamma_5\boldsymbol{\tau}\psi)^2 \right], \quad (90)$$

$$\mathcal{L}_{\text{det}} = G_2 \left[(\bar{\psi}\psi)^2 - (\bar{\psi}\boldsymbol{\tau}\psi)^2 - (\bar{\psi}i\gamma_5\psi)^2 + (\bar{\psi}i\gamma_5\boldsymbol{\tau}\psi)^2 \right], \quad (91)$$

where $\boldsymbol{\tau}$ are the Pauli spin matrices, and $\not{D} = \gamma^\mu D_\mu$. $D_\mu = \partial_\mu - iQA_\mu$ is the covariant derivative where $Q = \text{diag}(\frac{2}{3}, -\frac{1}{3})e$ is the charge matrix. G_1 and G_2 are coupling constants and m_0 is the mass matrix, $m_0 = \text{diag}(m_u, m_d)$. As is normally done in the literature, we use $m_u = m_d$. For $N_f = 2$, ψ is an isospin doublet,

$$\psi = \begin{pmatrix} u \\ d \end{pmatrix}. \quad (92)$$

The terms $\mathcal{L}_0 + \mathcal{L}_{\bar{q}q}$ are invariant under the global symmetries $SU(N_c) \times SU(2)_L \times SU(2)_R \times U(1)_B \times U(1)_A$ in the chiral limit and $SU(N_c) \times SU(2)_{L+R} \times U(1)_B$ at the physical point.³ These are the symmetries of QCD, except that the color symmetry is global and not local. The term \mathcal{L}_{det} breaks the $U(1)_A$ symmetry while preserving the others. This term is 't Hooft's instanton-induced interaction and mimics the breaking of the axial $U(1)_A$ symmetry in the QCD vacuum ('t Hooft, 1976). It is necessary to explain the relatively large mass of the η particle. We note that such a term is a six-quark interaction in three-flavor QCD.

We next consider the two nonzero quark condensates $\langle \bar{u}u \rangle$ and $\langle \bar{d}d \rangle$. These can be expressed in terms of $\langle \bar{\psi}\psi \rangle$ and $\langle \bar{\psi}\boldsymbol{\tau}_3\psi \rangle$ as $\langle \bar{u}u \rangle \pm \langle \bar{d}d \rangle$, and a nonzero $\langle \bar{\psi}\boldsymbol{\tau}_3\psi \rangle$ implies that $\langle \bar{u}u \rangle \neq \langle \bar{d}d \rangle$. Hence we can write $(\bar{\psi}\psi)^2 = (\bar{\psi}\psi - \langle \bar{\psi}\psi \rangle)^2 + 2\langle \bar{\psi}\psi \rangle \bar{\psi}\psi - \langle \bar{\psi}\psi \rangle^2$ and $(\bar{\psi}\boldsymbol{\tau}_3\psi)^2 = (\bar{\psi}\boldsymbol{\tau}_3\psi - \langle \bar{\psi}\boldsymbol{\tau}_3\psi \rangle)^2 + 2\langle \bar{\psi}\boldsymbol{\tau}_3\psi \rangle \bar{\psi}\boldsymbol{\tau}_3\psi - \langle \bar{\psi}\boldsymbol{\tau}_3\psi \rangle^2$.

³ This is for the case $m_u = m_d$. If $m_u \neq m_d$, the symmetry $SU(2)_{L+R}$ reduces to $U(1)_{I_3}$.

$\langle \bar{\psi}\tau_3\psi \rangle)^2 + 2\langle \bar{\psi}\tau_3\psi \rangle \bar{\psi}\tau_3\psi - \langle \bar{\psi}\tau_3\psi \rangle^2$. In the mean-field approximation, we linearize the interaction terms in presence of the two condensates $\langle \bar{\psi}\psi \rangle$ and $\langle \bar{\psi}\tau_3\psi \rangle$, i.e. we neglect the fluctuations around the mean field. Hence, we approximate the quartic terms by

$$(\bar{\psi}\psi)^2 \approx 2\langle \bar{\psi}\psi \rangle \bar{\psi}\psi - \langle \bar{\psi}\psi \rangle^2, \quad (93)$$

$$(\bar{\psi}\tau_3\psi)^2 \approx 2\langle \bar{\psi}\tau_3\psi \rangle \bar{\psi}\tau_3\psi - \langle \bar{\psi}\tau_3\psi \rangle^2. \quad (94)$$

Substituting Eqs. (93) and (94) into Eq. (88), we obtain the Lagrangian which is bilinear in the fermion fields:

$$\begin{aligned} \mathcal{L}_{\text{bilinear}} = & -\frac{(M_0 - m_0)^2}{4G_0} - \frac{M_3^2}{4(1-2c)G_0} \\ & + \bar{\psi} [\not{D}_\mu - M] \psi, \end{aligned} \quad (95)$$

where $M = M_0 + \tau_3 M_3$ and we have introduced

$$M_0 = m_0 - 2G_0 \langle \bar{\psi}\psi \rangle, \quad (96)$$

$$M_3 = -2(1-2c)G_0 \langle \bar{\psi}\tau_3\psi \rangle, \quad (97)$$

$$G_1 = (1-c)G_0, \quad (98)$$

$$G_2 = cG_0. \quad (99)$$

The parameter c controls the instanton interaction or the amount of explicit breaking of the

$U(1)_A$ symmetry. Beyond the mean-field approximation, the number of scalars and pseudo-scalars depends on c ; For $c = \frac{1}{2}$, only the sigma and the pions are present, while for all other values, also the η and the \mathbf{a} are in the spectrum. The constituent quark masses for the u and d quarks can be expressed as $M_u = M_0 + M_3$ and $M_d = M_0 - M_3$. Generally these constituent quark masses are different, only for $G_1 = G_2$ are they identical. This corresponds to $c = \frac{1}{2}$. The fact that $\langle \bar{u}u \rangle$ generally is different from $\langle \bar{d}d \rangle$ should come as no surprise as the electric charge of the u -quark is different from that of the d -quark.

The Lagrangian (95) is bilinear in the quark fields and we can integrate over them exactly. The vacuum energy is evaluated using dimensional regularization with zeta-function regularization in the usual way and whose M -independent (divergent and finite) terms are omitted⁴. The remaining divergences can be isolated by subtracting and adding the vacuum energy for $B = 0$. The difference between the two vacuum energies is finite, while the subtracted vacuum energy is evaluated using a hard three-dimensional cutoff Λ . This yields the free energy density (Boomsma and Boer, 2010; Menezes *et al.*, 2009)

$$\begin{aligned} \mathcal{F}_{0+1} = & \frac{(M_0 - m)^2}{4G_0} + \frac{M_3^2}{4(1-2c)G_0} + \frac{N_c}{8\pi^2} \sum_f \left[M_f^4 \ln \left(\frac{\Lambda}{M_f} + \sqrt{1 + \frac{\Lambda^2}{M_f^2}} \right) \right. \\ & \left. - M_f \Lambda \left(M_f^2 + 2\Lambda^2 \right) \sqrt{1 + \frac{\Lambda^2}{M_f^2}} \right] - \frac{8N_c}{(4\pi)^2} \sum_f (q_f B)^2 \left[\zeta^{(1,0)}(-1, x_f) \right. \\ & \left. + \frac{1}{4} x_f^2 - \frac{1}{2} x_f^2 \ln x_f + \frac{1}{2} x_f \ln x_f \right] - \frac{2N_c T^2}{(4\pi)^2} \sum_f K_0^B(\beta M_f) |q_f B|, \end{aligned} \quad (100)$$

where $x_f = M_f/|2q_f B|$. A similar expression can be found in the paper by Ebert and Klimenko (2000), where a four-dimensional cutoff is used, cf. Eq. (46).

⁴ This corresponds to ignoring wavefunction renormalization of the tree-level term $\frac{1}{2}B^2$ in the free energy density.

1. Quark condensates

The calculations discussed in this subsection were presented in the paper by Boomsma and Boer (2010). In these calculations, they used $m_0 = 6$ MeV, $\Lambda = 590$ MeV, and $G_0 \Lambda^2 = 2.435$. These values lead to a pion mass of 140.2 MeV, a pion decay

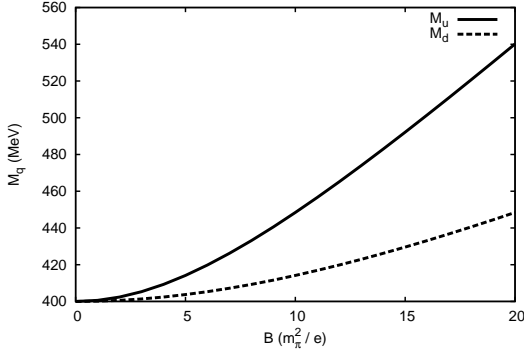


FIG. 5 Constituent quark masses M_u and M_d as functions of B measured in units of m_π^2/e for $c = 0$. Figure taken from Boomsma and Boer (2010).

constant of 92.6 MeV, and a quark condensate $\langle \bar{u}u \rangle = \langle \bar{d}d \rangle = (-241.3 \text{ MeV})^3$, all in the vacuum.

The values of M_u and M_d are obtained by solving the gap equations

$$\frac{\partial \mathcal{F}_{0+1}}{\partial M_f} = 0, \quad f = u, d. \quad (101)$$

In Fig. 5, the constituent quark masses M_u and M_d are shown as a function of B measured in units of m_π^2/e for $c = 0$, i.e. with the $U(1)_A$ symmetry intact. Notice that $M_u = M_d$ for $B = 0$, while they split for finite magnetic field and the splitting increases as B grows. A nonzero c will bring the masses closer together and at $c = \frac{1}{2}$ they are equal.

In Fig. 6, the constituent quark mass $M_u = M_d = M$ is shown as a function of T for three different values of the magnetic field. The results are in the chiral limit and for $c = \frac{1}{2}$. The transition is second order with mean-field critical exponents for all values of the magnetic field (Boomsma and Boer, 2010; Inagaki *et al.*, 2004). The order of the phase transition in various approximations will be discussed further in Secs. V.D and VII. The number x in x LL is the number of Landau levels one must include such that the error is less than 1%. The stronger the magnetic field, the fewer Landau levels are needed to be included in the sum in order to obtain a certain accuracy. The reason is that the effective mass of the fermions increases with the

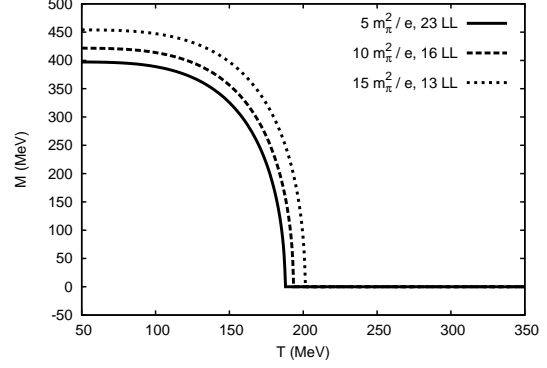


FIG. 6 Constituent quark mass M as a function of T for three different values of the magnetic field and in the chiral limit. Figure taken from Boomsma and Boer (2010).

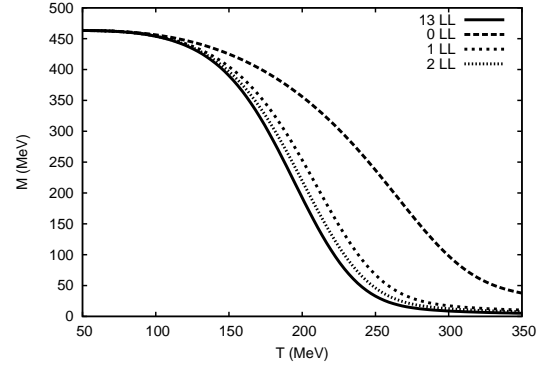


FIG. 7 Constituent quark mass M as a function of T for four different values of the magnetic field and at the physical point. Figure taken from Boomsma and Boer (2010).

magnetic field and that more Landau levels are effective Boltzmann suppressed.

In Fig. 7, the constituent quark mass $M_u = M_d = M$ for $c = \frac{1}{2}$ and at the physical point is shown as a function of T for four different values of the magnetic field. The constituent quark mass is a strictly positive continuous function of T and hence the transition is a crossover.

2. Other condensates

So far we have discussed the quark condensates $\langle \bar{u}u \rangle$ and $\langle \bar{d}d \rangle$ as functions of the magnetic field. However, due to the external magnetic field, the symmetry of the system is re-

duced and other nonzero condensates are possible. Ferrer *et al.* (2014b) considered a one-flavor NJL model in a constant external magnetic field. A constant magnetic field breaks Lorentz invariance down to $SO(1, 1) \times SO(2)$, where the latter corresponds to rotations around the axis in the direction of the magnetic field B . The standard interaction term they consider is

$$\mathcal{L}_{\text{int}}^{(1)} = \frac{G}{2} [(\bar{\psi}\psi)^2 + (\bar{\psi}i\gamma^5\psi)^2], \quad (102)$$

where G is the usual coupling in the NJL model. The new interaction term that respects chiral symmetry and is invariant under $SO(1, 1) \times SO(2)$ is

$$\mathcal{L}_{\text{int}}^{(2)} = \frac{G'}{2} [(\bar{\psi}\Sigma^3\psi)^2 + (\bar{\psi}i\gamma^5\Sigma^3\psi)^2], \quad (103)$$

where $\Sigma^3 = \frac{i}{2}[\gamma^1, \gamma^2]$ is the spin operator along the field direction and G' is a new coupling constant. The interaction terms in Eqs. (102)–(103) can be derived from one-gluon exchange in QCD using Fierz identities. The value of the coupling constant G' is unknown, but vanishes in the limit $B \rightarrow 0$. The reduced symmetry gives rise to a new nonzero condensate

$$\xi = \langle \bar{\psi}\gamma^1\gamma^2\psi \rangle, \quad (104)$$

in addition to the chiral condensate $\sigma = \langle \bar{\psi}\psi \rangle$. Calculating the thermodynamic potential Ω in the mean-field approximation and using the equations of motion $\frac{\partial\Omega}{\partial\sigma} = 0$ and $\frac{\partial\Omega}{\partial\xi} = 0$, they show that

$$\xi = \frac{G'}{G}\sigma. \quad (105)$$

Thus the spin condensate vanishes in zero magnetic field as expected and for nonzero magnetic field it is proportional to the quark condensate. Due to Eq. (105), the two condensates evaporate at the same critical temperature. The same behavior has been found on the lattice (Bali *et al.*, 2012b), where ξ and σ drop to zero at around $T = 160$ MeV.

The spectrum of fermionic excitations was calculated by Ferrer *et al.* (2014b) and reads

$$E_0^2 = p_z^2 + (\sigma + \xi)^2, \quad n = 0, \quad (106)$$

$$E_n^2 = p_z^2 + \sigma^2 + (\sqrt{2|q_f B|n \pm \xi})^2, \quad n \geq 1, \quad (107)$$

where \pm correspond to the positive and negative spin projections, respectively. Here we notice that there is a Zeeman splitting in the spectrum for $n \geq 1$ but not so for $n = 0$. The interpretation of the term involving ξ is that it arises from an anomalous magnetic moment of the quarks and antiquarks.

The critical temperature T_c for the system changes due to the existence of the condensate ξ . If the magnetic field is sufficiently strong that all the particles are in the lowest Landau level (LLL), one can calculate the critical temperature analytically. In this case, the dynamical mass of the quarks in the LLL is given by $M_\xi = \sigma + \xi$ and the critical temperature is proportional to M_ξ . A calculation by Ferrer *et al.* (2014b) shows that

$$T_c \approx 0.8M_\xi. \quad (108)$$

Thus the temperature increases linearly with M_ξ and is governed by the coupling G' .

We close this section with a brief discussion of a possible new phase in the QCD vacuum at very strong magnetic fields. In this phase, charged ρ^\pm mesons condense and as a result the vacuum behaves as a superconductor. The idea goes back to Ambjørn and Olesen (1989a,b); and Nielsen and Olesen (1978) who showed that the W^\pm condense in a sufficiently strong magnetic field: the energy of a W^\pm boson becomes purely imaginary signalling an instability of the electroweak vacuum and the formation of a condensate. The dispersion relation for a charged ρ meson in a magnetic field is

$$E_k^2 = m_\rho^2 + p_z^2 + |qB|(2k + 1 - 2s), \quad (109)$$

where $s = \pm 1$. For a particle in the lowest Landau level with zero longitudinal momentum p_z , the energy becomes purely imaginary when the magnetic field exceeds $B_c = m_\rho^2/q$, with $m_\rho = 775$ MeV. This suggests that the QCD vacuum is unstable against condensation of charged ρ mesons (Callebaut *et al.*, 2013; Chernodub, 2010, 2011). The condensate breaks a $U(1)$ symmetry, however this is not in conflict with the Vafa-Witten theorem as no massless Nambu-Goldstone bosons appear in the spectrum (Chernodub, 2014; Hidaka and Yamamoto, 2013).

D. Quark-meson model

Introducing the collective fields and integrating over the quark fields in the NJL model, leads to a fermion determinant in the expression for the effective action. This functional determinant is a function of the background fields σ and $\boldsymbol{\pi}$. As explained earlier, the mean-field approximation consists of setting σ equal to its expectation value and ignore fluctuations of the fields σ and $\boldsymbol{\pi}$. Expanding the fluctuation determinant around the expectation value of the σ field, one generates kinetic terms for the mesons as well as

interaction terms. The terms that are generated are in principle all those that are consistent with the symmetries of the NJL model. These terms can be organized according to the powers of the fields and their derivatives. If one truncates the series at second order in derivatives and fourth order in the fields, we are effectively left with a quark-meson model whose coupling constants depend on the parameters of the NJL model and some one-loop fermionic integrals.

The Euclidean Lagrangian of the two-flavor quark-meson model can be written as

$$\mathcal{L} = \bar{\psi} \left[\gamma_\mu D_\mu + g(\sigma - i\gamma_5 \boldsymbol{\tau} \cdot \boldsymbol{\pi}) \right] \psi + \frac{1}{2} \left[(\partial_\mu \sigma)^2 + (\partial_\mu \boldsymbol{\pi})^2 \right] + \frac{1}{2} m^2 \left[\sigma^2 + \boldsymbol{\pi}^2 \right] + \frac{\lambda}{24} \left[\sigma^2 + \boldsymbol{\pi}^2 \right]^2 - h\sigma. \quad (110)$$

This Lagrangian has an $O(4)$ symmetry for $h = 0$, which is explicitly broken to $O(3)$ for nonzero h .⁵ This term gives rise to nonzero pion masses after spontaneous symmetry breaking. However, once we couple the quark-meson model to an Abelian gauge field, the model is only $O(2) \times O(2)$ or $U(1)_V \times U(1)_A$ invariant. At the quark level, this was explained in Sec. V.B. At the mesonic level, the vector and axial phase transformations are

$$\Delta \rightarrow e^{2i\alpha} \Delta, \quad v \rightarrow v, \quad (111)$$

$$\Delta \rightarrow \Delta, \quad v \rightarrow e^{2i\gamma_5 \alpha} v, \quad (112)$$

where we have introduced $\Delta = \frac{1}{\sqrt{2}}(\pi_1 + i\pi_2) = \pi^+$ and $v = \frac{1}{\sqrt{2}}(\sigma + i\gamma_5 \pi_0)$. This implies that we have two invariants $\sigma^2 + \pi_0^2$ and $\pi^+ \pi^-$ instead of $\sigma^2 + \boldsymbol{\pi}^2$. We therefore have two mass parameters m_1^2 and m_2^2 instead of a single mass parameter m^2 , and three coupling constants λ_1 , λ_2 , and λ_3 instead of a single coupling λ . Finally, the Yukawa interaction term splits into the two terms $g_1 \bar{\psi}(\sigma - i\gamma_5 \tau_3 \pi_3) \psi$ and $-g_2 \bar{\psi} i\gamma_5 (\tau_1 \pi_1 + \tau_2 \pi_2) \psi$. These couplings are in principle functions of the magnetic field B but we do not know their B -dependence, only that their values are

identical for $B = 0$. As is commonly done in the literature, we therefore set all the couplings and masses equal and equal to their values in the vacuum.

At one loop, the effective potential receives contributions from the bosonic as well as the fermionic fields via the functional determinants. A common approximation in the QM model is to neglect the quantum and thermal fluctuations of the mesons (Fraga and Mizher, 2008; Scavenius *et al.*, 2001). We make this approximation in this section and discuss the inclusion of mesonic fluctuations in the section on the functional renormalization group.

We first shift the sigma field and write it as a sum of a classical background field ϕ and a quantum field $\tilde{\sigma}$

$$\sigma \rightarrow \phi + \tilde{\sigma}. \quad (113)$$

The tree-level potential then becomes

$$\mathcal{F}_0 = \frac{1}{2} B^2 + \frac{1}{2} m^2 \phi^2 + \frac{\lambda}{24} \phi^4 - h\phi. \quad (114)$$

The tree-level masses of the sigma, the pions, and the quark are (before coupling to B)

$$m_\sigma^2 = m^2 + \frac{\lambda}{2} \phi^2, \quad (115)$$

⁵ In addition to a global $SU(N_c)$ symmetry.

$$m_\pi^2 = m^2 + \frac{\lambda}{6}\phi^2, \quad (116)$$

$$m_q = g\phi. \quad (117)$$

The pion mass satisfies $h = \phi m_\pi^2$ at the minimum of the tree-level potential and therefore vanishes for $h = 0$, in agreement with the Goldstone theorem. The one-loop potential then becomes

$$\begin{aligned} \mathcal{F}_{0+1} = & \frac{1}{2}B^2 + \frac{1}{2}m^2\phi^2 + \frac{\lambda}{24}\phi^4 - h\phi - \frac{1}{4(4\pi)^2} \left(\frac{\Lambda^2}{m_\sigma^2} \right)^\epsilon \left[\left(\frac{1}{\epsilon} + \frac{3}{2} \right) m_\sigma^4 + 2J_0(\beta m_\sigma) \right] \\ & - \frac{1}{4(4\pi)^2} \left(\frac{\Lambda^2}{m_{\pi^0}^2} \right)^\epsilon \left[\left(\frac{1}{\epsilon} + \frac{3}{2} \right) m_{\pi^0}^4 + 2J_0(\beta m_{\pi^0}) \right] + \frac{1}{2(4\pi)^2} \left(\frac{\Lambda^2}{|2qB|} \right)^\epsilon \left[\left(\frac{(qB)^2}{3} - m_{\pi^0}^4 \right) \left(\frac{1}{\epsilon} + 1 \right) \right. \\ & + 8(qB)^2 \zeta^{(1,0)}(-1, \frac{1}{2} + x) - 2J_0^B(\beta m_{\pi^0}) \left. \right] + \frac{N_c}{(4\pi)^2} \sum_f \left(\frac{\Lambda^2}{2|q_f B|} \right)^\epsilon \left[\left(\frac{2(q_f B)^2}{3} + m_q^4 \right) \left(\frac{1}{\epsilon} + 1 \right) \right. \\ & \left. - 8(q_f B)^2 \zeta^{(1,0)}(-1, x_f) - 2|q_f B| m_q^2 \ln x_f - 2K_0^B(\beta m_q) |q_f B| T^2 + \mathcal{O}(\epsilon) \right]. \end{aligned} \quad (118)$$

The B -dependent divergence is removed in the usual way by making the replacement $B^2 \rightarrow Z^2 B^2$, where

$$Z^2 = \left[1 - \frac{q^2}{3(4\pi)^2 \epsilon} - N_c \sum_f \frac{4q_f^2}{3(4\pi)^2 \epsilon} \right] \quad (119)$$

The other divergences are removed by making the replacement $m^2 \rightarrow m^2 + \Delta m^2$, $\lambda \rightarrow \lambda + \Delta\lambda$, and adding a vacuum energy counterterm $\Delta\mathcal{E}_0$, where

$$\Delta m^2 = \frac{\lambda m^2}{(4\pi)^2 \epsilon}, \quad \Delta\lambda = \frac{\lambda^2}{8\pi^2} - \frac{3N_c N_f g^4}{2\pi^2 \epsilon}, \quad \Delta\mathcal{E} = \frac{m^4}{(4\pi)^2 \epsilon}. \quad (120)$$

The renormalized one-loop effective potential becomes

$$\begin{aligned} \mathcal{F}_{0+1} = & \frac{1}{2}B^2 \left[1 + \frac{q^2}{3(4\pi)^2} \ln \frac{\Lambda^2}{|2qB|} + N_c \sum_f \frac{4q_f^2}{3(4\pi)^2} \ln \frac{\Lambda^2}{|2q_f B|} \right] + \frac{1}{2}m^2\phi^2 + \frac{\lambda}{24}\phi^4 - h\phi \\ & - \frac{m_\sigma^4}{4(4\pi)^2} \left[\ln \frac{\Lambda^2}{m_\sigma^2} + \frac{3}{2} \right] - \frac{3m_{\pi^0}^4}{4(4\pi)^2} \left[\ln \frac{\Lambda^2}{m_{\pi^0}^2} + \frac{3}{2} \right] + \frac{N_c m_q^4}{(4\pi)^2} \sum_f \left[\ln \frac{\Lambda^2}{m_q^2} + \frac{3}{2} \right] \\ & + \frac{4(qB)^2}{(4\pi)^2} \left[\zeta^{(1,0)}(-1, \frac{1}{2} + x) + \frac{1}{4}x^2 - \frac{1}{2}x^2 \ln x + \frac{1}{24} \right] - \frac{8N_c}{(4\pi)^2} \sum_f (q_f B)^2 \left[\zeta^{(1,0)}(-1, x_f) \right. \\ & + \frac{1}{4}x_f^2 - \frac{1}{2}x_f^2 \ln x_f + \frac{1}{2}x_f \ln x_f - \frac{1}{12} \left. \right] - \frac{1}{2(4\pi)^2} \left[J_0(\beta m_\sigma) T^4 + J_0(\beta m_{\pi^0}) T^4 \right. \\ & \left. + 2J_0^B(\beta m_{\pi^0}) |qB| T^2 \right] - \frac{2N_c T^2}{(4\pi)^2} \sum_f K_0^B(\beta m_q) |q_f B|. \end{aligned} \quad (121)$$

As mentioned above, it a common approximation to neglect the bosonic contribution to the one-loop effective potential and as a result our expression reduces to

$$\mathcal{F}_{0+1} = \frac{1}{2}B^2 \left[1 + N_c \sum_f \frac{4q_f^2}{3(4\pi)^2} \ln \frac{\Lambda^2}{|2q_f B|} \right] + \frac{1}{2}m^2\phi^2 + \frac{\lambda}{24}\phi^4 - h\phi + \frac{N_c m_q^4}{(4\pi)^2} \sum_f \left[\ln \frac{\Lambda^2}{m_q^2} + \frac{3}{2} \right]$$

$$\begin{aligned}
& -\frac{8N_c}{(4\pi)^2} \sum_f (q_f B)^2 \left[\zeta^{(1,0)}(-1, x_f) + \frac{1}{4} x_f^2 - \frac{1}{2} x_f^2 \ln x_f + \frac{1}{2} x_f \ln x_f - \frac{1}{12} \right] \\
& -\frac{2N_c T^2}{(4\pi)^2} \sum_f K_0^B(\beta m_q) |q_f B|. \tag{122}
\end{aligned}$$

In the literature, the parameters are often fixed at tree level. The parameters in the Lagrangian (110) can then be expressed in terms of the sigma mass, the pion mass, and the pion decay constant as

$$m^2 = -\frac{1}{2}(m_\sigma^2 - 3m_\pi^2), \tag{123}$$

$$\lambda = \frac{3(m_\sigma^2 - m_\pi^2)}{f_\pi^2}, \tag{124}$$

$$h = f_\pi m_\pi^2. \tag{125}$$

Having determined the parameters as described above, the tree-level potential has its minimum at the correct value $\phi = f_\pi = 93$ MeV, while the minimum of the one-loop potential depends on the renormalization scale. We can choose Λ such that the minimum of the one-loop effective potential (122) in the vacuum, i.e. $T = B = 0$, still is at $\phi = f_\pi = 93$ MeV. This is done by requiring

$$\left. \frac{d\mathcal{F}_{0+1}}{d\phi} \right|_{\phi=f_\pi} = 0. \tag{126}$$

A straightforward calculation yields

$$\frac{N_c g^4 f_\pi^2}{(2\pi)^2} \left[\ln \frac{\Lambda^2}{g^2 f_\pi^2} + 1 \right] = 0. \tag{127}$$

Using $f_\pi = 93$ MeV and $g = 3.2258$ (see below), this yields $\Lambda = 181.96$ MeV. Even if we use this value for the renormalization scale such that \mathcal{F}_{0+1} has its minimum at $\phi = f_\pi$, it is strictly speaking not correct to use the parameters Eqs. (123)–(125) in the one-loop effective potential. The reason is that the sigma and pion masses receive radiative corrections, which must be taken into account in the equations that relate the physical masses and the parameters of the theory. In other words, Eqs. (123)–(125) receive corrections. The sigma mass is often defined by the curvature or the second derivative of the effective potential. At tree-level, this is given by

Eq. (115), but the expression for m_σ changes if we take the one-loop correction to the effective potential into account. To illustrate the dramatic difference, we have calculated the two. Using parameters such that the sigma mass at tree level is 750 MeV and the pion mass is 140 MeV, the curvature of the one-loop effective potential with $\Lambda = 182$ MeV, corresponds to a sigma mass of 530 MeV. Even if one takes radiative corrections into account and determine the parameters at the one-loop level, this procedure is not entirely correct. Determining the sigma mass by the curvature of the effective potential corresponds to including its self-energy evaluated at zero external momentum, $p^2 = 0$. However, the physical mass of the sigma is given by the pole of the propagator, which involves the self-energy evaluated self-consistently at $p^2 = -m_\sigma^2$. The difference between the self-energy evaluated at these two points gives rise to a finite shift of the sigma mass that is normally not taken into account. A similar remark applies to the pion mass at the physical point.

We next present some numerical results based on the effective potential (122). At the physical point, we use a pion mass of $m_\pi = 140$ MeV, a sigma mass of $m_\sigma = 800$ MeV, a constituent quark mass of $m_q = 300$ MeV, and a pion decay constant of $f_\pi = 93$ MeV. This yields the parameters $m^2 = -290600$ MeV², $\lambda = 215.29$, and $g = 3.2258$. In the chiral limit, we instead use $m_\pi = 0$, which yields $m^2 = -320000$ MeV², $\lambda = 222$, and $g = 3.2258$. We use these parameter values to generate the results presented in Figs. 8–11.

In Fig. 8, we show the renormalized effective potential at $T = 0$ normalized to f_π^4 as a function of ϕ for different values of the magnetic field. The minimum is moving to the right as the magnetic field increases and so the model exhibit magnetic catalysis as expected. Moreover, the effective potential is unstable for large values of

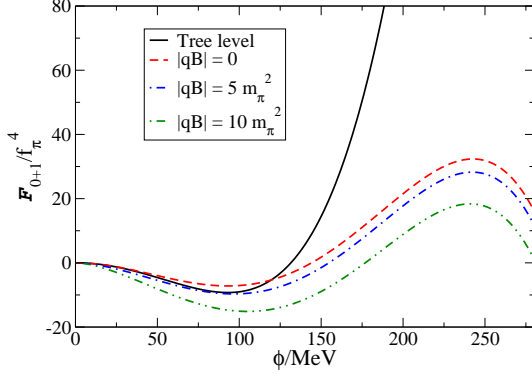


FIG. 8 Normalized effective potential $\mathcal{F}_{0+1}/f_\pi^4$ in the chiral limit for $T = 0$. Tree level (solid curve), one-loop with $|qB| = 0$ (dashed curve), one loop with $|qB| = 5m_\pi^2$ (dotted curve), and one loop with $|qB| = 10m_\pi^2$ (dash-dotted curve).

the field ϕ . This instability is present already for $B = 0$ and is due to a term $\sim m_q^4 \ln \frac{\Lambda^2}{m_q^2}$, which dominates the effective potential at large ϕ and goes negative for $m_q = g\phi \geq \Lambda$.⁶ The one-loop bosonic term is also of the form $m^4 \ln \frac{\Lambda^2}{m^2}$ with the opposite sign and may stabilize the effective potential if the prefactor is sufficiently large. However, perturbative calculations typically break down for large value of the field. In fact, a renormalization group improvement is necessary to make large values of ϕ accessible by removing large logarithms. These issues have been discussed in detail in e.g. Einhorn and Jones (2007); Ford *et al.* (1993); and Sher (1989).

In Fig. 9, we show the transition temperature for the QM model as a function of $|qB|/m_\pi^2$ in the chiral limit (black) and at the physical point (red). Both are growing functions of the magnetic field, which shows that the QM model exhibits magnetic catalysis.

In Fig. 10, we show the normalized effective potential for four different temperatures and $|qB| = 5m_\pi^2$ and with vacuum fluctuations (blue line: $T = 0$, pink line $T = 140$ MeV, orange line: $T = T_c = 177.9$ MeV, and green line: $T = 185$ MeV). The curves clearly show that the phase transition is of second order.

In Fig. 11, we show the normalized effective potential for four different temperatures,

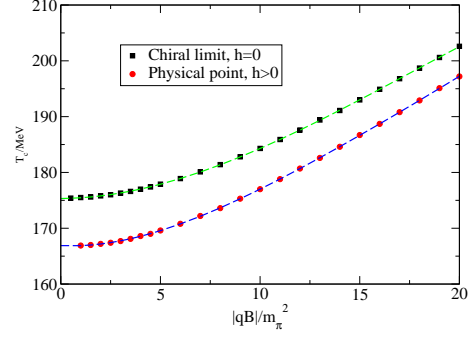


FIG. 9 The critical temperature for the chiral transition as a function of $|qB|/m_\pi^2$. Black points are the chiral limit and red points are the physical point.

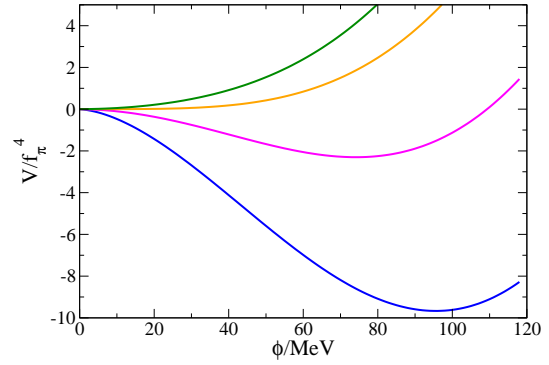


FIG. 10 The effective potential normalized by f_π^4 for four different temperatures and $|qB| = 5m_\pi^2$, where we have included the vacuum fluctuations.

$|qB| = 5m_\pi^2$ and no vacuum fluctuations (blue line: $T = 0$, pink line $T = 120$ MeV, orange line: $T = T_c = 158.0$ MeV, and green line: $T = 176$ MeV). The curves clearly show that the phase transition is of first order. Moreover, we notice that including the vacuum fluctuations gives a significantly higher critical temperature T_c .

We have now seen numerically that the phase transition is first order if the fermionic vacuum fluctuations are neglected and second order if they are included. It turns out that the role of vacuum fluctuations in the quark-meson model is the same also in the absence of a magnetic field. This case was carefully analyzed by Skokov *et al.* (2010) in the case of the chiral transition in the QM model with $B = 0$. Recently, the analysis was generalized to finite B field by Ruggieri *et al.* (2013).

One would like to get some analytic understanding of this result. The basic idea is to con-

⁶ This is the leading term in the large- x expansion (C5).

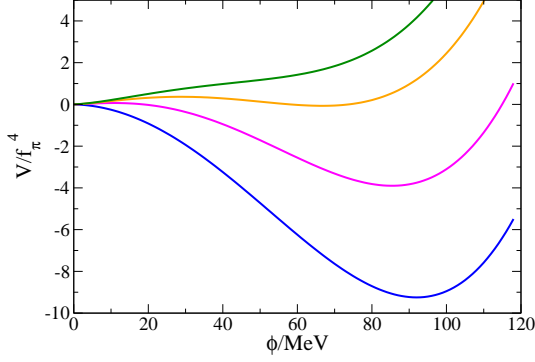


FIG. 11 The effective potential normalized by f_π^4 for four different temperatures and $|qB| = 5m_\pi^2$, where we have omitted the vacuum fluctuations.

struct a Ginzburg-Landau effective potential of the form

$$V_{\text{GL}} = \frac{1}{2}\alpha_2 m_q^2 + \frac{1}{4}\alpha_4 m_q^4, \quad (128)$$

where $m_q = g\phi$, and α_2 and α_4 are parameters that depend on the temperature T , the parameters of the Lagrangian, and the magnetic field B . A temperature T_c^* is defined by a vanishing coefficient α_2 , i.e. $\alpha_2(T_c^*) = 0$. If $\alpha_4(T_c^*) > 0$, then the transition is second order and the critical temperature is $T_c = T_c^*$. If $\alpha_4(T_c^*) < 0$, the effective potential has two minima for T slightly larger than T_c^* . The transition is first order and the critical temperature is $T_c > T_c^*$.

In the plots shown below, the authors used parameters that correspond to $f_\pi = 92.4$ MeV, $m_q = 335$ MeV, $m_\pi = 0$, and $m_\sigma = 700$ MeV. We first consider the renormalized case, i.e. the case where one adds counterterms for the mass and coupling and imposes some appropriate renormalization conditions. In Fig. 12, the normalized coefficient α_2/f_π^2 is shown as a function of T for different values of the magnetic field B . We see that α_2 is an increasing function of T and T_c^* is an increasing function of $|qB|$.

In Fig. 13, the dimensionless coefficient α_4 is shown as a function of T for different values of the magnetic field B . The coefficient is positive for all values of T implying that the transition is second order.

We next consider the unrenormalized case, i.e. the case where one regularizes the divergences by a sharp ultraviolet cutoff $\Lambda = 550$ MeV. In Fig. 14, the coefficient α_4 is shown as a function

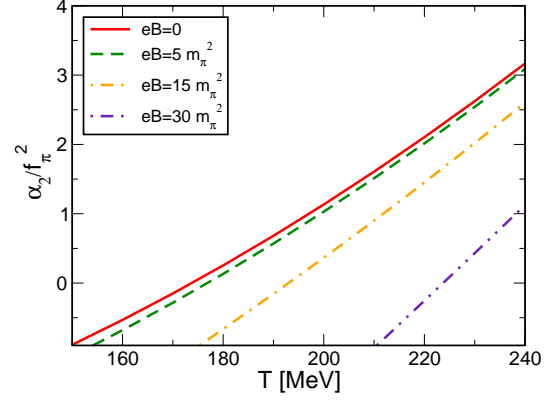


FIG. 12 Coefficient α_2 normalized by f_π^2 as a function of temperature T for different values of the magnetic field. Figure taken from Ruggieri *et al.* (2013).

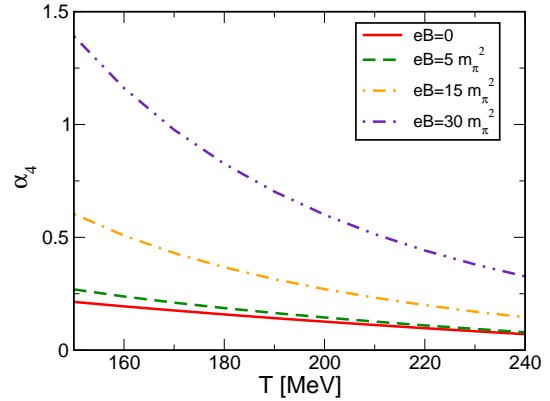


FIG. 13 Coefficient α_4 as a function of temperature T for different values of the magnetic field. Figure taken from Ruggieri *et al.* (2013).

of B evaluated at T_c^* . The coefficient is negative for $|qB| > |qB_c| \approx 47 m_\pi^2$ and so the transition is first order for large magnetic fields. The position of B_c obviously depends on Λ and for $\Lambda \rightarrow \infty$, one recovers the results in the renormalized case. On the other hand, if the cutoff Λ is below a critical value Λ_c , the transition is first order for all values of B . The sensitivity to the value of the sharp cutoff suggests that one should be careful and in particular not choose a cutoff below the scale set by the particles in the theory.

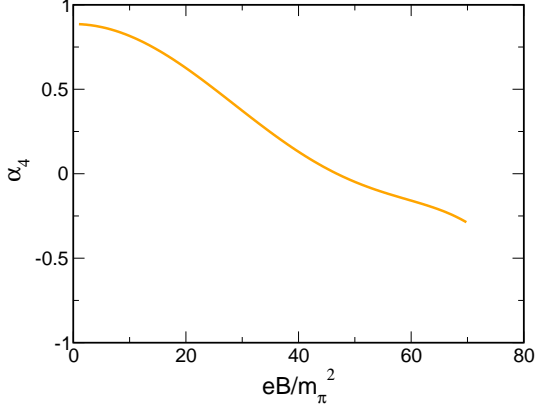


FIG. 14 Coefficient α_4 as a function of magnetic field B at T_c^* . Figure taken from Ruggieri *et al.* (2013).

E. Hadron resonance gas model

In this subsection, we briefly discuss the hadron resonance gas (HRG) model in a magnetic background. This model was studied in detail by Endrődi (2013). It can be used to access the low-temperature phase of QCD, even at nonzero chemical potential. The partition function is given by a sum of partition functions of noninteracting hadrons and resonances. This approach gives a surprisingly good description of the thermodynamics of QCD in the confined phase, up to temperatures just below the transition region (Borsanyi *et al.*, 2010;

Huovinen and Petreczky, 2010; Karsch *et al.*, 2003).

We can schematically write the free energy density as

$$\mathcal{F} = \sum_h d_h \mathcal{F}_h(B, T, m_h, q_h, s_h, g_h), \quad (129)$$

where d_h , m_h , q_h , s_h , and g_h are the multiplicity, mass, electric charge, spin, and gyromagnetic ratio of hadron h , respectively. For simplicity, the gyromagnetic ratio in the paper by Endrődi (2013) was set to $g_h = 2q_h/e$. The hadrons taken into account in the sum are $\pi^\pm, \pi^0, \dots, \Sigma^0$.

Since the free energy density is a sum of the free energy densities of noninteracting mesons and baryons, Eq. (129) is given by a sum of the one-loop terms Eqs. (B8) and (B10). Renormalization can be performed using minimal subtraction as discussed previously. However, the author used Schwinger's renormalization scheme which involves an extra logarithmic term. For example, the wavefunction counterterm is ⁷

$$Z^2 = \left[1 - \frac{q^2}{3(4\pi)^2 \epsilon} - \frac{q^2}{3(4\pi)^2} \ln \frac{m^2}{\Lambda^2} \right]. \quad (130)$$

Defining the renormalized magnetic field B_r via $B_r^2 = B^2 Z^2$ and subtracting the free energy density at $B = 0$, the one-loop free energy density from a boson is

$$\mathcal{F}_{0+1} = \frac{1}{2} B_r^2 + \frac{4(qB)^2}{(4\pi)^2} \left[\zeta^{(1,0)}(-1, \frac{1}{2} + x) + \frac{1}{4} x^2 - \frac{1}{2} x^2 \ln x + \frac{1}{24} (\ln x + 1) \right]. \quad (131)$$

This in turn implies that the renormalized free energy density approaches zero in the limit $m_h \rightarrow \infty$ instead of growing logarithmically. However, the prescription cannot be used in the massless limit due to infrared divergences coming from this extra term. Furthermore, the order- B^2 term is given by the first term in Eq. (130) as the leading term in the bracket starts at $\mathcal{O}(B^4)$. Figs. 15 and 16 show the individual

contributions to the HRG pressure as a function of the temperature T for zero magnetic field and for $|qB| = 0.2 \text{ GeV}^2$, respectively. We first note that the contribution from the neutral particles is independent of B as the gyromagnetic ratio was set to zero. The relative contribution of the charged particles is changing with B . The reason is that the effective mass is essentially $m_{\text{eff}} = \sqrt{m_h^2 + |q_h B|(1 - 2s)}$, and this increases for e.g. m_{π^\pm} ($s = 0$) and decreases for e.g. ρ^\pm ($s = 1$) and so the Boltzmann weight changes

⁷ There is an extra factor of $\ln \frac{4\pi}{e^2 E}$ since the MS-scheme is used.

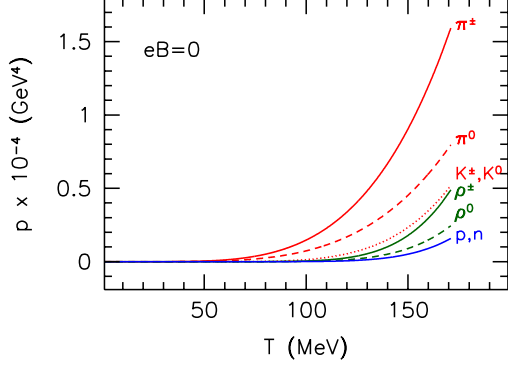


FIG. 15 Individual contributions to the HRG pressure as function of the temperature T for $B = 0$. Figure taken from Endrődi (2013).

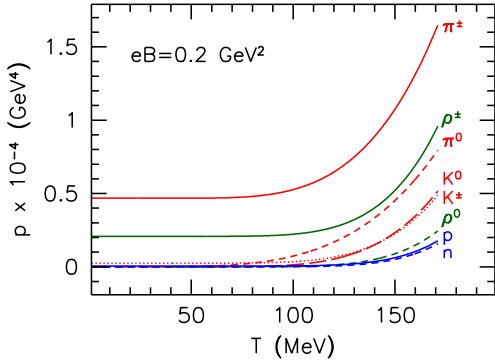


FIG. 16 Individual contributions to the HRG pressure as function of the temperature T for $|qB| = 0.2 \text{ GeV}^2$. Figure taken from Endrődi (2013).

with B . This is clearly seen in Figs. 15 and 16.

Moreover, the pressure is an increasing function of the magnetic field for fixed temperature T . This implies that the magnetization is positive and hence that the hadronic phase is paramagnetic. We will discuss this further in Sec. XI. The speed of sound c_s (not shown) displays a peak, which moves to lower temperatures as the magnetic fields grows. The position of the peak on the T -axis is a possible definition of the transition temperature and so the results suggest that T_c decreases with B . However, the HRG model is valid only at low temperatures and not too large magnetic fields ⁸ (Endrődi, 2013) so

⁸ Clearly, $m_{\text{eff}}^2 < 0$ for the ρ meson when $|qB| > m_\rho^2$.

one must be cautious.

VI. POLYAKOV-LOOP EXTENDED MODELS

As mentioned earlier, the NJL model is not confining. Likewise, the QM model is an effective theory that consists of deconfined quarks as well as mesons as effective degrees of freedom (Bowman and Kapusta, 2009). This is probably a good description at temperatures around the transition temperature, but for very low temperatures it is certainly not. At low temperatures, the thermodynamics is dominated by the light pions. While these models incorporate chiral symmetry breaking, they are not confining. This is a serious shortcoming as an effective low-energy description of QCD. Below, we shall see that we can mimic - in a statistical sense - the effects of confinement by coupling the chiral models to a nontrivial $SU(3)$ background gauge field A_μ (Fukushima, 2004). One can express this background gauge field in terms of the complex-valued Polyakov loop variable Φ and so the effective potential becomes a function of the expectation value of the chiral condensate as well as the expectation value of the Polyakov loop. Finally, one adds the contribution to the free energy density from the gluons via a Polyakov loop potential.

A. Coupling to the Polyakov loop

In pure gauge theory, the Polyakov loop Φ is an order parameter for deconfinement (Yaffe and Svetitsky, 1982a,b). For QCD with dynamical quarks, it is an approximate order parameter, just like the chiral condensate. It is defined as the trace of the thermal Wilson line, where the thermal Wilson L line is given by

$$L(\mathbf{x}) = \mathcal{P} \exp \left[i \int_0^\beta d\tau A_4(\mathbf{x}, \tau) \right], \quad (132)$$

where $A_4 = iA_0$ and $A_0 = t_a A_0^a$. Here A_μ^a are the $SU(3)_c$ gauge fields and the generators $t^a = \frac{1}{2}\lambda^a$, where λ^a are the Gell-Mann matrices. \mathcal{P} denotes path ordering. The Polyakov Φ and its complex

conjugate are then given by

$$\Phi = \frac{1}{N_c} \text{Tr} L, \quad (133)$$

$$\bar{\Phi} = \frac{1}{N_c} \text{Tr} L^\dagger. \quad (134)$$

The Polykov loop transforms nontrivially under the center group Z_{N_c} of the gauge group $SU(N_c)$, $\Phi \rightarrow e^{2\pi i n/N_c} \Phi$, where $n = 0, 1, 2, \dots, N_c - 1$. Its behavior in the pure gauge theory is

$$\langle \Phi \rangle \sim 0, \text{ confinement at low } T, \quad (135)$$

$$\langle \Phi \rangle \sim 1, \text{ deconfinement at high } T, \quad (136)$$

and so the center symmetry Z_{N_c} is broken in the high-temperature phase.

A constant nonabelian background is now introduced via the covariant derivative which takes the form

$$D_\mu = \partial_\mu - iq_f A_\mu^{\text{EM}} - iA_\mu, \quad (137)$$

where $A_\mu^{\text{EM}} = (0, 0, Bx, 0)$ and $A_\mu = \delta_{\mu 0} A_0$. In the Polyakov gauge, we can write the back-

ground gauge field $A_4 = iA_0$ as

$$A_4 = t_3 A_4^{(3)} + t_8 A_4^{(8)}, \quad (138)$$

For constant gauge fields, the thermal Wilson line can be written as

$$L = \begin{pmatrix} e^{i(\phi_1 + \phi_2)} & 0 & 0 \\ 0 & e^{i(-\phi_1 + \phi_2)} & 0 \\ 0 & 0 & e^{-2i\phi_2} \end{pmatrix}, \quad (139)$$

where $\phi_1 = \frac{1}{2}\beta A_4^{(3)}$ and $\phi_2 = \frac{1}{2\sqrt{3}}\beta A_4^{(8)}$. In the perturbative vacuum $\phi_1 = \phi_2 = 0$ and in the confining vacuum $\phi_1 = \phi_2 = \frac{\pi}{3}$. We can use $\phi_1 = \phi_2$ and the Polyakov loop variable itself reduces to

$$\Phi = \frac{1}{3} [1 + 2 \cos(\phi_1)]. \quad (140)$$

Note that the Polyakov loop is real for μ_B and therefore $\Phi = \bar{\Phi}$. In the expressions below, we will however, keep Φ and $\bar{\Phi}$ so the expressions below agree with those in the literature.

The zeroth component of the gauge field acts as a chemical potential in the covariant derivative (137). With this observation and the definition Eq. (132), we can immediately make the following replacement for a fermion in the background field:

$$\ln [1 + e^{-\beta E_q}] \rightarrow \frac{1}{2N_c} \text{Tr} \ln [1 + L e^{-\beta E_q}] + \frac{1}{2N_c} \text{Tr} \ln [1 + L^\dagger e^{-\beta E_q}], \quad (141)$$

where the trace on the right-hand side is in color space and E_q is the energy of the fermionic excitations. Performing the trace of the first term in Eq. (141) using Eq. (139), one obtains

$$\frac{1}{N_c} \text{Tr} \ln [1 + L e^{-\beta E_q}] = \frac{1}{3} \ln [1 + 3 (\Phi + \bar{\Phi} e^{-\beta E_q}) e^{-\beta E_q} + e^{-3\beta E_q}],$$

and where the second term in Eq. (141) can be obtained by Hermitean conjugation. The temperature-dependent part of the one-loop fermionic contribution to the free energy density can then be written as

$$\begin{aligned} \mathcal{F}_1^T = -T \sum_f \frac{|q_f B|}{\pi} \sum_{s=\pm 1} \sum_{k=0}^{\infty} \int_0^{\infty} \left\{ \ln [1 + 3 (\Phi + \bar{\Phi} e^{-\beta E_q}) e^{-\beta E_q} + e^{-3\beta E_q}] \right. \\ \left. + \ln [1 + 3 (\bar{\Phi} + \Phi e^{-\beta E_q}) e^{-\beta E_q} + e^{-3\beta E_q}] \right\}. \end{aligned} \quad (142)$$

It reduces to the second term in Eq. (35) in the limit $\Phi, \bar{\Phi} \rightarrow 1$, with an extra factor of $N_c = 3$, as it should. We note in passing that the vacuum part of the one-loop fermionic free energy density is unchanged and therefore the PNJL model reduces to the NJL model at $T = 0$.

Taking the trace in color space, the Fermi-Dirac distribution is generalized to

$$n_F(\beta E) = \frac{1 + 2\bar{\Phi}e^{\beta E_q} + \Phi e^{2\beta E_q}}{1 + 3\bar{\Phi}e^{\beta E_q} + 3\Phi e^{2\beta E_q} + e^{3\beta E_q}}. \quad (143)$$

It is instructive to look at the behavior of Eq. (143) at very low and at very high temperatures. At low temperatures, we have $\Phi \approx 0$ and therefore the Fermi-Dirac distribution reduces to

$$n_F(\beta E_q) \approx \frac{1}{e^{3\beta E_q} + 1}, \quad (144)$$

which is the distribution function of a fermion with energy $3E_q$. Thus the contribution from the fermions to the effective potential is suppressed at low temperature as compared to the corresponding chiral model without the Polyakov loop. This is referred to as statistical confinement. In the same manner, we see that Eq. (143) at high temperature behaves as

$$n_F(\beta E_q) \approx \frac{1}{e^{\beta E_q} + 1}, \quad (145)$$

where we have used that $\Phi \approx 1$. This is distribution function of a fermion with energy E_q , i.e. that of deconfined quarks. A word of caution here is appropriate. The same behavior as Eq. (144) is found in two-color

QCD with quarks in the adjoint representation (Zhang *et al.*, 2010) and so the number x in $x\beta E_q$ does not necessarily give the correct number of quarks to form a color singlet.

We have now coupled the Polyakov loop variable to the matter sector of theory. However, we must also include the contribution to the free energy density from the gauge sector and this is done by adding a phenomenological Polyakov loop potential $U(\Phi, \bar{\Phi})$. This potential is required to reproduce the pressure for pure-gluon QCD as calculated on the lattice for the temperatures around the transition temperature.

A number of forms for the Polyakov loop potentials have been proposed and investigated at the mean-field level for the PNJL model (Lourenco *et al.*, 2011) and the PQM model with $\mu_B = 0$ (Schaefer *et al.*, 2010). In the following we will review three different Polyakov loop potentials. Since the Polyakov loop variable is the order parameter for the Z_3 center symmetry of pure-gluon QCD, a Ginzburg-Landau type potential should incorporate this. A polynomial expansion then leads to (Ratti *et al.*, 2006)

$$\frac{U_{\text{poly}}}{T^4} = -\frac{1}{2}b_2(T)\Phi\bar{\Phi} - \frac{1}{6}b_3(\Phi^3 + \bar{\Phi}^3) + \frac{1}{4}b_4(\Phi\bar{\Phi})^2, \quad (146)$$

where the coefficients are

$$b_2(T) = 6.75 - 1.95\left(\frac{T_0}{T}\right) + 2.624\left(\frac{T_0}{T}\right)^2 - 7.44\left(\frac{T_0}{T}\right)^3, \quad (147)$$

$$b_3 = 0.75, \quad (148)$$

$$b_4 = 7.5. \quad (149)$$

The parameter T_0 is the transition temperature for pure-gluon QCD lattice calculations, $T_0 = 270$ MeV (Karsch *et al.*, 2001). Ratti *et al.* (2007a,b) proposed another form of the Polyakov loop potential based on the $SU(3)$ Haar measure:

$$\frac{U_{\text{log}}}{T^4} = -\frac{1}{2}a(T)\Phi\bar{\Phi} + b(T)\ln\left[1 - 6\Phi\bar{\Phi} + 4(\Phi^3 + \bar{\Phi}^3) - 3(\Phi\bar{\Phi})^2\right], \quad (150)$$

where the coefficients are

$$a(T) = 3.51 - 2.47 \left(\frac{T_0}{T} \right) + 15.2 \left(\frac{T_0}{T} \right)^2, \quad (151)$$

$$b(T) = -1.75 \left(\frac{T_0}{T} \right)^3. \quad (152)$$

We note that the logarithmic term ensures that the magnitude of Φ and $\bar{\Phi}$ are constrained to be in the region between -1 and 1 , i.e. the possible attainable values for the normalized trace of an element of $SU(3)$. The coefficient $a(T)$ approaches $16 \frac{\pi^2}{90} \approx 3.51$ as $T \rightarrow \infty$ such that the potential Eq. (150) reproduces the Stefan-Boltzmann limit. Finally, Fukushima (2008) proposed the following Polyakov loop potential

$$\frac{U_{\text{Fuku}}}{T^4} = -\frac{b}{T^3} \left(54e^{-aT_0/T} \Phi \bar{\Phi} + \ln \left[1 - 6\Phi \bar{\Phi} + 4(\Phi^3 + \bar{\Phi}^3) - 3(\Phi \bar{\Phi})^2 \right] \right), \quad (153)$$

where the constants are $a = 664/270$ and $b = (196.2 \text{ MeV})^3$. This potential differs from the logarithmic potential (150) only by the coefficient of the first term.

A problem with all the Polyakov loop potentials proposed is that they are independent of the number of flavors and of the baryon chemical potential. However, we know that, for example, the transition temperature for the deconfinement transition is a function of N_f . In other words, one ought to incorporate the back-reaction from the fermions to the gluonic sector. Schaefer *et al.* (2007) use perturbative arguments to estimate the effects of the number of flavors and the baryon chemical potential on the transition temperature T_0 . The functional form of T_0 is (Herbst *et al.*, 2011) for $\mu_B = 0$ is

$$T_0 = T_\tau e^{-1/(\alpha_0 b(N_f))}, \quad (154)$$

where

$$b(N_f) = \frac{1}{6\pi} (11N_c - 2N_f), \quad (155)$$

and the parameters are $T_\tau = 1.77 \text{ GeV}$ and $\alpha_0 = 0.304$. This yields a transition temperature of 240 MeV and 208 MeV for $N_f = 1$ and $N_f = 2$, respectively. Another way of including the back-reaction from the fermions has been implemented by Haas *et al.* (2013) and Herbst *et al.* (2014). They calculate the glue potential as a function of a background gauge field with and without dynamical fermions using the

functional renormalization group. They compare the two potentials and found a mapping between them and this mapping is used to modify the Polyakov loop potential discussed above.

The phase structure of the Polyakov-loop extended model is then found by solving simultaneously the gap equations

$$\frac{\partial \mathcal{F}}{\partial M_0} = 0, \quad \frac{\partial \mathcal{F}}{\partial \Phi} = 0, \quad (\text{PNJL}), \quad (156)$$

$$\frac{\partial \mathcal{F}}{\partial \phi} = 0, \quad \frac{\partial \mathcal{F}}{\partial \Phi} = 0, \quad (\text{PQM}). \quad (157)$$

where \mathcal{F} is the sum of the free energy density from the fermions and the Polyakov loop potential U .

Gatto and Ruggieri (2010) considered the PNJL model using the logarithmic potential Eq. (150). They used $G_1 = G_2$ and added an eight-quark interaction term of the form

$$\delta \mathcal{L} = G_8 \left[(\bar{\psi}\psi)^2 + (\bar{\psi}i\gamma_5 \boldsymbol{\tau} \psi)^2 \right]^2, \quad (158)$$

where G_8 is a coupling constant. In this case, the constituent quark mass reads $M_0 = m_0 - 2G_0 \langle \bar{\psi}\psi \rangle - 4G_8 \langle \bar{\psi}\psi \rangle^3$. They also used a form factor of the form

$$F(p) = \frac{\Lambda^{2N}}{\Lambda^{2N} + (p_z^2 + 2|q_f B|k)^N}, \quad (159)$$

choosing the value $N = 5$.

Fig. 17 shows the phase diagram in the B - T plane for the chiral (dot-dashed) as well as

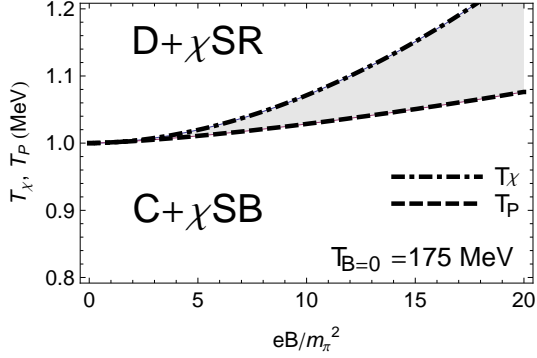


FIG. 17 Phase diagram in the B - T plane. Figure taken from Gatto and Ruggieri (2010).

the deconfinement transition (dashed). The critical temperatures T_χ and T_P have been normalized to the common pseudocritical temperature $T_0 = 175$ MeV at $B = 0$. We note that the transition temperature T_χ is increasing more with the magnetic field than T_P is. The shaded area corresponds to a phase where the quarks are deconfined but where chiral symmetry is still broken.

The PNJL model has been extended by several authors by using a non-local NJL vertex (Hell *et al.*, 2009; Kondo, 2010; Sasaki *et al.*, 2007). In the paper by Kondo (2010), he derives from QCD a non-local vertex that depends explicitly on T as well as the phase of the Polyakov loop. Such a model is called the entangled Polyakov loop model (EPNJL), which was used by Gatto and Ruggieri (2011) at finite B to study the chiral and deconfinement transitions. In contrast to the PNJL model, there is basically no splitting of the two transitions in the EPNJL model.

Another mean-field analysis was carried out by Mizher *et al.* (2010) using the PQM model focusing on the physical point. Renormalization is carried out by subtracting the divergent fluctuation determinant for $B = 0$. The authors make several interesting observations. If the fermionic vacuum fluctuations are neglected⁹, the transition temperature for the deconfinement transi-

tion coincides with that of the chiral transition, and they are both first order, except for very small values of the magnetic field, where they are crossovers. Moreover, the transition temperatures are decreasing with increasing B . If the vacuum fluctuations are included, the transition temperatures are increasing with B and the resulting phase diagram is qualitative the same as in Fig. 17. The chiral transition is now a crossover.

B. Two-color QCD

So far we have been discussing QCD with three colors. In this section, we consider two-color QCD. Two-color QCD is interesting for a number of reasons. In contrast to three-color QCD, one can perform lattice simulations at finite baryon chemical potential μ_B . This is a consequence of the special properties of the gauge group $SU(2)_c$ which leads to a real-valued Dirac determinant even for $\mu_B \neq 0$. Hence, the sign problem is absent in this case and one can use importance sampling techniques as usual. Moreover, the order of the deconfinement transition for pure-gluon QCD is different in $SU(2)_c$ and $SU(3)_c$. For $N_c = 2$ it is second order, while for $N_c = 3$ it is first order. In two-color QCD, the critical exponents are expected to be those of the two-state Potts model, which follows from universality arguments.

In this section, we discuss two-color QCD in a strong magnetic field. While there is a number of model calculations in two-color QCD at finite temperature and baryon chemical potential, there is only a single calculations at finite B (Cruz and Andersen, 2013).

In the Polyakov gauge, the background non-abelian gauge field is diagonal in color space,

$$A_4 = \sigma_z \theta, \quad (160)$$

where θ is real. The thermal Wilson line can then be written as

$$L = \begin{pmatrix} e^{i\phi} & 0 \\ 0 & e^{-i\phi} \end{pmatrix}, \quad (161)$$

where $\phi = \beta\theta$. The Polyakov loop variable becomes

$$\Phi = \cos(\phi), \quad (162)$$

⁹ Note that there are still some B -dependent vacuum terms that have not been removed by the renormalization procedure.

In analogy with Eq. (143), the Fermi-Dirac distribution function becomes

$$n_F(\beta E_q) = \frac{1 + \Phi e^{-\beta E_q}}{1 + 2\Phi e^{-\beta E_q} + e^{-2\beta E_q}}. \quad (163)$$

At low temperature, $\Phi \approx 0$ and so Eq. (163) describes excitations with energy $2E_q$, i.e. that of a bound state.¹⁰ Again this is referred to as statistical confinement. At high temperature, $\Phi \approx 1$ and Eq. (163) describes excitations with energy E_q , i.e. deconfined quarks.

The Polyakov loop potential in the gauge sector used is (Brauner *et al.*, 2010)

$$\Omega_{\text{gauge}} = -bT \left[24\Phi^2 e^{-\beta a} + \ln(1 - \Phi^2) \right], \quad (164)$$

where a and b are constants. This form is motivated by the lattice strong coupling expansion (Fukushima, 2008). In the gauge theory without dynamical quarks, one can find an explicit expression for the Polyakov-loop variable $\Phi = \sqrt{1 - \frac{1}{24}e^{-\beta a}}$ as a function of T and so $a = T_c \ln 24$. Moreover, Φ goes to zero in a continuous manner and the theory exhibits a second-order transition.

A few remarks about the parameters in 2-color QCD are in order. For $N_c = 2$, there are no experimental results to guide us in the determination of the parameters. A common way of determining them is to use N_c scaling arguments (Brauner *et al.*, 2010). The pion decay constant scales as $\sqrt{N_c}$ and the pion mass scales as N_c . This yields the two parameters $f_\pi = 75.4$ MeV and $m_\pi = 93.3$ MeV.

In Fig. 18, we show the Polyakov loop as a function of T/m_π (with $m_\pi = 140$ MeV) found by minimizing the Polyakov loop potential (164) (dotted line). We also show the normalized quark condensate obtained in the NJL model (dashed-dotted line). The dashed and solid lines show the Polyakov loop and normalized quark condensate as functions of T/m_π in the PNJL model. From the figure, we see that the coupling between the two variables, forces the curve

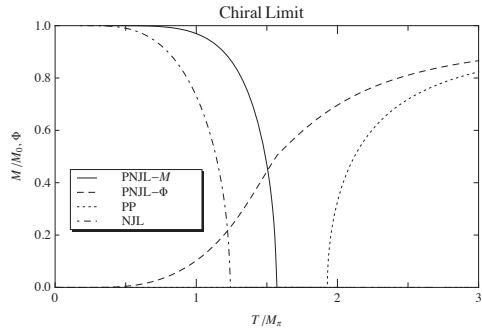


FIG. 18 Normalized constituent quark mass and Polyakov loop in the chiral limit as a function of T/m_π , where $m_\pi = 140$ MeV is the pion mass for $N_c = 3$. Figure taken from Cruz and Andersen (2013).

for the normalized quark condensate to the right and the curve for the Polyakov to the left so that the two transitions have a common transition temperature.

In Fig. 19, we show the transition temperatures for the chiral and deconfinement transitions as a function of $|qB|/m_\pi^2$ where $m_\pi = 140$ MeV is the physical pion mass for $N_c = 3$. The band shows the values of the order parameters $0.4 < M/M_0 < 0.6$ and $0.4 < \Phi < 0.6$, where M_0 is the chiral condensate at $T = 0$. For comparison we also show the chiral transition for NJL model. The transitions coincide for $B = 0$, cf. Fig. 18 but split at finite B . Note the similarity with the curves in Fig. 17 and that the deconfinement temperature is almost independent of temperature.

VII. FUNCTIONAL RENORMALIZATION GROUP

The functional renormalization group (FRG) (Wetterich, 1993) is a powerful nonperturbative method that has gained popularity since its formulation more than two decades ago. It is one way of implementing the renormalization group ideas of Wilson from the early 1970s. The average effective action, which is denoted by $\Gamma_k[\phi]$ is a function of a set of fields collective denoted by ϕ . The subscript k

¹⁰ For $N_c = 2$, two (anti)quarks can form a color singlet and belongs to the same multiplet as the usual three quark anti-quark bound states. These states are the "baryons" of two-color QCD.

$$\partial_k \Gamma_k = \frac{1}{2} \left(\text{solid circle} - \text{dashed circle} \right)$$

FIG. 20 Diagrammatic representation of the exact flow equation for the effective action $\Gamma_k[\phi]$. The lines denote the exact field-dependent propagators for bosons (solid) and fermions (dashed), while the circle denotes the insertion of the regulator function $R_k^B(p)$ or $R_k^F(p)$.

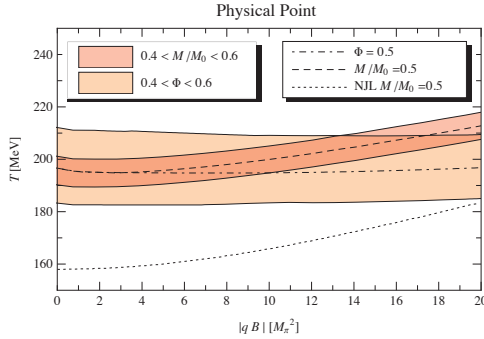


FIG. 19 Transition temperatures for the deconfinement and the chiral transition in the PNJL model as a function of $|qB|/m_\pi^2$ in 2-color QCD. Figure taken from Cruz and Andersen (2013).

indicates that the effective action is a function of a momentum scale.

This sliding scale acts as an infrared cutoff, such that all momenta q between k and the ultraviolet cutoff of the theory, Λ , have been integrated out. At $k = \Lambda$, no momenta have been integrated out and the effective action equals the bare action, $\Gamma_\Lambda[\phi] = S[\phi]$. Thus the value $S[\phi]$ is the boundary condition for the effective action. Moreover, when $k = 0$, all the quantum and thermal fluctuations have been integrated out and $\Gamma_0[\phi]$ is equal to the full quantum effective action. The average effective action satisfies a functional integro-differential equation, which reads

$$\partial_k \Gamma_k[\phi] = \frac{1}{2} \text{Tr} \left[\partial_k R_k^B(p) \left[\Gamma_k^{(2)} + R_k^B(p) \right]_{p,-p}^{-1} \right] - \text{Tr} \left[\partial_k R_k^F(p) \left[\Gamma_k^{(2)} + R_k^F(p) \right]_{p,-p}^{-1} \right], \quad (165)$$

where the superscript n means the n th functional derivative of $\Gamma_k[\phi]$. Moreover, the trace is over the variable p , which includes spacetime, field indices, and Dirac indices. The so-called regulator functions $R_k^B(p)$ and $R_k^F(p)$ are added to implement the renormalization group ideas mentioned above. These functions are large for $p < k$ and small for $p > k$ if $0 < k < \Lambda$. The regulator functions also satisfy $R_\Lambda^B(p) = R_\Lambda^F(p) = \infty$. These properties guarantee that the modes with $q < k$ are heavy and decouple and only the modes q between the sliding scale k and the ultraviolet cutoff Λ are light and integrated out. We will return to the choice of regulator functions below.

A. Local-potential approximation

Of course one cannot solve the flow equation exactly - then one would have solved the theory exactly - and so one needs to make approximations. A framework for systematic approximations is the derivative expansion. The leading-order approximation in the derivative expansion is called the local-potential approximation (LPA) since the full quantum effective action is approximated by the action

$$\Gamma[\phi] = \int_0^\beta d\tau \int d^3 \left\{ \frac{1}{2} (\partial_\mu \sigma)^2 + \frac{1}{2} (\partial_\mu \boldsymbol{\pi})^2 + U_k(|v|, |\Delta|) \right\}, \quad (166)$$

where $U_k(|v|, |\Delta|)$ is a k -dependent local potential and $v = \frac{1}{\sqrt{2}}(\sigma + i\gamma_5 \pi^0)$ and $\Delta = \frac{1}{\sqrt{2}}(\pi_1 + i\pi_2)$. Thus the potential depends on two $O(2)$ invariants in accordance with the discussion in Sec. V.D.

We are not including a pion condensate and therefore the local potential is evaluated at $|\Delta| = 0$. However, the flow equation still depends on the two partial derivatives $\frac{\partial U_k}{\partial |v|}$ and $\frac{\partial U_k}{\partial |\Delta|}$. In the mean-field approximation, these partial derivatives are identical, but beyond they generally are not. In order to make the flow equation numerically tractable, Andersen *et al.* (2014a) made the approximation that they are equal.

Using the chain rule, the matrix appearing in the first term in Eq. (165)

$$\left[\Gamma_k^{(2)} + R_k^B(p) \right]_{p,-p}^{-1} = \begin{pmatrix} p^2 + R_k^B(p) + U'_k + 2\rho U''_k & 0 & 0 & 0 \\ 0 & p^2 + R_k^B(p) + U'_k & 0 & 0 \\ 0 & 0 & \dots & 0 \\ 0 & 0 & 0 & \dots \end{pmatrix}, \quad (167)$$

where the indicates $p^2 + R_k^B(p) + U'_k$, $U'_k = \frac{\partial U_k}{\partial \rho}$ and $U''_k = \frac{\partial^2 U_k}{\partial \rho^2}$ with $\rho = \frac{1}{2}\phi^2$. We notice that the matrix Eq. (167) is simply the inverse tree-level propagator if we make the substitution $\mathcal{V}_0 \rightarrow U_k + R_k^B(p)$. The second term in Eq. (167) has the form of an inverse fermion tree-level propagator with a similar substitution. We will use a modification of the regulators (Litim, 2001; Stokic *et al.*, 2010)

$$R_k^B(p) = (k^2 - \mathbf{p}^2)\theta(k^2 - \mathbf{p}^2), \quad (168)$$

$$R_k^F(p) = \left(\sqrt{\frac{p_0^2 + k^2}{p_0^2 + \mathbf{p}^2}} - 1 \right) p\theta(k^2 - \mathbf{p}^2). \quad (169)$$

Knowing the spectrum in a constant magnetic field, we modify the regulators by making the replacements $\mathbf{p}^2 \rightarrow p_z^2 + (2n+1)|qB|$ and $\mathbf{p}^2 \rightarrow p_z^2 + (2n+1-s)|q_f B|$ above. Note that we here and in the remainder of this section denote the Landau levels by n so there is no confusion with the sliding scale k . The regulators Eq. (168)–(169) are very convenient in practical calculations since we can carry out the integral over the momentum p_z . The integro-differential flow equation reduces to a partial differential equation that is easier to solve numerically. Integrating over p_z and summing over Matsubara frequencies P_0 , the flow equation can be written as (Skokov, 2012)

$$\begin{aligned} \partial_k U_k = & \frac{k^4}{12\pi^2} \left[\frac{1}{\omega_{1,k}} (1 + 2n_B(\omega_{1,k})) + \frac{1}{\omega_{2,k}} (1 + 2n_B(\omega_{2,k})) \right] \\ & + \frac{|qB|}{2\pi^2} \sum_{n=0}^{\infty} \frac{k}{\omega_{1,k}} \sqrt{k^2 - p_{\perp}^2(q, n, 0)} \theta(k^2 - p_{\perp}^2(q, n, 0)) [1 + 2n_B(\omega_{1,k})] \\ & - \frac{N_c}{2\pi^2} \sum_{s,f,n=0}^{\infty} \frac{|q_f B|k}{\omega_{q,k}} \sqrt{k^2 - p_{\perp}^2(q_f, n, s)} \theta(k^2 - p_{\perp}^2(q_f, n, s)) [1 - 2n_F(\omega_{q_f,k})], \quad (170) \end{aligned}$$

where we have defined $\omega_{1,k} = \sqrt{k^2 + U'}$, $\omega_{2,k} = \sqrt{k^2 + U' + 2\rho U''}$, $\omega_{q,k} = \sqrt{k^2 + 2g^2\rho}$, $p_{\perp}^2(q, n, s) = (2n+1-s)|qB|$.

In the limit $B \rightarrow 0$, the sum over Landau levels becomes an integral via defining the variable $p_{\perp}^2 = 2|qB|m$ which yields $p_{\perp} dp_{\perp} = |qB|dm$. Replacing the sum by an integral one finds the flow equation first derived by Stokic *et al.* (2010)

$$\begin{aligned} \partial_k U_k = & \frac{k^4}{12\pi^2} \left[\frac{1}{\omega_{1,k}} (1 + 2n_B(\omega_{1,k})) + \frac{1}{\omega_{2,k}} (1 + 2n_B(\omega_{2,k})) \right] + \frac{k}{2\omega_{1,k}\pi^2} \int_0^{\infty} dp_{\perp} p_{\perp} \sqrt{k^2 - p_{\perp}^2} \\ & \times \theta(k^2 - p_{\perp}^2) [1 + 2n_B(\omega_{1,k})] - \frac{N_c N_f k}{\omega_{q,k}\pi^2} \int_0^{\infty} dp_{\perp} p_{\perp} \sqrt{k^2 - p_{\perp}^2} \theta(k^2 - p_{\perp}^2) [1 - 2n_F(\omega_k)] \end{aligned}$$

$$\begin{aligned}
&= \frac{k^4}{12\pi^2} \left\{ \frac{3}{\omega_{1,k}} [1 + 2n_B(\omega_{1,k})] + \frac{1}{\omega_{2,k}} [1 + 2n_B(\omega_{2,k})] \right\} \\
&\quad - \frac{N_c N_f k^4}{3\pi^2} \left\{ \left[\frac{1}{\omega_{q,k}} (1 - 2n_F(\omega_{q,k})) \right] \right\} .
\end{aligned} \tag{171}$$

Sometimes, one defines a so-called extended mean-field equation by omitting the bosonic terms on the right-hand side of the flow equation. Then the terms that depend on the derivatives of U_k on the right-hand side drop out and one can formally integrate the flow equation to obtain the effective potential (Kamikado *et al.*, 2012). For $T = 0$, this can be done analytically even for nonzero magnetic field B .

The k -dependent minimum $f_{\pi,k}$ is found by solving

$$\left. \frac{\partial U_k}{\partial \phi} \right|_{\phi=f_{\pi,k}} = h , \tag{172}$$

i.e. by minimizing the modified effective potential $\tilde{U}_k = U_k - h\phi$. The k -dependent masses $m_{\pi,k}^2$ and $m_{\sigma,k}^2$ can be expressed in terms of the second derivatives of the k -dependent (modified) effective potential at the k -dependent minimum $f_{\pi,k}$ as follows

$$m_{\pi,k}^2 = \left. \frac{\partial \tilde{U}_k}{\partial \rho} \right|_{\phi=f_{\pi,k}} , \tag{173}$$

$$m_{\sigma,k}^2 = m_{\pi}^2 + \rho \left. \frac{\partial^2 \tilde{U}_k}{\partial \rho^2} \right|_{\phi=f_{\pi,k}} . \tag{174}$$

Combining Eqs. (172) and (173), we find $f_{\pi,k} m_{\pi,k}^2 = h$. For $k = h = 0$, this is Goldstone's theorem.

The boundary condition for the effective potential at $k = \Lambda$ is chosen to have the form

$$U_{\Lambda} = \frac{1}{2} m_{\Lambda} \phi^2 + \frac{\lambda_{\Lambda}}{24} \phi^4 . \tag{175}$$

The bare parameters m_{Λ}^2 and λ_{Λ} are tuned such that one obtains the correct pion mass and pion decay constant in the vacuum at $k = 0$. In the calculation we use an ultraviolet cutoff $\Lambda = 800$ MeV, although the results are not too sensitive to the exact value. We ignore the running of the Yukawa coupling and set $g = g_k = 3.2258$ for all values of k . This gives a constituent

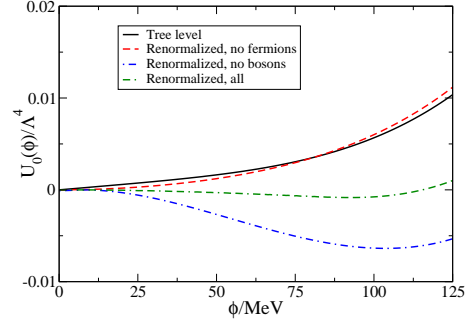


FIG. 21 Tree-level potential and renormalized potential $U_0(\phi)$ in different approximations.

quark mass of $m_q = g\phi_0 = gf_{\pi} = 300$ MeV. Further details of the numerical implementation can be found in Andersen *et al.* (2014a) and Andersen and Tranberg (2012).

In Fig. 21, we show the effective potential $U_0(\phi)$ normalized to Λ^4 in various approximations. The black curve is the tree-level potential i.e. the boundary condition $U_{\Lambda}(\phi)$ that gives the correct quantum effective potential given by the green curve. In order to investigate the effects of the different terms in the flow equation, we have solved it with the same boundary condition, but omitted the bosonic terms (blue curve) and omitted the fermionic terms (red curve). We see that the bosonic vacuum fluctuations have a tendency to decrease symmetry breaking in the vacuum while fermions vacuum fluctuations have a tendency to enhance symmetry breaking. Thus we have competition between the two terms in the flow equation and their relative importance depends on the momentum scale k .

In Fig. 22, we show the scale-dependent effective potential $U_k(\phi)$ for different values of $t = \ln \frac{\Lambda}{k}$. The black curve is the tree-level potential and the green line is the fully renormalized potential $U_0(\phi)$. It is interesting to note that the potential at intermediate stages, here shown as the red, blue, and orange curves, do not evolve

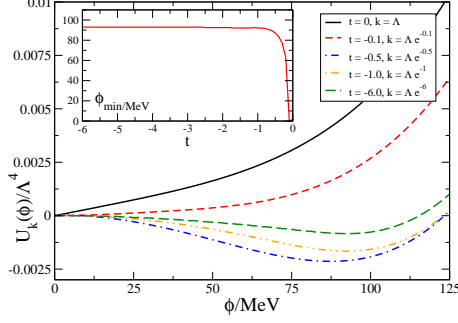


FIG. 22 Effective potential $U_k(\phi)$ for different values of $t = \ln \frac{\Lambda}{k}$. Inset: t -dependent minimum of $U_k(\phi)$. See main text for details.

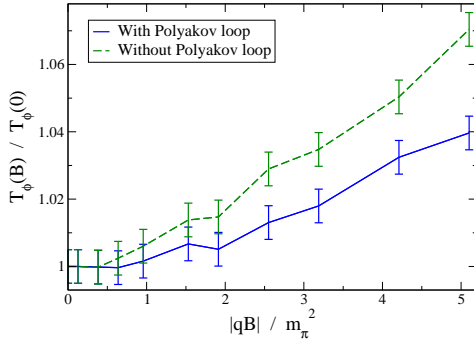


FIG. 23 Normalized critical temperature $T_\phi(B)/T_\phi(0)$ for the chiral transition as a function of the magnetic field B with and without the inclusion of the Polyakov loop.

monotonically. This shows that the bosonic and fermionic terms in the flow equation dominate in different regions of integration. The inset shows how the k -dependent minimum $f_{\pi,k}$ expressed in terms of dimensionless variable $t = \ln \frac{\Lambda}{k}$. We see that the minimum mainly gets renormalized for t between $t = 0$ and $t = -2$, whereafter it levels off.

In Fig. 23, we show the critical temperature as a function of the magnetic field B at the physical point. The dashed curve is the quark-meson model and solid curve is the Polyakov-loop extended quark-meson model. In agreement with various mean-field results, the critical temperature is an increasing function of B . It is interesting to note that the coupling to the Polyakov-loop variable Φ lowers T_c . This is an interesting observation, in particular since the Polyakov

loop has no influence on magnetic catalysis at zero temperature. This effect can be understood by calculating the free energy density in a given background ϕ_1 and comparing it with the free energy density in the deconfining background $\phi_1 = 0$ (Bruckmann *et al.*, 2013).¹¹ The difference between these two free energy densities is

$$\Delta\mathcal{F} = \frac{|q_f B|}{\pi^2} \int_0^\infty \frac{ds}{s^2} e^{-m^2 s} \coth(|q_f B|s) \left[\theta_3\left(\phi_1 + \frac{1}{2}\pi, e^{-\frac{1}{4sT^2}}\right) - \theta_3\left(\frac{1}{2}\pi, e^{-\frac{1}{4sT^2}}\right) \right], \quad (176)$$

where the elliptic theta function $\theta_3(u, q)$ is defined by

$$\theta_3(u, q) = 1 + 2 \sum_{n=1}^\infty q^{n^2} \cos(2nu). \quad (177)$$

The function $|q_f B| \coth(|q_f B|s)$ increases with s for all values of s . Thus a magnetic field favors deconfined Polyakov loops and therefore tends to lower the transition temperature. We also note that this effect decreases with larger quark masses m .

We are not aware of any mean-field calculations that directly compare the chiral transition temperature with and without the Polyakov loop.¹² However, based on the above argument as well as the renormalization group calculations, we expect to see the same behavior in the mean-field approximation.

B. Beyond the LPA

The results we have been discussing so far are obtained using the local-potential approximation. In a recent paper, Kamikado and Kanazawa (2014a) go beyond the LPA by including the wave-functional renormalization terms Z_\perp and Z_\parallel . In order to avoid the complication of having two invariants

¹¹ Recall $\Phi = \frac{1}{3}[1 + 2 \cos(\phi_1)] = 1$ for $\phi_1 = 0$.

¹² There are of course many mean-field calculations with and without the Polyakov loop, but a comparison between them requires that physical observables in the vacuum are the same.

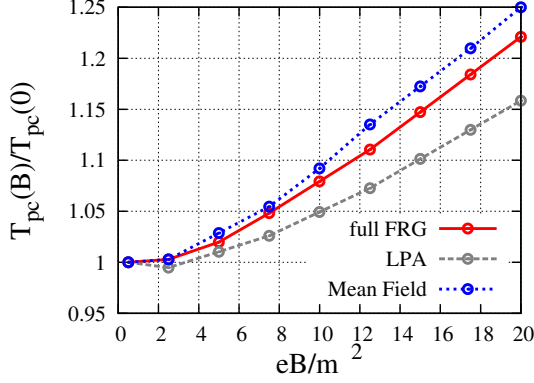


FIG. 24 The transition temperature for the chiral transition as a function of $|qB|$ for three different approximations normalized to the transition temperature at $B = 0$. Figure taken from Kamikado and Kanazawa (2014a).

ρ and Δ on which the effective potential U_k depends, they consider the case $N_f = 1$. In this case, the symmetry is $U(1)_V \times U(1)_A$ in the chiral limit or $U(1)_V$ at the physical point. Either way, the quark condensate gives rise to a single (pseudo)Goldstone boson. One expects the charged pions to decouple for sufficiently large magnetic fields since they become heavy and therefore the $N_f = 2$ model essentially reduces to the model they considered. Moreover, their calculations were at the physical point.

One of the interesting aspects of this work is the systematic study of the various approximations. For example, they studied the transition temperature in the mean-field approximation, using the LPA, and beyond the LPA. The transition temperature is determined by the peak of dM_q/dT , where M_q is the constituent quark mass. The result is shown in Fig. 24, where the blue, grey, and red lines show the normalized transition temperature in the three approximations. The inclusion of the mesonic fluctuations lowers the transition temperature compared to the mean-field approximation, while the inclusion of wavefunction renormalization effects increases the slope somewhat. It would be of interest to see the effects of including the Polyakov loop as well.

The constituent quark mass normalized to the constituent quark mass for $B = 0$ as a function of the temperature normalized to the

transition temperature $T_{pc,B=0}$ for $B = 0$ for the three different approximations is shown in Fig. 25. For all temperatures, we see that the constituent quark mass is an increasing function of the magnetic field, thus the system shows magnetic catalysis. This is the reason for the increase of the transition temperature as a function of B displayed in Fig. 24. We note that magnetic catalysis is less pronounced in the LPA as compared to the mean-field approximation and this can probably be attributed to the mesonic fluctuations that tend to counteract symmetry breaking (c.f. Fig. 21). The inclusion of the wavefunction renormalization terms increases magnetic catalysis as a function of B such that the transition temperature lies between the mean-field and the LPA curves. Again, it would be of interest to see the effects of adding the Polyakov loop variable.

We next consider the wavefunction renormalization terms Z_k^\parallel and Z_k^\perp . The regulator functions chosen are the anisotropic functions

$$R_k^B(p) = (k^2 - p_z^2) Z_\parallel \theta(k^2 - p_z^2) \quad (178)$$

$$R_k^F(p) = -\not{p}_z \left(\frac{k}{|p_z|} - 1 \right) \theta(k^2 - p_z^2), \quad (179)$$

where $\not{p}_z = \gamma^3 p_z$. The regulators clearly break rotational invariance also for $B = 0$. However, they give rise to a very simple scale-dependent fermion propagator and so it is very useful for practical calculations. The boundary condition for the wavefunction renormalization terms at $k = \Lambda$ and $B = 0$ is $Z_{k=\Lambda}^\parallel = Z_{k=\Lambda}^\perp = 1$. Due to the $O(4)$ symmetry at $B = 0$, we have $Z_{k=0}^\parallel = Z_{k=0}^\perp$. However, due to the above-mentioned breaking of rotational invariance, the authors instead fine-tuned the $Z_{k=\Lambda}^\parallel$ and $Z_{k=\Lambda}^\perp$, such that $Z_{k=0}^\parallel = Z_{k=0}^\perp$ at $T = 3$ MeV and $|qB| = 0.5m_\pi^2$. This gives the values $Z_{k=\Lambda}^\parallel = 0.002$ and $Z_{k=\Lambda}^\perp = 0.236$, respectively.

The wavefunction renormalization terms Z^\parallel and Z^\perp as functions of the normalized temperature for various strengths of the magnetic field is shown in Fig. 26. We first notice that while $Z_{k=0}^\parallel$ increases with the magnetic field, $Z_{k=0}^\perp$ decreases. This can probably be attributed to the fact that the flow equation of the former has an explicit B -dependence, while the flow equation

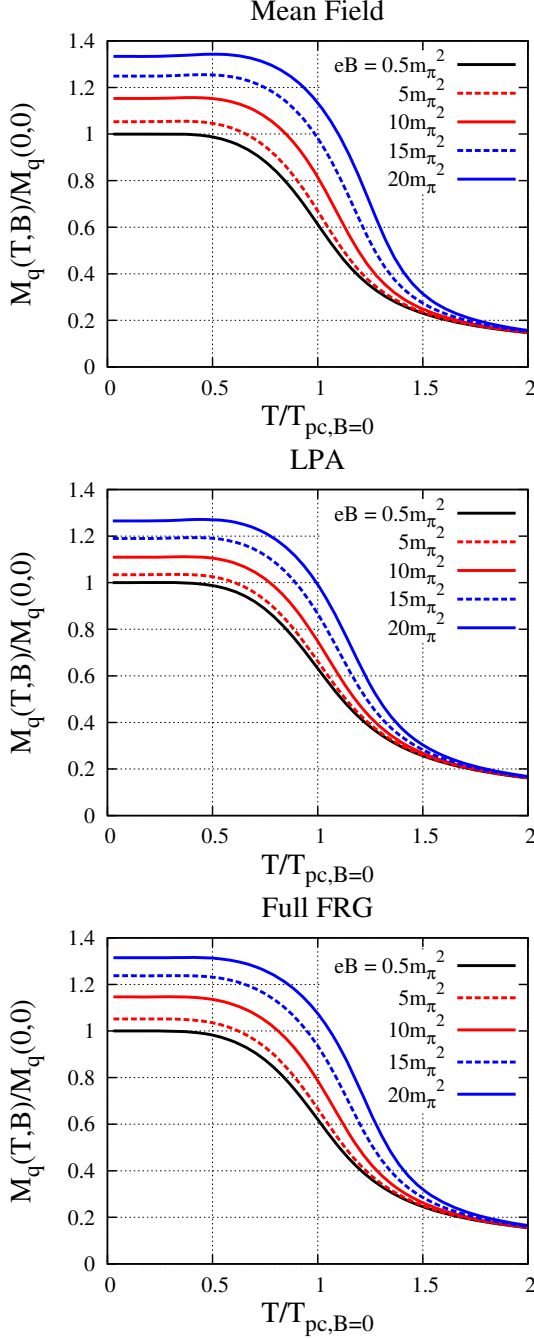


FIG. 25 Normalized constituent quark mass as a function of the normalized temperature for the three different approximations and different values $|qB|$. Figures taken from Kamikado and Kanazawa (2014a).

of the latter does not. Secondly, all curves meet for sufficiently large temperatures and that the curves for Z_{\perp} have done so already before the transition temperature.

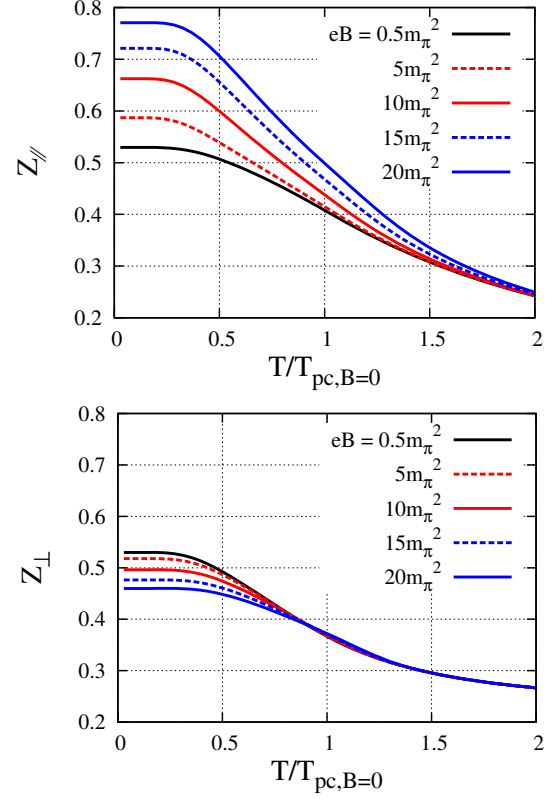


FIG. 26 Wavefunction renormalization terms $Z_{k=0}^{\parallel}$ and $Z_{k=0}^{\perp}$ as a function of the normalized temperature for various magnetic fields. Figures taken from Kamikado and Kanazawa (2014a).

VIII. MAGNETIC CATALYSIS

In this section, we discuss magnetic catalysis at $T = 0$. Magnetic catalysis is the effect that either

- (1) The magnitude of a condensate is enhanced by the presence of an external magnetic field B if the condensate is already present for zero magnetic field.
- (2) An external magnetic field induces symmetry breaking and the appearance of a condensate when the symmetry is intact for $B = 0$.

Case (2) is also referred to as dynamical symmetry breaking by a magnetic field. In context of low-energy effective theories of QCD, the condensate is the nonzero expectation value of the sigma field or the quark condensate. The early

works on magnetic catalysis date back to the late 80s and early 90s, and focused on the NJL model in 2+1 dimensions (Klimenko, 1992a,b,c) and in 3+1 dimensions (Ebert and Klimenko, 2000; Klevansky and Lemmer, 1989; Klimenko and Zhukovsky, 2008), and QED (Gusynin *et al.*, 1994). Other applications are in QCD (Miransky and Shovkovy, 2002; Ozaki, 2013) and the Walecka model in nuclear physics (Haber *et al.*, 2014). Magnetic catalysis is now considered a generic feature of matter in an external magnetic field (Shovkovy, 2013).

Inspecting the dispersion relation for fermions in a magnetic field, $E_k = \sqrt{m_f^2 + p_z^2 + (2k+1-s)|q_f B|}$, we see that it resembles the dispersion relation for a massive

particle in one spatial dimension with an effective mass $M_{\text{eff}}^2 = m_f^2 + (2k+s-1)|q_f B|$. Only for the lowest Landau level, is this effective mass independent of the magnetic field. When the fermionic mass scale is much smaller than the magnetic mass scale, $m_f^2 \ll |q_f B|$, the higher Landau levels decouple from the long low-energy dynamics and the long-distance behavior is determined by the lowest Landau level. Since the particles in the lowest Landau level essentially are confined to move along the magnetic field, i.e. the z -axis, the system becomes effectively one-dimensional and the system exhibits dimensional reduction, $D = 3 + 1 \rightarrow 1 + 1$. The 1 + 1-dimensional character of the lowest Landau at low momentum can also be inferred from the form of fermion propagator given by Eq. (18). Isolating the $k = 0$ contribution, we find

$$\tilde{S}_0(p) = i \exp\left(-\frac{p_\perp^2}{|q_f B|}\right) \frac{\gamma^0 p_0 - \gamma^3 p_3 + m}{p_0^2 - p_3^2 - m_f^2} [1 - i s_\perp \gamma^1 \gamma^2] , \quad (180)$$

where we have used $L_{-1}^a(x) = 0$. Note that dimensional reduction is not taking place for bosons as the ground-state energy is not vanishingly small compared to the energy of the first excited state, $k = 0$ and $k = 1$ in Eq. (20).

At this point, a few remarks on dimensional reduction and spontaneous symmetry breaking are in order. We have seen that a magnetic field enhances (spontaneous) symmetry breaking as well as reduces the system to being essentially 1+1 dimensional. However, we know from the Coleman theorem that there is no spontaneous symmetry breaking of a continuous symmetry in 1+1 dimension and therefore no massless Nambu-Goldstone boson can exist (Coleman, 1973).¹³ The point here is that $\langle \bar{\psi}\psi \rangle$ is neutral with respect to the magnetic field and that the Goldstone boson π^0 is a neutral excitation with respect to the magnetic field (Gusynin *et al.*, 1996). The motion of the center of mass of π^0 is not restricted to being along the magnetic field as it is an electrically neutral particle.

Let us discuss the NJL model first. For simplicity, we consider the case $N_c = N_f = 1$. If we denote the quark condensate by M , the mean-field contribution to the free energy density is given by $\frac{M^2}{2G}$, cf. the first two terms in Eq. (100) with $M_0 = M_3 = M$ for $c = 0$. Using a four-dimensional ultraviolet cutoff Λ , the one-loop contribution to the effective potential for $B = T = 0$ is given by Eq. (46). In the limit $M \ll \Lambda$, we find

$$\mathcal{F} = \frac{M^2}{2G} + \frac{1}{(4\pi)^2} \left[\frac{1}{2} \Lambda^4 - 2\Lambda^2 M^2 + \frac{1}{2} M^4 + M^4 \ln \frac{\Lambda^2}{M^2} \right] . \quad (181)$$

¹³ This applies to massless excitations that are linear in the momentum p for small p . Magnons are massless excitations in ferromagnets that are quadratic in the

momentum p for small p and exist in 1+1 dimension. Linear Goldstone modes exist in 2+1 dimensions at $T = 0$. See e.g. Watanabe and Murayama (2014) for a detailed discussion.

The minimum is found by solving the gap equation, which reads

$$M \left[\frac{4\pi^2}{G} - \Lambda^2 + M^2 \ln \frac{\Lambda^2}{M^2} \right] = 0. \quad (182)$$

$M = 0$ is always a solution. However a nontrivial solution exists for $G > G_c = \frac{4\pi^2}{\Lambda^2}$. Hence, for couplings larger than the critical value G_c , quantum fluctuations induce symmetry breaking in the model. The possible solutions to the gap equation in a constant magnetic field were first considered by Klevansky and Lemmer (1989). For finite magnetic field, the gap equation is

$$\frac{4\pi^2}{G} - \Lambda^2 + M^2 \ln \left(\frac{\Lambda^2}{M^2} \right) - \frac{|2q_f B|}{(4\pi)^2} \left[\zeta^{(1,0)}(0, x_f) + x_f - \frac{1}{2}(2x_f - 1) \ln x_f \right] = 0, \quad (183)$$

where $x_f = \frac{M^2}{2|q_f B|}$ as before. For nonzero magnetic field B and any G , this equation has only a nonzero solution for M . Consequently, for $G < G_c$, a nonzero magnetic field induces symmetry breaking when the symmetry is intact for $B = 0$. This effect was first observed in the context of the NJL model in 2+1 dimensions by Klimenko (1992a,b,c). For $G < G_c$, one finds (Gusynin *et al.*, 1996)

$$M^2 = \frac{|q_f B|}{\pi} \exp \left[-\frac{1}{|q_f B|} \left(\frac{4\pi^2}{G} - \Lambda^2 \right) \right]. \quad (184)$$

The gap vanishes in the limit $|q_f B| \rightarrow 0$ as it should. Moreover, Eq. (184) has an essential singularity at $G = 0$, which shows its nonperturbative nature: i.e. it is obtained by summing Feynman graphs from all orders of perturbation theory. Any finite-order perturbative calculation yields a vanishing gap.¹⁴ Furthermore, it is interesting to note the dependence on G in (184) is the same dependence as the solution to the gap equation in the BCS theory for superconductivity (albeit at zero magnetic field) (Shovkovy, 2013).

We next turn to the QM meson model. The value ϕ of the scalar field is determined by solving $\frac{d\mathcal{F}_{0+1}}{d\phi} = 0$. The value ϕ is an increasing function of the magnetic field in the same manner as $\langle \bar{\psi}\psi \rangle$ is in the NJL model. From Eq. (121), we find for small values of ϕ

$$\frac{d\mathcal{F}_{0+1}}{d\phi} \approx \phi \left[m^2 + \frac{N_c g^2}{4\pi^2} \sum_f |q_f B| \ln \frac{\pi m_q^2}{2|q_f B|} \right]$$

¹⁴ Recall that the N_c -expansion is nonperturbative in the sense that each order corresponds to a sum of Feynman diagrams from all orders of perturbation theory. The large- N_c is a sum of all daisy and superdaisy graphs.

$$= 0, \quad (185)$$

whose to nonzero solution is approximately

$$\phi^2 \approx \frac{|qB|}{g^2} \exp \left[-\frac{m^2}{N_c g^2 |qB|} \right]. \quad (186)$$

If the mass parameter m^2 is positive, there is no symmetry breaking at tree level. Eq. (186) then shows that quantum fluctuations induce symmetry breaking in the same manner as in the NJL model, cf. Eq. (184).

In Fig. 27, we show the minimum of the effective potential $U_{k=0}(\phi)$ at $T = 0$ as a function of $(|qB|)^{\frac{1}{2}}/\Lambda$ in the quark-meson model using the functional renormalization group. We see that the minimum is an increasing function of the magnetic field, so the system shows magnetic catalysis.

There have been a number of lattice calculations of the chiral condensate at $T = 0$ as a function of the magnetic field both in the quenched approximation (Braguta *et al.*, 2012; Buividovich *et al.*, 2010a,b) and with dynamical quarks (D'Elia and Negro, 2011; Endr di, 2013).

In Fig. 28, the results for the condensates $\langle \bar{u}u \rangle$ and $\langle \bar{d}d \rangle$ as well as their average are shown as functions of the magnetic

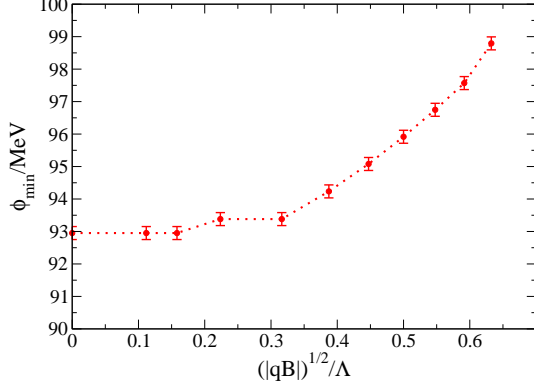


FIG. 27 Magnetic catalysis in the quark-meson model at the physical point and at $T = 0$. The vacuum expectation value of the field ϕ as a function of

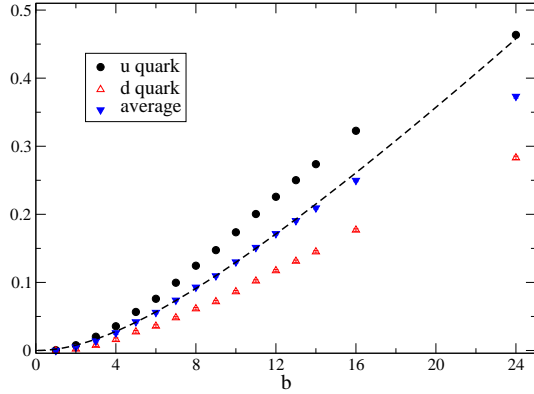


FIG. 28 The $\langle \bar{u}u \rangle$ (black points) and $\langle \bar{d}d \rangle$ (red points) condensates as well as their average (blue points) as a function of B . Figure taken from D'Elia and Negro (2011).

field (D'Elia and Negro, 2011). We notice that the $\bar{u}u$ condensate is larger than the $\bar{d}d$ in agreement with model calculations, cf. Fig. 5.

In Fig. 29, the change of the condensate $\frac{1}{2}\Delta(\langle \Sigma_u \rangle + \langle \Sigma_d \rangle)$ is shown as a function of $|qB|$ at $T = 0$ and at the physical point (Endrődi, 2013). The lattice results are continuum extrapolated. The model calculations are from one-loop chiral perturbation theory (Andersen, 2012a,b; Cohen *et al.*, 2007) as well as the Polyakov-loop extended NJL model (Gatto and Ruggieri, 2011). Notice that at $T = 0$, the PNJL model reduces to the NJL model. Clearly, the result of the Chpt results are in quantitative agreement with lattice simulations for magnetic fields up to $|qB| \approx 0.15 \text{ GeV}^2$. For the (P)NJL model, the

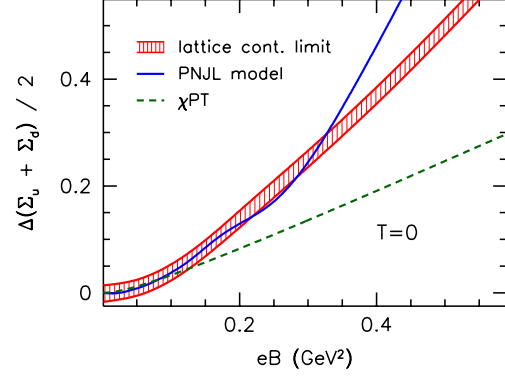


FIG. 29 Comparison of the continuum limit of the change of the condensate to with that of chiral perturbation theory (Andersen, 2012a,b; Cohen *et al.*, 2007) and the (P)NJL model (Gatto and Ruggieri, 2011). Figure taken from Bali *et al.* (2012c).

agreement with lattice extends up to $|qB| \approx 0.30 \text{ GeV}^2$. The quark condensate in chiral perturbation theory is given by Eq. (77). Expanding around $B = 0$ to at $T = 0$ using Eq. (C7), we find the shift due to the magnetic field

$$\Delta\langle \bar{q}q \rangle = \frac{1}{2}(qB)^2 \frac{1}{3(4\pi)^2} \frac{\langle \bar{q}q \rangle}{m_\pi^2 f_\pi^2} + \mathcal{O}(B^4) \quad (187)$$

where we have identified $M = m_\pi$ and $F = f_\pi$, correct at this order. The interesting observation here, first made by Endrődi (2013), is that the prefactor is proportional to the one-loop β -function of scalar QED, $\beta = \frac{1}{3(4\pi)^2}$. A similar result is obtained for fermions, which can be shown using the relation $\langle \bar{q}q \rangle \sim \frac{\partial \mathcal{F}}{\partial m_f}$ (Bali *et al.*, 2014).

The behavior of the quark condensate as a function of B can be understood in terms of the Banks-Casher relation (Banks and Casher, 1980). The quark condensate $\langle \bar{\psi}\psi \rangle$ is proportional to the spectral density $\rho(\lambda)$ of the Dirac operator around zero. The Dirac operator depends on the magnetic field, and therefore the spectral density depends on B . A constant magnetic field enhances the spectral density around zero and as a result it enhances the quark condensate, see also the discussion in Sec. IX. This behavior of the spectral density is already found in the quenched approximation (Braguta *et al.*, 2012; Buividovich *et al.*, 2010a,b) in which there is no back-reaction from the quarks to the non-abelian gauge fields. In model calculations, the

quark condensate is given by the expectation value of the operator $\text{Tr}(\not{D}(B) + m)^{-1}$, which is enhanced by the magnetic field. This enhancement is due to an increase of the spectral density, which is a consequence of the degeneracy being proportional to the magnetic flux, cf the discussion after Eq. (11).

In a recent paper, Mueller *et al.* (2014) investigate dynamical quark mass generation and spin polarization in a strong magnetic field B using the Dyson-Schwinger (DS) equations. They do this in both the quenched and unquenched approximations at $T = \mu_B = 0$. The starting point is the Dyson-Schwinger equation for the fermion

propagator $S(x, y)$ in coordinate space

$$S^{-1}(x, y) = S_0^{-1}(x, y) + \Sigma(x, y), \quad (188)$$

where $S_0(x, y)$ is the free fermion propagator and $\Sigma(x, y)$ is the fermion self-energy

$$\Sigma(x, y) = ig^2 C_F \gamma^\mu S(x, y) \Gamma^\nu(y) D_{\mu\nu}(x, y), \quad (189)$$

where $C_F = \frac{N_c^2 - 1}{2N_c}$, $\Gamma^\nu(y)$ is the dressed fermion vertex and $D_{\mu\nu}(x, y)$ is the quenched gluon propagator. The quenched gluon propagator in momentum space can be written as $D_{\mu\nu}(k^2) = D(k^2)P_{\mu\nu}$, where the projection operator is $P_{\mu\nu} = \delta_{\mu\nu} - k_\mu k_\nu / k^2$. The fermion propagator in the Ritus representation (Ritus, 1978) is

$$S(x, y) = \sum_{k=0}^{\infty} \int \frac{d^2 p_{\parallel}}{(2\pi)^4} \int_{-\infty}^{\infty} dp_2 E_p(x) \frac{1}{i\gamma \cdot p_{\parallel} A_{\parallel}(p) + i\gamma \cdot p_{\perp} A_{\perp}(p) + B(p)} \bar{E}_p(y), \quad (190)$$

where $A_{\parallel}(p)$, $A_{\perp}(p)$, and $B(p)$ are the so called dressing functions. By taking the trace in the Dyson-Schwinger equation, one finds a set of coupled equations for the dressing functions.

The gluon propagator function $D(k^2)$ is written in terms of the dressing function $Z(k^2)$ via $D(k^2) = Z(k^2)/k^2$. The function $D(k^2)$ has been calculated to high precision both on the lattice (Leinweber, 1999, 2000) and by solving the Dyson-Schwinger equations (Fischer *et al.*, 2009; Huber and von Smekal, 2013). The quenched gluon propagator is used as input to the Dyson-Schwinger equation together with the dressed vertex $\Gamma^\mu(p)$. The latter is, however, poorly known, and Mueller *et al.* (2014) made a simple ansatz for it.

In the unquenched approximation, the gluon propagator is improved by taking into account the quark loop in the Dyson-Schwinger equation. This is shown diagrammatically in Fig. 30 and the Dyson-Schwinger equation in momentum space can then be written as

$$\begin{aligned} D_{\mu\nu}^{-1}(k) &= (D_{\mu\nu}^{-1})_0(k) + \Pi_{\mu\nu}^g(k) + \Pi_{\mu\nu}^q(k) \\ &\approx D_{\mu\nu}^{-1, \text{eff}}(k) + \Pi_{\mu\nu}^q(k), \end{aligned} \quad (191)$$

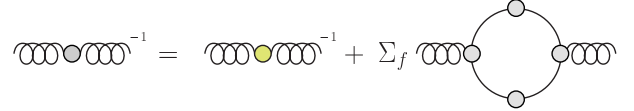


FIG. 30 Dyson-Schwinger equation for the inverse gluon propagator.

where $D_{\mu\nu}^{-1}(k)$ is an effective inverse propagator corresponding to the first diagram on the right-hand side in Fig. 30. The self-energy $\Pi_{\mu\nu}^q(k)$ corresponds to the quark loop in Fig. 30. The big blobs represent dressed propagators and dresses vertices. Since the term $D_{\mu\nu}^{-1, \text{eff}}(k)$ is isotropic, it is the quark loop that generates the anisotropies in the dressed gluon propagator.

Fig. 31 displays the $\langle \bar{u}u \rangle$ (solid black line) and $\langle \bar{d}d \rangle$ quark condensates (solid red line) in the unquenched approximation as a function of the magnetic field. For comparison, the $\langle \bar{u}u \rangle$ condensate (dashed black line) in the quenched approximation has been shown as well. One observes that the condensates are different. This simply reflects the isospin breaking due to the different electric charges of the u and the d

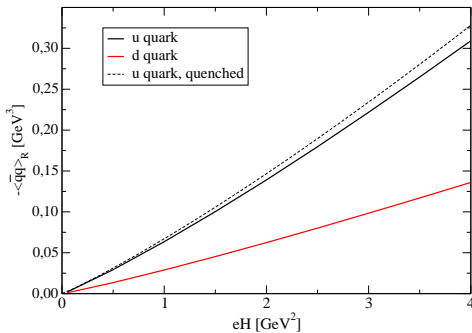


FIG. 31 $\langle \bar{u}u \rangle$ (black) and $\langle \bar{d}d \rangle$ quark condensates (red) together with the $\langle \bar{u}u \rangle$ condensate in the quenched approximation (dashed). Figure taken from Mueller *et al.* (2014).

quark. The most interesting result is that the quenched condensate is larger than the unquenched condensate. Taking the back-reaction of the quarks on the gluonic sector leads to reduced magnetic catalysis. Whether this leads to inverse magnetic catalysis around T_c is an open question, but it is certainly of interest to investigate it.

A similar approach was used by Watson and Reinhardt (2014), in which the Dyson-Schwinger equation was studied in the rainbow approximation. In this approximation, the dressed quark-gluon vertex is replaced with the bare (tree-level) vertex, while the quark propagator and its inverse are dressed. The gluon dressing function has a phenomenological form that has been used to study dynamical chiral symmetry breaking. The authors pay particular attention to the weak-field limit and so this is complementary to the paper by Mueller *et al.* (2014). In order to connect to the case $B = 0$, a nonperturbative approximation to the quark propagator is constructed, which involves a summation over the Landau levels. If one does sum over Landau levels, the mass gap vanishes in the limit $B \rightarrow 0$, which is incorrect (see Fig. 31). In Fig. 32, the relative increment (see also Eq. (196) below) is shown using the Dyson-Schwinger approach as well lattice results from by D’Elia and Negro (2011). The agreement is very good up to field strengths

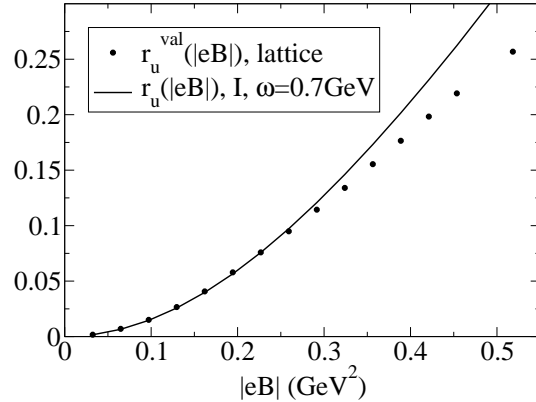


FIG. 32 Comparison of the up-quark relative increment with the lattice results of D’Elia and Negro (2011). ω is a parameter of the gluon dressing function. Figure taken from Watson and Reinhardt (2014).

of approximately $|qB| = 0.3 \text{ GeV}^2$. One must be cautious, however, as the DS equations are solved in the chiral limit, while the lattice results are for quark masses that correspond to $m_\pi \approx 200 \text{ MeV}$.

IX. LATTICE SIMULATIONS AND INVERSE MAGNETIC CATALYSIS

As discussed in the introduction, QCD at zero baryon chemical potential μ_B in an Abelian background field A_μ is free of the sign problem and so QCD can in principle be straightforwardly simulated on the lattice using standard Monte Carlo algorithms. This statement is independent of the color gauge group, which opens up the possibility for doing lattice simulations for the theories where the physics is very different. For example, for two colors, $N_c = 2$, and two massless flavors, $N_f = 2$, the symmetry group of the Lagrangian is $SU(4) \sim SO(6)$, which is broken down in the vacuum to the group $Sp(2) \sim SO(5)$. In the process, five generators are broken leading to five massless bosons according to Goldstone’s theorem. These Goldstone particles are the pions, π^\pm and π_0 as well a diquark Δ and an antidiquark Δ^* . Due to the color group $SU(2)_c$, two quarks can form color singlets and therefore are part of the physical spectrum. The diquarks are thus the “fermions”

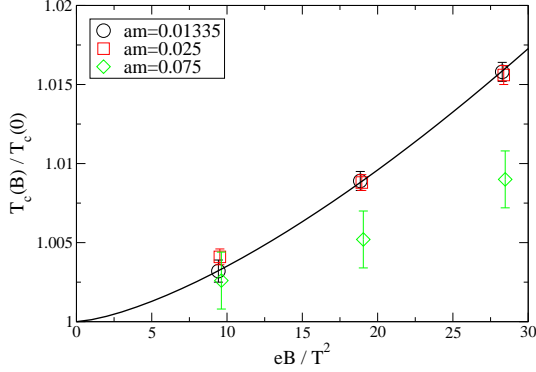


FIG. 33 Transition temperature normalized to T_c at $B = 0$ for the deconfinement and the chiral transition as a function $|qB|/T^2$. Figure taken from D’Elia *et al.* (2010).

of two-color QCD. However, being bosons, they behave differently. For example, they Bose condense when the baryon chemical potential exceeds the mass of the diquarks.¹⁵

A. $SU(3)_c$

In the physical case $N_c = 3$ and with $N_f = 2$, the first lattice simulations at finite magnetic field were carried out by D’Elia *et al.* (2010). They used different values of the bare quark masses corresponding to a pion mass in the 200–480 MeV range. The magnetic field strengths were up to $|qB| \sim 0.75 \text{ GeV}^2$ and the calculations were carried out with a lattice spacing of 0.3 fm and the results were not continuum extrapolated. The authors found no evidence for a splitting between the chiral and deconfinement transition as found in PNJL and PQM model calculations. They also found that the critical temperature increases very slowly with the magnetic field as can be seen in Fig. 33. These results have later been confirmed by Bali *et al.*

(2012c,d) and seem to be in agreement with model calculations presented in Secs. V and VII.

Bali *et al.* (2012c,d) have also carried out lattice simulation using a physical pion mass of

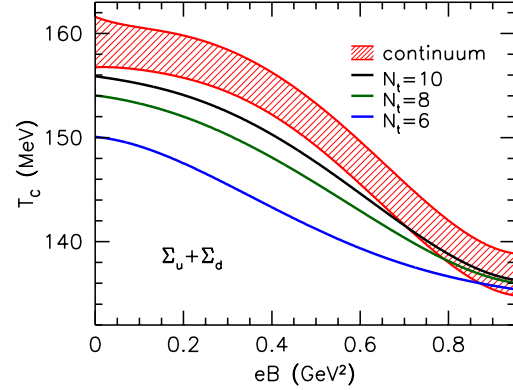


FIG. 34 Transition temperature for the deconfinement as a function of $|qB|$ for different lattice spacings (solid curves) and the continuum-extrapolated result (band) Figure taken from Bali *et al.* (2012a).

$m_\pi = 140 \text{ MeV}$. Their results are shown in Fig. 34. Their results have been continuum extrapolated and show, perhaps somewhat surprisingly, that the transition temperature is decreasing with the magnetic field B . The fact that T_c is a decreasing function of the magnetic field suggests that the results obtained for larger pion masses will survive the continuum extrapolation. If this is correct, the transition temperature is a complicated function of the magnetic field and the quark masses.

In the recent papers of Bali *et al.* (2012c,d) and Bruckmann *et al.* (2013), the authors analyze in detail lattice results and thereby explain the discrepancy for T_c as a function of B between the model calculations such as (P)NJL and (P)QM models and their results.

The chiral condensate can be written as

$$\langle \bar{\psi}\psi \rangle = \frac{1}{Z(B)} \int d\mathcal{U} e^{-S_g} \det(\mathcal{D}(B) + m) \text{Tr}(\mathcal{D}(B) + m)^{-1}, \quad (192)$$

¹⁵ Note that due to the special properties of the Pauli matrices, $SU(2)_c$ does not have a sign problem and so

one can perform lattice simulations at finite μ_B .

where the partition function $\mathcal{Z}(B)$ is

$$\mathcal{Z}(B) = \int d\mathcal{U} e^{-S_g} \det(\mathcal{D}(B) + m) , \quad (193)$$

and S_g is the pure-gluon action. The magnetic field enters via the operator $\text{Tr}(\mathcal{D}(B) + m)^{-1}$ as well as the fermion functional determinant $\det(\mathcal{D}(B) + m)$. We can think of $\mathcal{P}(m, U, B) \equiv \frac{1}{\mathcal{Z}(B)} e^{-S_g} \det(\mathcal{D}(B) + m)$, where U denotes the gauge-field configuration that corresponds to e^{-S_g} , as a measure. In order to study the contributions to magnetic catalysis coming separately from the change in the operator and in measure, one defines the two condensates

$$\langle \bar{\psi}\psi \rangle^{\text{val}} = \frac{1}{\mathcal{Z}(0)} \int d\mathcal{U} e^{-S_g} \det(\mathcal{D}(0) + m) \text{Tr}(\mathcal{D}(B) + m)^{-1} , \quad (194)$$

$$\langle \bar{\psi}\psi \rangle^{\text{sea}} = \frac{1}{\mathcal{Z}(B)} \int d\mathcal{U} e^{-S_g} \det(\mathcal{D}(B) + m) \text{Tr}(\mathcal{D}(0) + m)^{-1} . \quad (195)$$

These are the so-called valence and sea condensates. The valence condensate is the average of the trace of the propagator in a constant magnetic background, but where the sampling of the nonabelian gauge configurations is done at $B = 0$. The sea contribution is the average of the same operator in zero magnetic field, but where the sampling is done at nonzero B . The sea effect is absent in the quenched approximation. More generally, a sea observable is an observable that does not depend explicitly on the magnetic field. The Polyakov loop is another example of a sea observable. We note that the sea condensate equals a condensate of a neutral quark in a two-flavor theory with one electrically charged and one neutral quark since the magnetic field does not appear in the operator, but in the determinant.

A useful quantity is the relative increment $r(B)$ of the quark condensate as a function of B , which is defined by

$$r(B) = \frac{\langle \bar{\psi}\psi \rangle(B)}{\langle \bar{\psi}\psi \rangle(0)} - 1 . \quad (196)$$

The relative increments $r^{\text{val/sea}}(B)$ are defined in a similar manner. D'Elia and Negro (2011) calculated the three quantities $r(B)$, $r^{\text{val}}(B)$, and $r^{\text{sea}}(B)$ at zero temperature. The result is shown in Fig. 35. The valence contribution $r^{\text{val}}(B)$ (red data points) and the sea contribution $r^{\text{sea}}(B)$ (blue data points) are both positive. The sum of the two (open circles) and $r(B)$ (full circles) are shown as well. We notice that the open circles

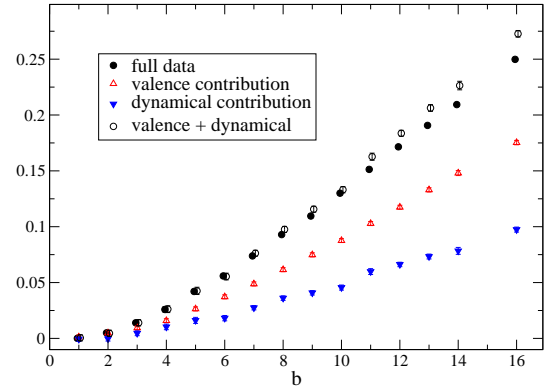


FIG. 35 Relative increments $r(B)$, $r^{\text{val}}(B)$, and $r^{\text{sea}}(B)$ at zero temperature. See main text for details. Figure taken from D'Elia and Negro (2011).

are very close to the full circles, except for very large values of B , which suggests that the relative increment can be written as a sum of the valence and sea contributions. The same behavior of $r^{\text{val}}(B)$, and $r^{\text{sea}}(B)$ are found in the simulations by Bruckmann *et al.* (2013) for physical quark masses at $T = 0$.

As mentioned, earlier, it is possible to understand the behavior of the valence condensate by employing the Banks-Casher relation (Banks and Casher, 1980). In the chiral limit, the chiral condensate is proportional to the spectral density $\rho(\lambda)$ of the Dirac operator around zero. In Fig. 36, Bruckmann *et al.* (2013) show the spectral density for three values of the magnetic field B . The ensemble of non-

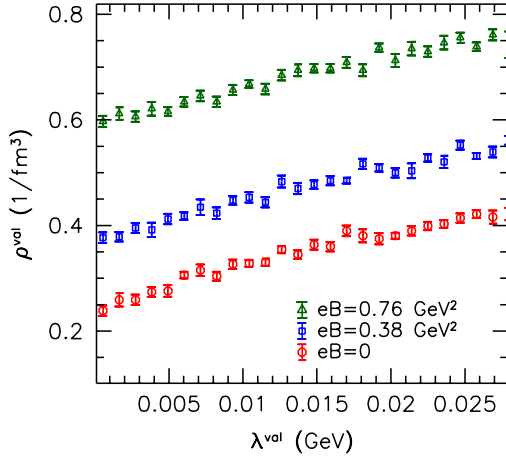


FIG. 36 Spectral density of the Dirac operator for three different values of the magnetic field B . Figure taken from Bruckmann *et al.* (2013).

abelian gauge field backgrounds are generated at zero magnetic field and at $T = 142$ MeV. It is evident from Fig. 36 that the spectral density and therefore the valence condensate increases with the strength of the magnetic field. This behavior is independent of the temperature.

At temperatures around the transition temperature, the valence condensate is still positive while the sea condensate is negative. Hence there is a competition between the two, leading to a net inverse catalysis. The sea contribution can be viewed as a back reaction of the fermions on the gauge fields and this effect is not present in the model calculations as there are no dynamical gauge fields. The behavior of the sea contribution was also carefully analyzed by Bruckmann *et al.* (2013). Introducing $\Delta S_f(B) = \log \det(\not{D}(B) + m) - \log \det(\not{D}(0) + m)$, one can rewrite the full condensate as

$$\langle \bar{\psi}\psi \rangle = \frac{\langle e^{-\Delta S_f(B)} \text{Tr}(\not{D}(B) + m)^{-1} \rangle_0}{\langle e^{-\Delta S_f(B)} \rangle_0}, \quad (197)$$

where the subscript 0 indicates that the expectation values are at $B = 0$. We note that Eq. (197) reduces to the valence condensate if we replace the exponential factor $e^{-\Delta S_f(B)}$ by unity.

In Fig. 37, Bruckmann *et al.* (2013) show a scatter plot of the condensate as a function of the change in the action $\Delta S_f(B)$ due to the magnetic field for a magnetic field strength of $|qB| \approx$

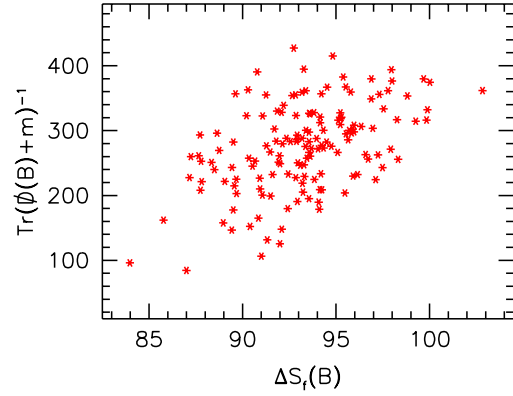


FIG. 37 Scatter plot of the down-quark condensate as a function of $\Delta S_f(B)$. The magnetic field strength is $|qB| \approx 0.5$ GeV² and $T \sim T_c$. Figure taken from Bruckmann *et al.* (2013).

0.5 GeV² and T around the transition temperature. Each point represents a gauge configuration and they were generated at $B = 0$, and therefore a simple averaging of $\text{Tr}(\not{D}(B) + m)^{-1}$ without weighting each configuration in the ensemble with the Boltzmann factor $e^{-\Delta S_f(B)}$ gives the valence condensate. In order to calculate the full quark condensate, one must average $\text{Tr}(\not{D}(B) + m)^{-1}$ over the gauge configurations including the weight factor $e^{-\Delta S_f(B)}$. Generally, larger values of the condensate correspond to larger values of $\Delta S_f(B)$ and as a result, the weight of the associated gauge configuration is suppressed. This suppression is particularly effective around T_c and in fact overwhelms the valence effect and therefore leads to inverse magnetic catalysis in the transition region. This suppression is not present for larger quark masses, cf. Fig. 35. One therefore might expect the sea effect to be even more pronounced in the chiral limit. Let us finally add that the recent simulations of Bornyakov *et al.* (2014) with large quark masses that correspond to a pion mass of approximately 500 MeV show a different behavior. Using chiral fermions instead of staggered fermions, the authors find clear evidence for inverse magnetic catalysis also for large pion masses. The analysis was based on the behavior of the chiral condensate, the expectation value of the Polyakov loop as well as the spectral density

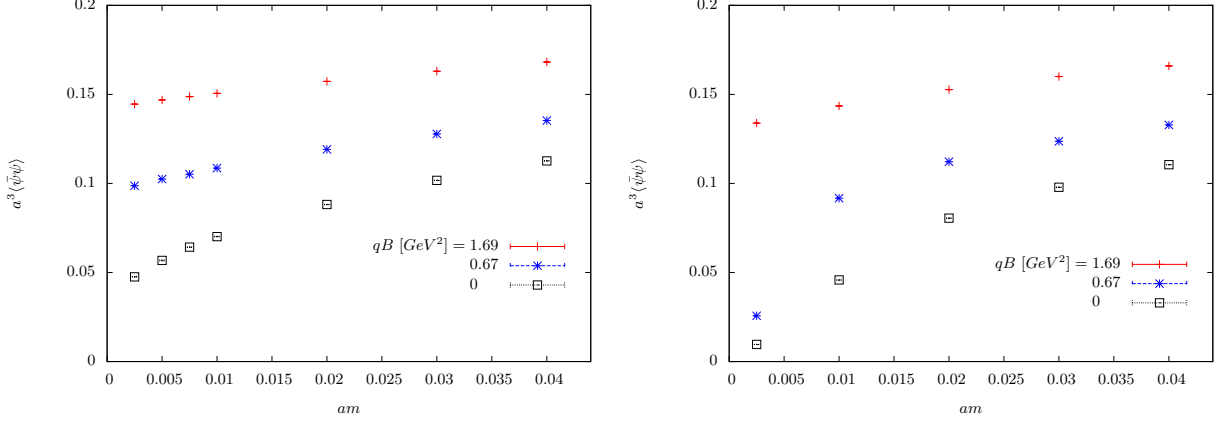


FIG. 38 Mass dependence of the bare chiral condensate for three different values of the magnetic field and two different temperatures: 147 MeV (left) and 195 MeV (right). Figure taken from Ilgenfritz *et al.* (2014).

as functions of B for two different values of the temperature. The results seem to indicate that the chiral properties are an important ingredient in inverse magnetic catalysis.

B. $SU(2)_c$

Recently, Ilgenfritz *et al.* (2012, 2014) have carried out lattice simulations with dynamical fermions. We focus on their second paper, which is extension of the first to smaller quark masses. They used $N_f = 4$ and equal electric charge as well as quark masses that correspond to a pion mass m_π of approximately 175 MeV. The transition temperature for $B = 0$ is in this case $T_c \approx m_\pi$.

Fig. 38 shows the mass dependence of the bare chiral condensate for three different values of the magnetic field, $B = 0$ (grey), $|qB| = 0.67 \text{ GeV}^2$ (blue), and $|qB| = 1.69 \text{ GeV}^2$ (red) and two different temperatures: 147 MeV (left) and 195 MeV (right). Inspecting the left panel, the data points suggest that the system is in the chirally broken phase for all three values of the magnetic field. In contrast, the data points in right panel indicate that the chiral condensate is zero (extrapolating to the chiral limit) for $B = 0$ and $|qB| = 0.67 \text{ GeV}^2$, while the chiral condensate is nonzero for $|qB| = 1.69 \text{ GeV}^2$. This behavior suggests that the critical temperature grows with B for very strong magnetic fields.

Further insight can be gained from Fig. 39, where the authors show the expectation values of the Polyakov loop (left panel) and the chiral condensate (right panel) at $T = 195 \text{ MeV}$ as functions of $|qB|$ up to $|qB| = 1.69 \text{ GeV}^2$. The left panel shows a rise of the Polyakov loop for magnetic fields up to approximately $|qB| = 0.7 \text{ GeV}^2$. This suggests that one goes deeper into the deconfinement region and that the system exhibits inverse magnetic catalysis at low values of the magnetic field. For values of the magnetic field larger than $|qB| = 0.7 \text{ GeV}^2$, there is a significant drop of the expectation value of the Polyakov loop. This indicates that we are going back into the confinement region and that the system exhibits magnetic catalysis for large values of the magnetic field.

The results suggest that the critical temperature decreases for weak magnetic fields and in-

creases for strong magnetic fields. A conjectured phase diagram based on these observa-

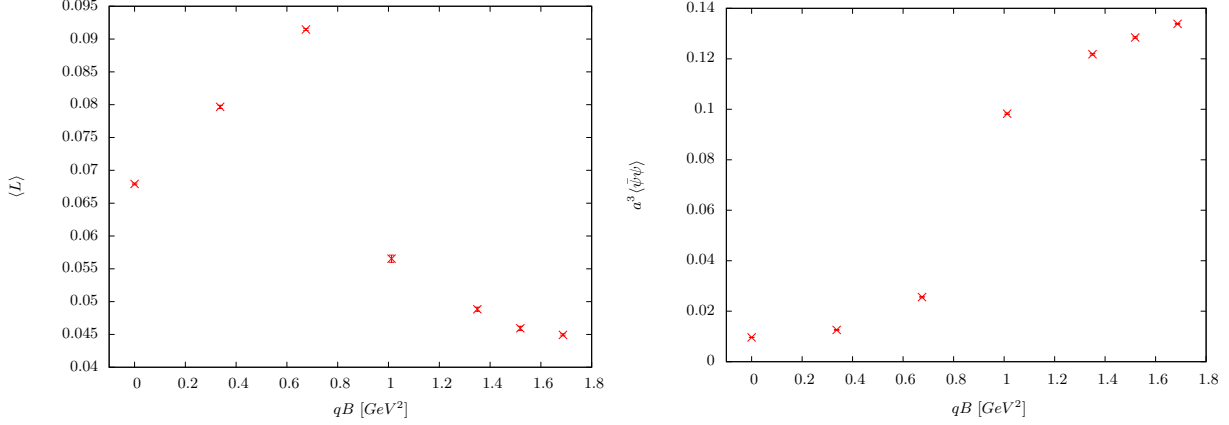


FIG. 39 Expectation values of the Polyakov loop (left) and the chiral condensate (right) vs $|qB|$ at $T = 195$ MeV. Figure taken from Ilgenfritz *et al.* (2014).

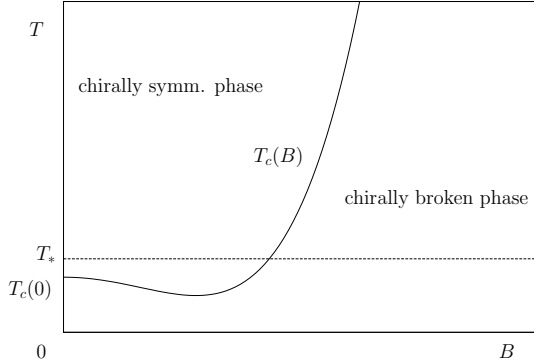


FIG. 40 Conjectured phase diagram in the B - T plane. The horizontal line is $T^* = 195$ MeV. Figure taken from Ilgenfritz *et al.* (2014).

tions is shown in Fig. 40. A direct comparison with the only model calculation that exists (Cruz and Andersen, 2013) is not straightforward since $N_f = 2$ with $q_u = \frac{2}{3}$ and $q_d = -\frac{1}{3}$ were used. Nevertheless, note the similarity with Fig. 19, where a small minimum can be seen. However, to firmly conclude, a thorough analysis involving separating the valence and sea effects along the lines of Bruckmann *et al.* (2013) would be of interest.

X. MODEL CALCULATIONS REVISITED

After it was realized that most model calculations were in disagreement with the lattice calculations, there has been significant efforts to

modify them such that they reproduce the correct behavior of T_c as a function of B , or to propose a mechanism for inverse magnetic catalysis around T_c (Ayala *et al.*, 2014a,b; Braun *et al.*, 2014; Chao *et al.*, 2013; Farias *et al.*, 2014; Fayazbakhsh and Sadooghi, 2014; Ferreira *et al.*, 2014a,b,c; Ferrer *et al.*, 2014a; Fraga *et al.*, 2014, 2013; Fukushima and Hidaka, 2013; Fukushima and Pawłowski, 2012; Kojo and Su, 2013; Twafik and Magdy, 2014; Yu *et al.*, 2014a,b). A large number of papers have been focusing on B -dependent coupling constants or B -dependent parameters in the model and we discuss some of them below.

A. B -dependent transition temperature T_0

The parameter T_0 that enters the Polyakov loop potential depends on the number of quarks (and on the chemical potential at finite density). At finite B , one expects T_0 to depend on the magnetic field as well as N_f , which can be taken into account by using a B -dependent function $b = b(N_f, B)$ in analogy with Eq. (154). The first attempt to incorporate a B -dependent transition temperature $T_0(qB)$ was made by Ferreira *et al.* (2014b) using the (E)PNJL model. They made the ansatz

$$T_0(qB) = T_0(qB = 0) + \zeta(qB)^2 + \xi(qB)^4, \quad (198)$$

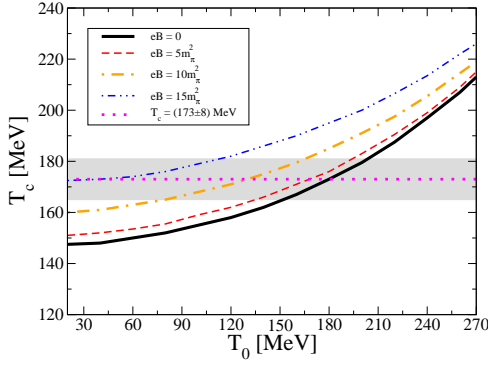


FIG. 41 Transition temperature T_c for the chiral transition as a function of T_0 for different values of the magnetic field. Figure taken from Fraga *et al.* (2014).

and fitted the parameters ζ and ξ to reproduce the transition temperature extracted from the strange quark number susceptibility data (Bali *et al.*, 2012c). This approach gives a crossover for $|qB| < 0.25 \text{ GeV}^2$ and a first-order transition for $|qB| > 0.25 \text{ GeV}^2$, when $T_0(qB) = 186 \text{ MeV}$, which corresponds to the critical temperature for 2+1 massless flavors. The range of crossover transitions increases significantly by using $T_0(qB = 0) = 270 \text{ MeV}$, which corresponds to the transition temperature for pure-gluon, i.e. by omitting the backreaction from the fermions at $B = 0$.

Recently Fraga *et al.* (2014) analyzed the possibility of inverse magnetic catalysis by allowing the model parameter T_0 to be a function of B . They calculated the transition temperature T_c for the chiral transition as a function of the parameter T_0 in the PQM model in the mean-field approximation.

Any parametrization of $T_0(B)$ gives rise to a continuous curve that starts at some point on the black curve corresponding to $B = 0$ and crosses the other curves as B is varied. T_c as a function of B can be a decreasing function only if $T_0(B)$ decreases sufficiently fast. This can be the case for low values of the magnetic field, if the point $T_0(B = 0)$ is sufficiently far to the right on the black curve. However, since the curves become flatter as one moves to the left in the figure, it is clear that this behavior

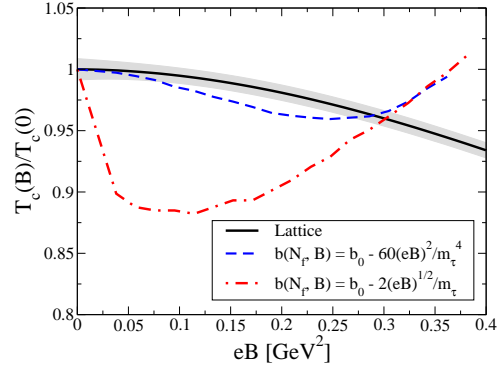


FIG. 42 Normalized transition temperature T_c for the chiral transition as a function of $|qB|$. The grey band is the lattice results from Bali *et al.* (2012d) Figure taken from Fraga *et al.* (2014).

cannot be sustained. In other words, even if the critical temperature initially is decreasing with B , eventually it will have a minimum and start increasing again for larger values of B . Specific parametrizations $b(n_f, B) = b(N_f) - 60(qB)^2/m_\tau^4$ and $b(n_f, B) = b_0 - 60\sqrt{|qB|}/m_\tau$ were given by Fraga *et al.* (2014) to illustrate this point. The result is shown in Fig. 42.

Andersen *et al.* (2014b) have very recently performed the same type of calculations using the functional renormalization group. The inclusion of mesonic fluctuations does not change the results and conclusions, as anticipated by Fraga *et al.* (2014).

B. B -dependent coupling constant

Farias *et al.* (2014) investigated the possibility of obtaining inverse magnetic catalysis in the NJL model by using an effective coupling constant that is a function of the magnetic field and the temperature T . Motivated by the running of the QCD coupling, they proposed a B -dependent coupling $G(B)$ given by

$$G(B) = \frac{G_0}{1 + \alpha \ln \left(1 + \beta \frac{|qB|}{\Lambda_{\text{QCD}}^2} \right)}, \quad (199)$$

where $G_0 = 5.022 \text{ GeV}^{-2}$ is the value of the coupling at $B = 0$. We notice that $G(B) \rightarrow 0$ as

$B \rightarrow \infty$, a behavior that is inspired by the running of α_s at very large magnetic fields $|qB| \gg \Lambda_{\text{QCD}}^2$: $\frac{1}{\alpha_s} \sim \ln \frac{|qB|}{\Lambda_{\text{QCD}}^2}$ (Miransky and Shovkovy, 2002). Here α and β are free parameters that are determined such that one obtains a reasonable description of the average $\frac{1}{2}(\Sigma_u + \Sigma_d)$ calculated on the lattice at $T = 0$, where the dimensionless quantity Σ_f is defined by

$$\Sigma_f = \frac{2m_f}{m_\pi^2 f_\pi^2} (\langle \bar{\psi}_f \psi_f \rangle_B - \langle \bar{\psi}_f \psi_f \rangle_0) + 1 \quad (200)$$

At finite temperature the authors propose a coupling $G(B, T)$ given by

$$G(B, T) = G(B) \left(1 - \gamma \frac{|qB|}{\Lambda_{\text{QCD}}^2} \frac{T}{\Lambda_{\text{QCD}}} \right) \quad (201)$$

Here γ is another parameter that is fitted to reproduce the lattice results of Bali *et al.* (2012d) for $\frac{1}{2}(\Sigma_u + \Sigma_d)$ at the highest temperatures available.

In Fig. 43, the average $\frac{1}{2}(\Sigma_u + \Sigma_d)$ is shown as a function of temperature T for different values of the magnetic field. The data points are from the lattice simulations of Bali *et al.* (2012d).

The ansätze for the coupling, Eqs. (199) and (201) then give a reasonable description of the lattice data. At $T = 0$, increasing magnetic field implies larger average $\frac{1}{2}(\Sigma_u + \Sigma_d)$. However, for $T \approx 140$ MeV, the curves cross each other and the order of the curves is reversed beyond this temperature. This shows inverse magnetic catalysis around the transition temperature. The curves in Fig. 43 become steeper around the transition temperature as the magnetic field increases, suggesting that transition becomes first order for sufficiently large values of B .

The chiral susceptibility is defined by

$$\chi = \frac{\partial \sigma}{\partial T}, \quad (202)$$

where

$$\sigma = -m_\pi \frac{(\langle \bar{u}u \rangle + \langle \bar{d}d \rangle)(B, T)}{(\langle \bar{u}u \rangle + \langle \bar{d}d \rangle)(B, 0)}, \quad (203)$$

and is shown in Fig. 44 as a function of T for different values of B . The peaks move to the left as a function of the magnetic field. The peak

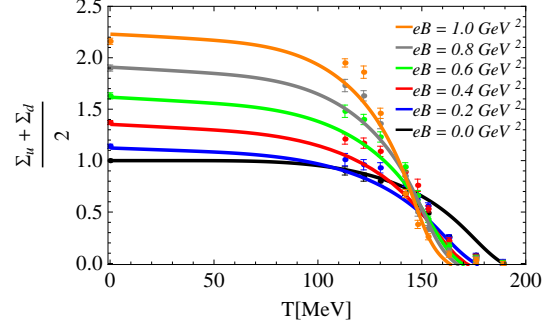


FIG. 43 The average $\frac{1}{2}(\Sigma_u + \Sigma_d)$ as a function of temperature T for different values of the magnetic field. The data points are the lattice results from Bali *et al.* (2012d). Figure taken from Farias *et al.* (2014).

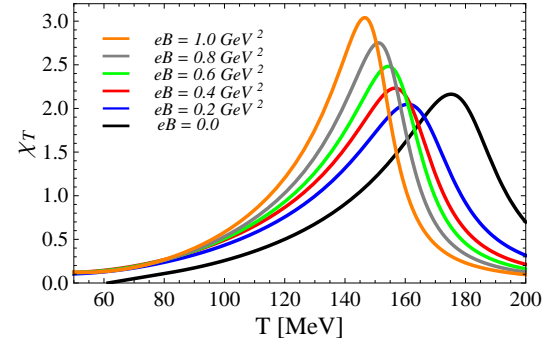


FIG. 44 Susceptibility χ as a function of the temperature T for different values of the magnetic field. Figure taken from Farias *et al.* (2014).

of the susceptibility χ defines the pseudocritical temperature T_{pc} and in Fig. 45 the pseudocritical temperature is shown as a function of $|qB|$.

A similar approach was used by Ferreira *et al.* (2014a), where an effective coupling $G_s(|qB|/\Lambda_{\text{QCD}}^2)$ was determined such that the NJL model reproduces the normalized transition temperature determined on the lattice. In the fit, the lattice data points are for magnetic fields in the range $0 < |qB| < 1$ GeV^2 . This way of determining the effective coupling leads to a temperature-dependent average $\frac{1}{2}(\Sigma_u + \Sigma_d)$ that qualitatively looks like the plot in Fig. 43. The resulting normalized transition temperature $T_c^x/T_c^x(B=0)$ together with lattice data points are shown in Fig. 46.

The B -dependent coupling $G_s(|qB|/\Lambda_{\text{QCD}}^2)$ was subsequently used as input to a PNJL cal-

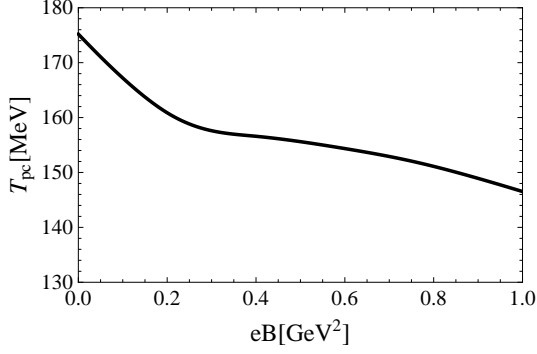


FIG. 45 Pseudocritical temperature T_{pc} temperature as a function of the magnetic field B in the NJL model. Figure taken from Farias *et al.* (2014).

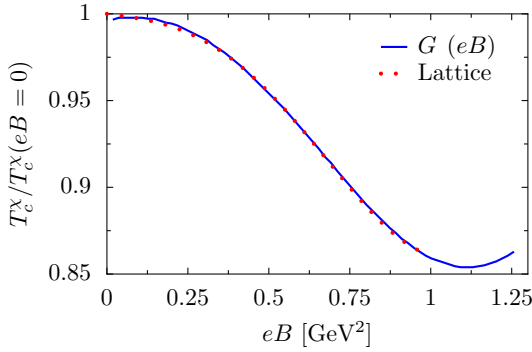


FIG. 46 Normalized pseudocritical temperature $T_c^X/T_c^X(B=0)$ as a function of $|qB|$ in the NJL model. Figure taken from Ferreira *et al.* (2014a).

ulation of the critical temperature for the chiral as well as the deconfinement transition. In the calculations, they used the value $T_0 = 210$ MeV for the parameter in the Polyakov loop potential. The result is displayed in Fig. 47, where it is seen that a gap of approximately 30 MeV between the two transitions persists for all values of $|qB|$, with T_c for the chiral transition being higher as before. The interesting feature here is not the gap as such since this can probably be tuned by using a different value of T_0 ; rather it is the similar behavior of the curves.

In a recent paper, Ferrer *et al.* (2014a) studied the possibility of inverse magnetic catalysis using the NJL model in the lowest-Landau-level approximation. The starting point is the gap M

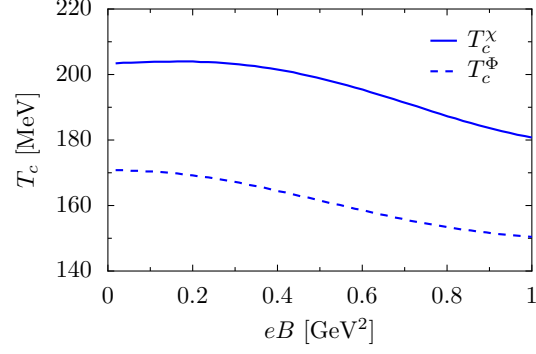


FIG. 47 Pseudocritical temperatures for the chiral (solid line) and deconfinement (dashed line) transitions as functions of $|qB|$ in the PNJL model. Figure taken from Ferreira *et al.* (2014a).

at zero temperature, which is given by

$$M = \frac{2G\Lambda}{G + G'} \exp \left[\frac{-2\pi^2}{(G + G')N_c|q_f B|} \right] \quad (204)$$

where G' is given by Eq. (103) and the condensate ξ is given by Eq. (105). In this approximation, the phase transition is of second order and the critical temperature is given by

$$T_c = 1.16\sqrt{|q_f B|} \exp \left[-\frac{2\pi^2}{(G + G')N_c|q_f B|} \right]. \quad (205)$$

In the absence of a magnetic field, the coupling constant G is related to the strong coupling constant α_s via one-gluon exchange as $G = 4\pi\alpha_s/\Lambda^2$. In a magnetic field, the strong coupling splits into α_s^\parallel and α_s^\perp , and only the latter depends on B . Since $|q_f B|$ effectively acts as a cutoff in the LLL approximation, the effective coupling becomes $G = 4\pi\alpha_s^\parallel/|q_f B|$ and so the critical temperature goes like

$$T_c = 1.16\sqrt{|q_f B|} \exp \left[-\frac{\pi}{2N_c\alpha_s^\parallel} \right]. \quad (206)$$

Since α_s^\parallel is a decreasing function of the magnetic field (Ferrer *et al.*, 2014a), it is clear that T_c decreases with B .

Finally, we mention that there have been attempts at obtaining inverse magnetic catalysis by varying the Yukawa coupling g in the QM

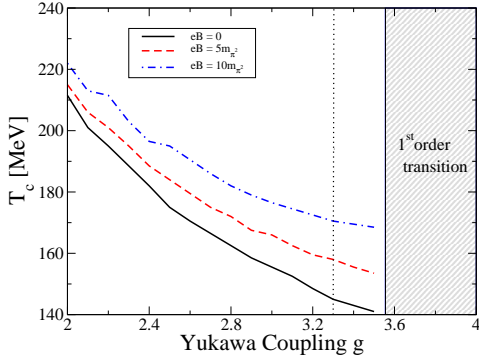


FIG. 48 T_c as a function of the Yukawa coupling g for various values of B . $B = 0$: black solid line, $|qB| = 5m_\pi^2$: red dashed line, and $|qB| = 10m_\pi^2$: blue dash-dotted line. Figure taken from Fraga *et al.* (2014).

model (Fraga *et al.*, 2014). This is possible if g is an increasing function of B , see Fig. 48. However, any curve $g(B)$ must start at $g(0) = 3.22$ (indicated by the vertical dotted line) and successively cross the red and black curves. One therefore soon enters the shaded region which indicates a first-order transition in the QM model. Since lattice results show that the transition is a crossover, magnetic catalysis is ruled out.

Motivated by the recent work on inverse magnetic catalysis at finite temperature, Andersen *et al.* (2014b) studied the quark-meson model using both dimensional regularization and a sharp cutoff Λ_{UV} . The critical temperature for the chiral transition was calculated as a function of the Yukawa coupling using different values of a sharp cutoff. The results are shown in Fig. 49. The results using dimensional regularization and a renormalization scale of $\Lambda = 100$ MeV and a low value for the sharp cutoff are in qualitative agreement with the results of Fraga *et al.* (2014), namely a decreasing transition temperature as a function of g .¹⁶ At larger values of the sharp cutoff, i.e. for more reasonable cutoffs, the transition temperature is an increasing function of the Yukawa coupling. This suggests that magnetic catalysis is much more delicate than using a B -dependent cou-

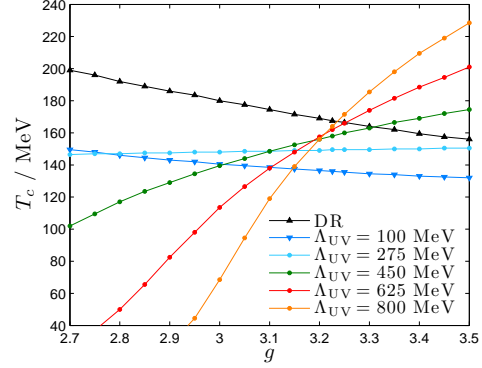


FIG. 49 Critical temperature as a function of the Yukawa coupling g for various values of the sharp cutoff as well as a renormalization scale of $\Lambda = 100$ MeV. Figure taken from Andersen *et al.* (2014b).

pling constant, cf. the discussion of the sea and valence effects in Sec. IX.

XI. ANISOTROPIC PRESSURE AND MAGNETIZATION

A constant magnetic field B along the z -axis breaks Lorentz invariance. One of the consequences is that the pressure is anisotropic: the pressure parallel to the magnetic field $\mathcal{P}_\parallel \equiv \mathcal{P}_z$ is different from the pressure perpendicular to the magnetic field $\mathcal{P}_\perp \equiv \frac{1}{2}(\mathcal{P}_x + \mathcal{P}_y)$. In this section, we review this topic and show how \mathcal{P}_\parallel and \mathcal{P}_\perp are related to the different components of the energy-momentum tensor (Strickland *et al.*, 2012). We will use a Bose gas as a specific example.

The energy density \mathcal{E} and the components of the pressure \mathcal{P}_i ($i = x, y, z$) are given by the total derivatives of the partition function

$$\mathcal{E} = -\frac{1}{V} \frac{d \ln \mathcal{Z}}{d\beta}, \quad (207)$$

$$\mathcal{P}_i = \frac{L_i}{\beta V} \frac{d \ln \mathcal{Z}}{dL_i}, \quad (208)$$

where the quantization volume is $V = L_x L_y L_z$. Taking the derivatives in Eq. (208) with respect to L_x or L_y , it is essential to distinguish between two cases; in the first case, one keeps the magnetic field B fixed and in the second case, one keeps the magnetic flux Φ fixed (Bali *et al.*,

¹⁶ The result in DR is insensitive to precise value of Λ .

2013). In the first case, a total derivative with respect to L_x or L_y can be replaced by a partial derivative, while in the second case, we must take into account the implicit dependence of L_x or L_y on the magnetic field B into account. These two cases are referred to as the B -scheme and the Φ -scheme, respectively. With obvious notation, we can write the pressures as

$$\mathcal{P}_i^B = \frac{L_i}{\beta V} \frac{\partial \ln \mathcal{Z}}{\partial L_i}, \quad (209)$$

$$\mathcal{P}_i^\Phi = \frac{L_i}{\beta V} \frac{\partial \ln \mathcal{Z}}{\partial L_i} + \frac{L_i}{\beta V} \frac{\partial \ln \mathcal{Z}}{\partial B} \frac{\partial B}{\partial L_i}. \quad (210)$$

Using the definition of the magnetization, $q\mathcal{M} = \frac{1}{\beta V} \frac{\partial \ln \mathcal{Z}}{\partial B}$ and $BL_x L_y = \Phi = \text{const}$, we can write

$$\mathcal{P}_{x,y}^P = \mathcal{P}_z^B, \quad (211)$$

$$\mathcal{P}_z^\Phi = \mathcal{P}_z^B, \quad (212)$$

$$\mathcal{P}_{x,y}^\Phi = \mathcal{P}_{x,y}^B - qBM. \quad (213)$$

Finally, we note that the energy density is the same, $\mathcal{E}^B = \mathcal{E}^\Phi$.

We next relate the pressure defined above to the expectation value of various components of the energy-momentum tensor. The conventional energy-momentum tensor $\mathcal{T}_{\mu\nu}$ in a constant magnetic background is given by

$$\mathcal{T}_{\mu\nu} = \frac{\partial \mathcal{L}}{\partial (\partial^\mu \phi)} \partial_\nu \phi - \eta_{\mu\nu} \mathcal{L}. \quad (214)$$

For a massive complex bosonic field coupled to an external Abelian gauge field A_μ with Lagrangian $\mathcal{L} = (D_\mu \Phi)^\dagger (D^\mu \Phi) - m^2 \Phi^\dagger \Phi$, the energy-momentum tensor reads

$$\mathcal{T}_{\mu\nu} = (\partial_\mu \Phi)^\dagger (D_\nu \Phi) + (D_\mu \Phi)^\dagger (\partial_\nu \Phi) - \eta_{\mu\nu} \mathcal{L}. \quad (215)$$

However, this definition is neither gauge invariant nor symmetric (Ferrer *et al.*, 2010; Strickland *et al.*, 2012). There is another definition of $\mathcal{T}_{\mu\nu}$ that guarantees it is gauge invariant and symmetric. The method is that of

metric perturbations, which is based on the fact that matter fields couple to gravity and that the energy-momentum tensor acts as a source for it. The energy-momentum tensor is found by calculating the relation between the variation of the metric and the variation of the action according to

$$\delta S = \frac{1}{2} \int d^4x \sqrt{-g} \mathcal{T}^{\mu\nu} \delta g_{\mu\nu},$$

where the action is

$$S = \int d^4x \sqrt{-g} [\mathcal{L}_{\text{scalar}} + \mathcal{L}_{\text{EM}}]. \quad (216)$$

Here g is minus the determinant of the metric $g_{\mu\nu}$ and the Lagrangian densities are (Birrell and Davies, 1982)

$$\mathcal{L}_{\text{EM}} = -\frac{1}{4} F^{\alpha\beta} F^{\gamma\delta} g_{\alpha\gamma} g_{\beta\delta}, \quad (217)$$

$$\mathcal{L}_{\text{scalar}} = (D^\alpha \Phi)^\dagger (D^\beta \Phi) g_{\alpha\beta} - m^2 \Phi^\dagger \Phi. \quad (218)$$

In order to proceed, we need the variation of $\sqrt{-g}$, which is given by $\delta\sqrt{-g} = -\frac{1}{2}\sqrt{-g}g^{\mu\nu}\delta g_{\mu\nu}$. Using this and calculating the variation of the terms in Eqs. (217) and (218), one can calculate the variation δS and read off the energy-momentum tensor using Eq. (216). This yields $\mathcal{T}_{\mu\nu} = \mathcal{T}_{\mu\nu}^{\text{EM}} + \mathcal{T}_{\mu\nu}^{\text{scalar}}$, where

$$\mathcal{T}_{\mu\nu}^{\text{EM}} = -\mathcal{F}_{\mu\alpha} F_\nu^\alpha - \eta_{\mu\nu} \mathcal{L}_{\text{EM}}, \quad (219)$$

$$\mathcal{T}_{\mu\nu}^{\text{scalar}} = 2(D_\mu \Phi)^\dagger (D_\nu \Phi) - \eta_{\mu\nu} \mathcal{L}_{\text{scalar}}, \quad (220)$$

where we have made the replacement $g_{\mu\nu} \rightarrow \eta_{\mu\nu}$ at the end. Clearly, the expressions Eqs. (219) and (220) are symmetric and gauge invariant. Note that $\mathcal{T}_{\mu\nu}^{\text{EM}}$ is traceless, while $\mathcal{T}_{\mu\nu}^{\text{scalar}}$ is traceless only in the massless case in 1+1 dimensions.

Specializing to a constant magnetic field B , one finds $\mathcal{T}_{\mu\nu}^{\text{EM}} = \frac{1}{2} \text{diag}(B^2, B^2, B^2, -B^2)$ and

$$\mathcal{T}_{00}^{\text{scalar}} = (\partial_0 \Phi)^\dagger (\partial_0 \Phi) + (\partial_z \Phi)^\dagger (\partial_z \Phi) + (D_\perp \Phi)^\dagger (D_\perp \Phi) + m^2 \Phi^\dagger \Phi, \quad (221)$$

$$\mathcal{T}_{zz}^{\text{scalar}} = (\partial_0 \Phi)^\dagger (\partial_0 \Phi) + (\partial_z \Phi)^\dagger (\partial_z \Phi) - (D_\perp \Phi)^\dagger (D_\perp \Phi) - m^2 \Phi^\dagger \Phi, \quad (222)$$

$$\frac{1}{2}(\mathcal{T}_{xx}^{\text{scalar}} + \mathcal{T}_{yy}^{\text{scalar}}) = (\partial_0 \Phi)^\dagger (\partial_0 \Phi) - (\partial_z \Phi)^\dagger (\partial_z \Phi) - m^2 \Phi^\dagger \Phi, \quad (223)$$

where we have defined $(D_\perp \Phi)^\dagger (D_\perp \Phi) = (D_x \Phi)^\dagger (D_x \Phi) + (D_y \Phi)^\dagger (D_y \Phi)$. The next step is to calculate expectation values of the different components of $\mathcal{T}_{\mu\nu}$. By scaling the coordinate z by a factor ξ , the partial derivative transforms as $\partial_z \rightarrow \frac{1}{\xi} \partial_z$. One can show that the expectation value of \mathcal{T}_{zz} can be expressed as a derivative of the partition function (Ferrer *et al.*, 2010),

$$\langle \mathcal{T}_{zz} \rangle = \frac{L_z}{\beta V} \frac{d \ln \mathcal{Z}}{d L_z}, \quad (224)$$

and equals the pressure \mathcal{P}_{zz} in both schemes. If one scales the x and y coordinates in the same manner, the covariant derivative transforms in the same way as a partial derivative only if the strength of the magnetic field transforms as $B \rightarrow \frac{B}{\xi^2}$. This is the Φ -scheme as defined above. One then finds

$$\frac{1}{2} \langle \mathcal{T}_{xx}^{\text{scalar}} + \mathcal{T}_{yy}^{\text{scalar}} \rangle = \frac{1}{2} \frac{1}{\beta V} \left[L_x \frac{d \ln \mathcal{Z}}{d L_x} + L_y \frac{d \ln \mathcal{Z}}{d L_y} \right]. \quad (225)$$

Since this corresponds to the Φ -scheme, we conclude that

$$\langle \mathcal{T}_{xx} + \mathcal{T}_{yy} \rangle = \mathcal{P}_{xx}^\Phi + \mathcal{P}_{yy}^\Phi. \quad (226)$$

Let us close this section by discussing the magnetization, which is defined by

$$\mathcal{M} = \frac{1}{\beta V} \frac{1}{q} \frac{\partial \ln \mathcal{Z}}{\partial B}. \quad (227)$$

One is not interested in the $\mathcal{O}(B^2)$ contribution to the pressure coming from the external magnetic field. Using the renormalization given by Eq. (130), this term is given by B_r^2 in Eq. (131) and is subtracted (Bali *et al.*, 2013; Endrődi, 2013). The magnetization as a function of the magnetic field at $T = 0$ has been calculated on the lattice by Bali *et al.* (2013) using various lattice spacings and the results are shown in Fig. 50. For comparison, the result from the HRG calculation of Endrődi (2013) is also shown (red line). Note that as a result of the subtraction mentioned above, the magnetization is positive, suggesting that the QCD vacuum is paramagnetic.

XII. CONCLUSIONS AND OUTLOOK

In this review, we have discussed a number of low-energy models and theories that are used to describe QCD in a magnetic background at zero and finite temperature.

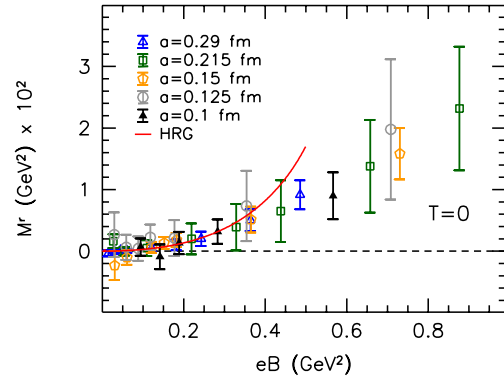


FIG. 50 Magnetization at zero temperature as a function of the magnetic field calculated on the lattice for different lattice spacings. Red curve is the result from the HRG calculation by Endrődi (2013). Figure taken from Bali *et al.* (2013).

One aspect we think is missing in the literature is systematic studies of various approximations. As we have discussed, parameter fixing is important and nontrivial. There are many papers in which the authors employ a certain model and a specific set of parameters. However, it would be very useful to compare various approximations and levels of sophistication using the same values for physical quantities. For example, it would be useful to calculate the critical temperature or the magnetization in the

NJL model and its Polyakov-loop extended version and compare the two. One of the few papers where a systematic study is carried out is by Kamikado and Kanazawa (2014a), where the critical temperature is calculated in the mean-field approximation, in the LPA, and beyond the LPA.

It is instructive to compare the results of the (P)NJL model and the (P)QM model at the mean-field level. In this case, only fermionic fluctuations are taken into account. If one takes into account the vacuum fluctuations of the (P)QM model, the results are similar. For example, the nature of the transition is the same and the phase diagrams closely resemble each other. This is not surprising as one is essentially evaluating the same fermionic functional determinant. However, we have seen that if the vacuum contribution is omitted in the (P)QM model, the crossover at finite pion mass turns into a first-order transition. In the same manner, the second-order transition in the chiral limit becomes first order. In the (P)NJL model it makes no sense to subtract the vacuum fluctuations as they are responsible for spontaneous symmetry breaking in the vacuum. In the (P)QM model, spontaneous symmetry breaking is present already at tree level provided by the quartic Higgs potential.

Regarding the calculations using the functional renormalization group, there are several directions for further improvement. For the physically most interesting cases $N_f = 2$ and $N_f = 3$ (see Kamikado and Kanazawa (2014b) for a recent application with $N_f = 2 + 1$), one should solve the flow equation for the effective potential as a function of the two invariants ρ and Δ , including wavefunction renormalization terms in the calculations. One might consider another regulator function that ensures $Z_{k=0}^{\parallel} = Z_{k=0}^{\perp}$ in the vacuum. Finally, including new condensates that are invariant under rotations about the z -axis is of interest. However, this requires the inclusion of new interaction terms in the Lagrangian of the quark-meson model and the problem is that one does not know the value of their couplings.

The most important issue that we have discussed, is the disagreement between model and

lattice calculations regarding the behavior of the transition temperature as a function of the magnetic field. On the lattice, two contributions to the quark condensate have been identified, namely the valence and the sea contribution. While the former increases as a function of B for all temperatures, the behavior of the latter is more complicated. At zero temperature the sea contribution is also increasing with the magnetic field and together with the valence contribution, they give rise to magnetic catalysis. Around the transition temperature, however, it decreases as a function of B for physical quark masses. The sea contribution overwhelms the valence contribution such that there is a net suppression of the condensate, which leads to inverse magnetic catalysis and a decrease of the transition temperature as a function of B . The mechanism behind this effect is that the magnetic field in the quark determinant changes the relative weight of the gauge configurations and that gauge configurations with larger values of the condensate are suppressed by the quark determinant (Bruckmann *et al.*, 2013). Moreover, using staggered fermions, the back-reaction of the quark determinant on the glue sector is very delicate; small quark masses lead to inverse catalysis while large values lead to magnetic catalysis. This dependence on the quark mass may very well be different if one uses chiral fermions. Calculations employing the (P)NJL model or the (P)QM show a different behavior; the transition temperature increases with the strength of the magnetic field. In hindsight, this disagreement should perhaps not be surprising as there is no sea effect in the (P)NJL and (P)QM models. However, it is interesting to notice that the coupling to the Polyakov loop in the QM model, gives less magnetic catalysis around the transition temperature than without, cf. Fig. 23. Regarding the attempts to modify models to accommodate inverse magnetic catalysis, most of them do not couple the Polyakov loop variable to the quark determinant and therefore does not include the underlying mechanism. The idea of using a B -dependent parameter T_0 in the Polyakov loop potential was implemented by Fraga *et al.* (2014); however, it was shown not to lead to magnetic catalysis.

In conclusion, although the level of complexity and sophistication in model calculations of the QCD transition in a magnetic background are steadily improving, it remains a challenge to properly incorporate the phenomenon of inverse magnetic catalysis.

ACKNOWLEDGMENTS

The authors would like to thank G. Bali, D. Boer, T. Brauner, F. Bruckmann, M. Chernodub, P. Costa, G. Endrodi, E. S. Fraga, V. de la Incera, T. Kalaydzhyan K. Kamikado, T. Kanazawa, S. Ozaki, M. B. Pinto, A. Schmitt, L. von Smekal, R. Stiele, M. Strickland, and P. Watson. for useful discussions. We also thank the authors who have granted us permission to use their figures in this review.

Appendix A: Notation and conventions

We use the Minkowski metric $g_{\mu\nu} = \text{diag}(1, -1, -1, -1)$ and natural units such that $k_B = \hbar = c = 1$.

We will be using the Dirac and chiral representations of the γ -matrices. In Minkowski space they are given respectively by

$$\gamma^0 = \begin{pmatrix} 1 & 0 \\ 0 & -1 \end{pmatrix}, \quad \gamma = \begin{pmatrix} 0 & \boldsymbol{\sigma} \\ -\boldsymbol{\sigma} & 0 \end{pmatrix}, \quad (\text{A1})$$

$$\gamma^0 = \begin{pmatrix} 0 & 1 \\ 1 & 0 \end{pmatrix}, \quad \gamma = \begin{pmatrix} 0 & \boldsymbol{\sigma} \\ -\boldsymbol{\sigma} & 0 \end{pmatrix}, \quad (\text{A2})$$

where $\boldsymbol{\sigma} = (\sigma_x, \sigma_y, \sigma_z)$ are the Pauli spin matrices. The Euclidean γ -matrices are related to the γ^μ -matrices in Minkowski space by $\gamma_j = i\gamma^j$ and $\gamma_4 = \gamma^0$. They satisfy

$$\{\gamma_\mu, \gamma_\nu\} = 2\delta_{\mu\nu} \mathbf{1}, \quad \text{Tr}[\gamma_\mu \gamma_\nu] = 4\delta_{\mu\nu}, \quad (\text{A3})$$

where $\mathbf{1}$ is the unit matrix in four dimensions.

Appendix B: Sum-integrals

The bosonic and fermionic sum-integrals are defined by

$$\oint_P = T \sum_{P_0=2\pi nT} \int_p, \quad (\text{B1})$$

$$\oint_{\{P\}} = T \sum_{P_0=(2\pi+1)nT} \int_p, \quad (\text{B2})$$

where $P_0 = 2\pi nT$ for bosons and $P_0 = (2n+1)\pi T$ for fermions. where the integral over p is

$$\int_p = \left(\frac{e^{\gamma_E} \Lambda^2}{4\pi} \right)^\epsilon \int \frac{d^d p}{(2\pi)^d}, \quad (\text{B3})$$

and where $d = 3 - 2\epsilon$. The prefactor $\left(\frac{e^{\gamma_E} \Lambda^2}{4\pi} \right)^\epsilon$ is chosen such that Λ is associated with renormalization scale in the modified minimal subtraction scheme $\overline{\text{MS}}$. Here γ_E is the Euler-Mascheroni constant. In the case of particles with electric charge q moving in a constant magnetic field, the sum-integral is a sum over Matsubara frequencies P_0 , a sum of Landau levels k , and an integral over momenta in $d = 1 - 2\epsilon$ dimensions. For fermions, we also sum over spin s . We define for bosons and fermions, respectively

$$\oint_P^B = \frac{|qB|}{2\pi} T \sum_{k=0}^{\infty} \sum_{P_0=2\pi nT} \int_{p_z}, \quad (\text{B4})$$

$$\oint_{\{P\}}^B = \frac{|q_f B|}{2\pi} T \sum_{s=\pm 1} \sum_{k=0}^{\infty} \sum_{P_0=(2n+1)\pi T} \int_{p_z} \quad (\text{B5})$$

where the integral is

$$\int_{p_z} = \left(\frac{e^{\gamma_E} \Lambda^2}{4\pi} \right)^\epsilon \int \frac{d^{d-2} p}{(2\pi)^{d-2}}. \quad (\text{B6})$$

Eqs. (B4) and (B5) reduce to Eqs. (B1) and (B2) in the limit $B \rightarrow 0$.

The specific sum-integrals we need are

$$\oint_P \ln [P_0^2 + p^2 + m^2] = -\frac{1}{2(4\pi)^2} \left(\frac{\Lambda^2}{m^2} \right)^\epsilon \left[\left(\frac{1}{\epsilon} + \frac{3}{2} \right) m^4 + 2J_0(\beta m) T^4 + \mathcal{O}(\epsilon) \right], \quad (\text{B7})$$

$$\begin{aligned} \oint_P^B \ln [P_0^2 + p_z^2 + M_B^2] &= \frac{1}{2(4\pi)^2} \left(\frac{\Lambda^2}{|2qB|} \right)^\epsilon \left[\left(\frac{(qB)^2}{3} - m^4 \right) \left(\frac{1}{\epsilon} + 1 \right) \right. \\ &\quad \left. + 8(qB)^2 \zeta^{(1,0)}(-1, \frac{1}{2} + x) - 2J_0^B(\beta m) |qB| T^2 + \mathcal{O}(\epsilon) \right], \end{aligned} \quad (\text{B8})$$

$$\oint_{\{P\}} \ln [P_0^2 + p^2 + m_f^2] = -\frac{1}{2(4\pi)^2} \left(\frac{\Lambda^2}{m_f^2} \right)^\epsilon \left[\left(\frac{1}{\epsilon} + \frac{3}{2} \right) m_f^4 - 2K_0(\beta m_f) T^4 + \mathcal{O}(\epsilon) \right], \quad (\text{B9})$$

$$\begin{aligned} \oint_{\{P\}}^B \ln [P_0^2 + p_z^2 + M_B^2] &= -\frac{1}{(4\pi)^2} \left(\frac{\Lambda^2}{|2qB|} \right)^\epsilon \left[\left(\frac{2(qB)^2}{3} + m_f^4 \right) \left(\frac{1}{\epsilon} + 1 \right) - 8(qB)^2 \zeta^{(1,0)}(-1, x) \right. \\ &\quad \left. - 2|q_f B| m_f^2 \ln x_f - 2K_0^B(\beta m_f) |q_f B| T^2 + \mathcal{O}(\epsilon) \right], \end{aligned} \quad (\text{B10})$$

$$\oint_P \frac{1}{(P_0^2 + p^2 + m^2)} = -\frac{1}{(4\pi)^2} \left(\frac{\Lambda^2}{m^2} \right)^\epsilon \left[\left(\frac{1}{\epsilon} + 1 \right) m^2 - J_1(\beta m) T^2 + \mathcal{O}(\epsilon) \right], \quad (\text{B11})$$

$$\begin{aligned} \oint_P^B \frac{1}{(P_0^2 + p_z^2 + M_B^2)} &= -\frac{1}{(4\pi)^2} \left(\frac{\Lambda^2}{|2qB|} \right)^\epsilon \left[\frac{1}{\epsilon} m^2 - \zeta^{(1,0)}(0, \frac{1}{2} + x_f) |qB| \right. \\ &\quad \left. - J_1^B(\beta m) |qB| + \mathcal{O}(\epsilon) \right], \end{aligned} \quad (\text{B12})$$

$$\oint_{\{P\}} \frac{1}{(P_0^2 + p_z^2 + m_f^2)} = -\frac{1}{(4\pi)^2} \left(\frac{\Lambda^2}{m_f^2} \right)^\epsilon \left[\left(\frac{1}{\epsilon} + 1 \right) m_f^2 + K_1(\beta m_f) T^2 + \mathcal{O}(\epsilon) \right] \quad (\text{B13})$$

$$\begin{aligned} \oint_{\{P\}}^B \frac{1}{(P_0^2 + p_z^2 + M_B^2)} &= -\frac{1}{(4\pi)^2} \left(\frac{\Lambda^2}{|2qB|} \right)^\epsilon \left[\frac{1}{\epsilon} m_f^2 - 2\zeta^{(1,0)}(0, x) |q_f B| + K_1^B(\beta m_f) |q_f B| + \mathcal{O}(\epsilon) \right], \end{aligned} \quad (\text{B14})$$

where $x = \frac{m^2}{2|qB|}$, $x_f = \frac{m_f^2}{2|q_f B|}$. The bosonic and fermionic masses are $M_B = \sqrt{p_z^2 + m^2 + |qB|(2k+1)}$ and $M_B = \sqrt{p_z^2 + m_f^2 + |q_f B|(2k+1-s)}$, respectively. The generalized zeta-function is defined by $\zeta(s, q) = \sum_{k=0}^{\infty} \frac{1}{(q+k)^s}$. The thermal functions $J_n(\beta M)$, $J_n^B(\beta M)$, $K_n(\beta m_f)$, and $K_n^B(\beta m_f)$ are defined

$$J_n(\beta m) = \frac{4e^{\gamma_E \epsilon} \Gamma(\frac{1}{2})}{\Gamma(\frac{5}{2} - n - \epsilon)} \beta^{4-2n} m^{2\epsilon} \int_0^\infty \frac{p^{4-2n-2\epsilon} dp}{\sqrt{p^2 + m^2}} \frac{1}{e^{\beta \sqrt{p^2 + m^2}} - 1}, \quad (\text{B15})$$

$$J_n^B(\beta m) = \frac{8e^{\gamma_E \epsilon} \Gamma(\frac{1}{2})}{\Gamma(\frac{3}{2} - n - \epsilon)} \beta^{2-2n} (|2qB|)^\epsilon \sum_{k=0}^{\infty} \int_0^\infty \frac{p_z^{2-2n-2\epsilon} dp_z}{\sqrt{p_z^2 + M_B^2}} \frac{1}{e^{\beta \sqrt{p_z^2 + M_B^2}} - 1}, \quad (\text{B16})$$

$$K_n(\beta m_f) = \frac{4e^{\gamma_E \epsilon} \Gamma(\frac{1}{2})}{\Gamma(\frac{5}{2} - n - \epsilon)} \beta^{4-2n} m_f^{2\epsilon} \int_0^\infty \frac{p^{4-2n-2\epsilon} dp}{\sqrt{p^2 + m_f^2}} \frac{1}{e^{\beta \sqrt{p^2 + m_f^2}} + 1}, \quad (\text{B17})$$

$$K_n^B(\beta m_f) = \frac{4e^{\gamma_E \epsilon} \Gamma(\frac{1}{2})}{\Gamma(\frac{3}{2} - n - \epsilon)} \beta^{2-2n} (|2qB|)^\epsilon \sum_{s=\pm 1} \sum_{k=0}^{\infty} \int_0^\infty \frac{p_z^{2-2n-2\epsilon} dp_z}{\sqrt{p_z^2 + M_B^2}} \frac{1}{e^{\beta \sqrt{p_z^2 + M_B^2}} + 1}. \quad (\text{B18})$$

The sum over Matsubara frequencies is

$$\frac{1}{2} T \sum_{P_0} \ln [P_0^2 + \omega^2] = \frac{1}{2} \omega + T \ln [1 \pm e^{-\beta \omega}], \quad (\text{B19})$$

where the upper sign is for fermions and the lower signs is for bosons.

Appendix C: Small and large- B expansions

In this appendix we list a number small and large- B expansions of various ζ -functions. The small- x expansions of the various derivatives of the Hurwitz zeta-functions are

$$\zeta^{(1,0)}(-1, x) = \zeta'(-1) + \frac{1}{2}x - \frac{1}{2}\ln(2\pi)x - x\ln x + \mathcal{O}(x^2) , \quad (\text{C1})$$

$$\zeta^{(1,0)}(-1, \frac{1}{2} + x) = -\frac{1}{2}\zeta'(-1) - \frac{1}{24}\ln 2 - \frac{1}{2}x\ln 2 + \mathcal{O}(x^2) , \quad (\text{C2})$$

$$\zeta^{(1,0)}(0, x) = -\frac{1}{2}\ln(2\pi) - \ln x - \gamma_E x + \mathcal{O}(x^2) , \quad (\text{C3})$$

$$\zeta^{(1,0)}(0, \frac{1}{2} + x) = -\frac{1}{2}\ln 2 - 2\ln 2x - x\gamma_E + \mathcal{O}(x^2) , \quad (\text{C4})$$

where $\zeta'(-1) = \frac{1}{12} - \ln(A) \approx -0.165421$ and A is the Glaisher-Kinkelin constant. The large- x expansion of the the various derivatives of the Hurwitz zeta-functions are

$$\zeta^{(1,0)}(-1, x) = -\frac{1}{4}x^2 + \frac{1}{2}x^2\ln x - \frac{1}{2}x\ln x + \frac{1}{12}\ln x + \frac{1}{12} + \mathcal{O}\left(\frac{1}{x^2}\right) , \quad (\text{C5})$$

$$\zeta^{(1,0)}(-1, \frac{1}{2} + x) = -\frac{1}{4}x^2 + \frac{1}{2}x^2\ln x - \frac{1}{24}\ln x - \frac{1}{24} + \mathcal{O}\left(\frac{1}{x^2}\right) , \quad (\text{C6})$$

$$\zeta^{(1,0)}(0, x) = x\ln x - x - \frac{1}{2}\ln x + \frac{1}{12x} + \mathcal{O}\left(\frac{1}{x^3}\right) , \quad (\text{C7})$$

$$\zeta^{(1,0)}(0, \frac{1}{2} + x) = x\ln x - x - \frac{1}{24x} + \mathcal{O}\left(\frac{1}{x^3}\right) . \quad (\text{C8})$$

Appendix D: Propagators in a magnetic background

In this Appendix, we briefly discuss the boson and propagator in a constant magnetic background. Denoting the bosonic propagator in coordinate space by $\Delta(x, x')$, it satisfies the equation

$$\left[\partial_{x^0}^2 - \partial_{x^3}^2 - \partial_{x^1}^2 - (\partial_{x^2} - iqA_2)^2 + m^2 \right] \Delta(x, x') = \delta^4(x - x') , \quad (\text{D1})$$

where we have chosen the Landau gauge, $A^\mu = (0, 0, Bx, 0)$. We next introduce the propagator $\Delta(\mathbf{p}_\parallel, \mathbf{x}_\perp, \mathbf{x}'_\perp)$ via the Fourier transform

$$\Delta(x, x') = \int \frac{d^2 p_\parallel}{(2\pi)^2} e^{-i\mathbf{p}_\parallel(\mathbf{x}_\parallel - \mathbf{x}'_\parallel)} \Delta(\mathbf{p}_\parallel, \mathbf{x}_\perp, \mathbf{x}'_\perp) , \quad (\text{D2})$$

where $\mathbf{p}_\parallel = (p_0, p_3)$, $\mathbf{x}_\parallel = (x^0, x^3)$, and $\mathbf{x}_\perp = (x^1, x^2)$. Inserting Eq. (D2) into Eq. (D1), we obtain

$$\left[-p_0^2 + p_3^2 + m^2 - \partial_{x^1}^2 - \left(\frac{\partial}{\partial x^2} - iqBx \right)^2 \right] \Delta(\mathbf{p}_\parallel, \mathbf{x}_\perp, \mathbf{x}'_\perp) = \delta^2(\mathbf{x}_\perp - \mathbf{x}'_\perp) . \quad (\text{D3})$$

We next need a complete set of eigenfunctions of the operator $\partial_{x^1}^2 + \left(\frac{\partial}{\partial x^2} + iqBx \right)^2$, which are the well-known solutions involving the Hermite polynomials $H_k(x)$. The normalized wavefunctions are

$$\psi_{k,p_2}(\mathbf{x}_\perp) = \frac{1}{\sqrt{2\pi l}} \frac{1}{\sqrt{2^k k! \sqrt{\pi}}} H_k\left(\frac{x^1}{l} + p_2 l\right) e^{-\frac{1}{2l^2}(x^1 + p_2 l^2)^2} e^{isx^2 p_2} , \quad (\text{D4})$$

where $s_{\perp} = \text{sign}(qB)$ and $l^2 = 1/|qB|$. These functions satisfy the usual orthonormality and completeness relations:

$$\int d^2x_{\perp} \psi_{k,p_2}^*(\mathbf{x}_{\perp}) \psi_{k',p'_2}(\mathbf{x}_{\perp}) = \delta_{kk'} \delta(p_2 - p'_2), \quad (\text{D5})$$

$$\int_{-\infty}^{\infty} dp_2 \sum_{k=0}^{\infty} \psi_{k,p_2}(\mathbf{x}_{\perp}) \psi_{k,p_2}^*(\mathbf{x}'_{\perp}) = \delta^2(\mathbf{x}_{\perp} - \mathbf{x}'_{\perp}). \quad (\text{D6})$$

Using the completeness relation (D6), the propagator can be written as

$$\Delta(\mathbf{p}_{\parallel}, \mathbf{x}_{\perp}, \mathbf{x}'_{\perp}) = \int_{-\infty}^{\infty} dp_2 \sum_{k=0}^{\infty} \left[-p_0^2 + p_3^2 + m^2 + |qB|(2k+1) \right]^{-1} \psi_{k,p_2}(\mathbf{x}_{\perp}) \psi_{k,p_2}^*(\mathbf{x}'_{\perp}), \quad (\text{D7})$$

which after some algebra can be written as

$$\begin{aligned} \Delta(\mathbf{p}_{\parallel}, \mathbf{x}_{\perp}, \mathbf{x}'_{\perp}) &= \frac{1}{2\pi l} \int_{-\infty}^{\infty} dp_2 \sum_{k=0}^{\infty} \left[-p_0^2 + p_3^2 + m^2 + |qB|(2k+1) \right]^{-1} \frac{1}{2^k k! \sqrt{\pi}} \\ &\times H_k\left(\frac{x^1}{l} + p_2 l\right) H_k\left(\frac{x'^1}{l} + p_2 l\right) e^{-[p_2 l + (x^1 + x'^1)/2l - is(x^2 - x'^2)/2l]^2} \\ &\times e^{-\frac{1}{4l^2}(x^2 - x'^2)^2} e^{\frac{1}{4l^2}(x^1 - x'^1)^2} e^{-\frac{is}{2l^2}(x^1 + x'^1)(x^2 - x'^2)}. \end{aligned} \quad (\text{D8})$$

We next need the following integral

$$\int_{-\infty}^{\infty} dx e^{-x^2} H_k(x+z) H_k(x+w) = 2^k k! \sqrt{\pi} L_k(-2zw), \quad (\text{D9})$$

where $L_k(x)$ is a Laguerre polynomial of order k . In Eq. (D8), we make the substitution $p'_2 = p_2 + (x^1 + x'^1)/2l^2 - i(x^2 - x'^2)/2l^2$ and so we identify $z = (x^1 - x'^1)/2l - i(x^2 - x'^2)/2l$ and $w = -(x^1 - x'^1)/2l - i(x^2 - x'^2)/2l$. This implies that $-2zw = (\mathbf{x}_{\perp} - \mathbf{x}'_{\perp})^2/2l^2$ and we can write

$$\begin{aligned} \Delta(\mathbf{p}_{\parallel}, \mathbf{x}_{\perp}, \mathbf{x}'_{\perp}) &= \frac{1}{2\pi l^2} \sum_{k=0}^{\infty} \left[-p_0^2 + m^2 + p_3^2 + |qB|(2k+1) \right]^{-1} e^{-\frac{1}{4l^2}(\mathbf{x}_{\perp} - \mathbf{x}'_{\perp})^2} L_k\left(\frac{(\mathbf{x}_{\perp} - \mathbf{x}'_{\perp})^2}{2l^2}\right) \\ &\times e^{-is\Phi(\mathbf{x}_{\perp}, \mathbf{x}'_{\perp})}, \end{aligned} \quad (\text{D10})$$

where the so-called Schwinger phase is

$$\Phi(\mathbf{x}_{\perp}, \mathbf{x}'_{\perp}) = \frac{(x^1 + x'^1)(x^2 - x'^2)}{2l^2}. \quad (\text{D11})$$

The propagator in Eq. (D10) is now a product of a translationally invariant part and the Schwinger phase. The Fourier transform $\Delta(p_{\perp}, p_{\parallel})$ of the translationally invariant part is

$$\Delta(\mathbf{p}_{\perp}, \mathbf{p}_{\parallel}) = -2e^{-p_{\perp}^2 l^2} \sum_{k=0}^{\infty} \frac{(-1)^k}{p_0^2 - p_z^2 - m^2 - |qB|(2k+1)} L_k(2p_{\perp}^2 l^2). \quad (\text{D12})$$

The term $[p_0^2 - p_z^2 - m^2 - |qB|(2k+1)]$ is rewritten using Schwinger's trick

$$\frac{i}{p_0^2 - p_z^2 - m^2 - |qB|(2k+1)} = \int_0^{\infty} ds e^{is[p_0^2 - p_z^2 - m^2 - |qB|(2k+1)]}. \quad (\text{D13})$$

Using the summation formula for the generalized Laguerre polynomials $L_n^{\alpha}(x)$

$$\sum_{k=0}^{\infty} L_k^{\alpha}(x) z^k = (1-z)^{-(\alpha+1)} e^{\frac{xz}{z-1}}, \quad (\text{D14})$$

the translationally invariant propagator can be written as

$$\Delta(\mathbf{p}_\perp, \mathbf{p}_\parallel) = i \int \frac{ds}{\cos(|qB|s)} \exp \left\{ is \left[\mathbf{p}_\parallel^2 - m^2 \right] - i \mathbf{p}_\perp^2 \frac{\tan(|qB|s)}{|qB|} \right\}, \quad (\text{D15})$$

Finally, the propagator $\Delta(x, x')$ takes the form

$$\Delta(x, x') = e^{i\Phi(\mathbf{x}_\perp, \mathbf{x}'_\perp)} \int \frac{d^4p}{(2\pi)^4} e^{-ip(x-x')} \Delta(\mathbf{p}_\perp, \mathbf{p}_\parallel). \quad (\text{D16})$$

REFERENCES

- Agasian, N. O., and S. M. Fedorov (2008), Phys. Lett. B **663**, 445.
- Agasian, N. O., and I. A. Shushpanov (2000), Phys. Lett. B **472**, 143.
- Agasian, N. O., and I. A. Shushpanov (2001), JHEP **0110**, 006.
- Alford, M., J. Berges, and K. Rajagopal (2000), Nucl. Phys. B **571**, 269.
- Alford, M. G., A. Schmitt, and K. Rajagopal (2008), Rev. Mod. Phys. **80**, 1455.
- Ambjørn, J., and P. Olesen (1989a), Nucl. Phys. B **315**, 606.
- Ambjørn, J., and P. Olesen (1989b), Phys. Lett. B **218**, 67.
- Andersen, J. O. (2012a), Phys. Rev. D **85**, 065026.
- Andersen, J. O. (2012b), JHEP **10**, 005.
- Andersen, J. O., W. R. Naylor, and A. Tranberg (2014a), JHEP **04**, 187.
- Andersen, J. O., W. R. Naylor, and A. Tranberg (2014b), arXiv:1410.5247 [hep-ph].
- Andersen, J. O., and A. Tranberg (2012), JHEP **08**, 002.
- Ayala, A., M. Loewe, A. J. Mizher, and R. Zamora (2014a), Phys. Rev. D **90**, 036001.
- Ayala, A., M. Loewe, and R. Zamora (2014b), arXiv:1406.7408 [hep-ph].
- Bali, G., F. Bruckmann, G. Endrődi, F. Gruber, and A. Schafer (2013), JHEP **04**, 130.
- Bali, G. S., F. Bruckmann, M. Constantinou, M. Costa, G. Endrődi, Z. Fodor, S. D. Katz, S. Krieg, H. Panagopoulos, and A. Schafer (2012a), PoS Confinement , 197.
- Bali, G. S., F. Bruckmann, M. Constantinou, M. Costa, G. Endrődi, S. D. Katz, H. Panagopoulos, and A. Schafer (2012b), Phys. Rev. D **86**, 09412.
- Bali, G. S., F. Bruckmann, G. Endrődi, Z. Fodor, S. D. Katz, S. Krieg, A. Schafer, and K. K. Szabo (2012c), JHEP **1202**, 44.
- Bali, G. S., F. Bruckmann, G. Endrődi, Z. Fodor, S. D. Katz, and A. Schafer (2012d), Phys. Rev. D **86**, 071502.
- Bali, G. S., F. Bruckmann, G. Endrődi, and A. Schafer (2014), PoS LATTICE2013 , 182.
- Banks, T., and A. Casher (1980), Nucl. Phys. B **169**, 103.
- Baym, G., D. Bödeker, and L. D. McLerran (1996), Phys. Rev. D **53**, 662.
- Birrell, N. D., and P. C. W. Davies (1982), *Quantum fields in curved space* (Cambridge University Press, Cambridge, Great Britain).
- Bochkarev, A., and J. I. Kapusta (1996), Phys. Rev. D **54**, 4066.
- Boomsma, J. K., and D. Boer (2009), Phys. Rev. D **80**, 034019.
- Boomsma, J. K., and D. Boer (2010), Phys. Rev. D **81**, 074005.
- Bornyakov, V. G., P. V. Buividovich, N. Cundy, O. A. Kochetkov, and A. Schafer (2014), Phys. Rev. D **90**, 034501.
- Borsanyi, S., G. Endrődi, Z. Fodor, A. Jakovac, S. Krieg, C. Ratti, and K. K. Szabo (2010), JHEP **11**, 077.
- Bowman, E. S., and J. I. Kapusta (2009), Phys. Rev. C **79**, 015202.
- Braguta, V. V., P. V. Buividovich, T. Kalaydzhyan, S. V. Kuznetsov, and M. I. Polikarpov (2012), Phys. Atom. Nucl. **75**, 488.
- Braun, J., W. A. Mian, and S. Rechenberger (2014), arXiv:1412.6025 [hep-ph].
- Brauner, T. (2010), Symmetry **2**, 609.
- Brauner, T., K. Fukushima, and Y. Hidaka (2010), Phys. Rev. D **79**, 074035.
- Bruckmann, F., G. Endrődi, and T. G. Kovacs (2013), JHEP **1304**, 112.
- Buballa, M. (2005), Phys. Rept. **407**, 205.
- Buividovich, P. V., M. N. Chernodub, E. V. Luschevskaya, and M. I. Polikarpov (2010a), Phys. Lett. B **682**, 484.
- Buividovich, P. V., M. N. Chernodub, E. V. Luschevskaya, and M. I. Polikarpov (2010b), Nucl. Phys. B **826**, 313.
- Bzdak, A., and V. Skokov (2012), Phys. Lett. B **710**, 171.

- Callebaut, N., D. Dudal, and H. Verschelde (2013), JHEP **03**, 033.
- Chakrabarty, S. (1996), Phys. Rev. D **54**, 1306.
- Chao, J., P. Chu, and M. Huang (2013), Phys. Rev. D **88**, 054009.
- Chernodub, M. (2010), Phys. Rev. D **82**, 085011.
- Chernodub, M. (2011), Phys. Rev. Lett. **106**, 142003.
- Chernodub, M. (2014), Phys. Rev. D **89**, 018501.
- Chodos, A., R. L. Jaffe, K. Johnson, and C. B. Thorn (1974), Phys. Rev. D **10**, 2599.
- Cohen, T. D., D. A. McGady, and E. S. Werbos (2007), Phys. Rev. C **76**, 055201.
- Coleman, S. (1973), Commun. Math. Phys. **31**, 259.
- Cruz, A. A., and J. O. Andersen (2013), Phys. Rev. D **88**, 025016.
- De Simone, A., G. Nardini, M. Quiros, and A. Riotto (2011), JCAP **1110**, 30.
- D’Elia, M., S. Mukherjee, and F. Sanfilippo (2010), Phys. Rev. D **82**, 051501.
- D’Elia, M., and F. Negro (2011), Phys. Rev. D **83**, 114028.
- Duncan, R. C., and C. Thompson (1992), Astrophys. J. **392**, L9.
- Ebert, D. B., and K. G. Klimenko (2000), Phys. Rev. D **61**, 025005.
- Eguchi, T. (1976), Phys. Rev. D **14**, 2755.
- Einhorn, M. B., and D. R. T. Jones (2007), JHEP **04**, 051.
- Endr di, G. (2013), JHEP **04**, 23.
- Farias, R. L. S., K. P. Gomes, G. I. Krein, and M. B. Pinto (2014), arXiv:1404.3931 [hep-ph].
- Fayazbakhsh, S., and N. Sadooghi (2013), Phys. Rev. D **88**, 065030.
- Fayazbakhsh, S., and N. Sadooghi (2014), arXiv:1408.5457.
- Ferreira, M., P. Costa, O. Lourenco, T. Frederico, and C. Provid ncia (2014a), Phys. Rev. D **89**, 116011.
- Ferreira, M., P. Costa, D. P. Menezes, C. Provid ncia, and N. Scoccola (2014b), Phys. Rev. D **89**, 016002.
- Ferreira, M., P. Costa, and C. Provid ncia (2014c), Phys. Rev. D **90**, 016012.
- Ferrer, E. J., and V. de la Incera (2007), Phys. Rev. D **76**, 045011.
- Ferrer, E. J., V. de la Incera, J. P. Keith, I. Portillo, and P. L. Springsteen (2010), Phys. Rev. C **82**, 065802.
- Ferrer, E. J., V. de la Incera, and C. Manuel (2005), Phys. Rev. Lett. **95**, 152002.
- Ferrer, E. J., V. de la Incera, and C. Manuel (2006), Nucl. Phys. B **747**, 88.
- Ferrer, E. J., V. de la Incera, and X. J. Wen (2014a), arXiv:1407.3503 [nucl-th].
- Ferrer, I., V. de la Incera, I. Portillo, and M. Quiroz (2014b), Phys. Rev. D **89**, 085034.
- Fischer, C. S., A. Maas, and J. M. Pawłowski (2009), Annals of Phys. **324**, 2408.
- Ford, C., D. R. T. Jones, P. W. Stephenson, and M. B. Einhorn (1993), Nucl. Phys. **395**, 17.
- Fraga, E. S., B. W. Mintz, and J. Schaffner-Bielich (2014), Phys. Lett. B **731**, 154.
- Fraga, E. S., and Mizher (2008), Phys. Rev. D **78**, 025016.
- Fraga, E. S., J. Noronha, and L. Palhares (2013), Phys. Rev. D **87**, 114014.
- Fraga, E. S., and L. F. Palhares (2012), Phys. Rev. D **86**, 016008.
- Fukushima, K. (2004), Phys. Lett. B **591**, 277.
- Fukushima, K. (2008), Phys. Rev. D **77**, 114028.
- Fukushima, K., and T. Hatsuda (2011), Rept. Prog. Phys. **74**, 014001.
- Fukushima, K., and Y. Hidaka (2013), Phys. Rev. Lett. **110**, 031601.
- Fukushima, K., and J. M. Pawłowski (2012), Phys. Rev. D **86**, 076013.
- Fukushima, K., and H. J. Warringa (2008), Phys. Rev. Lett. **100**, 032007.
- Gasser, J., and H. Leutwyler (1984), Annals Phys. **158**, 142.
- Gasser, J., and H. Leutwyler (1985), Nucl. Phys. B **250**, 465.
- Gatto, R., and M. Ruggieri (2010), Phys. Rev. D **82**, 054027.
- Gatto, R., and M. Ruggieri (2011), Phys. Rev. D **83**, 034016.
- Gerber, P., and H. Leutwyler (1989), Nucl. Phys. B **321**, 387.
- Giovanni, M., and M. E. Shaposhnikov (1998), Phys. Rev. D **57**, 199.
- Gusynin, V. P., V. A. Miransky, and I. A. Shovkovy (1994), Phys. Rev. Lett. **73**, 3499.
- Gusynin, V. P., V. A. Miransky, and I. A. Shovkovy (1996), Nucl. Phys. B **462**, 249.
- Haas, L. M., R. Stiele, J. Braun, J. M. Pawłowski, and J. Schaffner-Bielich (2013), Phys. Rev. D **87**, 076004.
- Haber, A., F. Preis, and A. Schmitt (2014), arXiv:1409.0425 [nucl-th].
- Hell, T., S. Roessner, M. Cristoforetti, and W. Weise (2009), Phys. Rev. D **79**, 014022.
- Herbst, T. K., M. Mitter, B.-J. Pawłowski, J. M. Schaefer, and R. Stiele (2014), Phys. Lett. B **731**, 248.
- Herbst, T. K., J. M. Pawłowski, and B.-J. Schaefer (2011), Phys. Lett. B **696**, 58.
- Hidaka, Y., and A. Yamamoto (2013), Phys. Rev. D **87**, 094502.
- ’t Hooft, G. (1976), Phys. Rev. D **14**, 3432.

- Hsu, S., and M. Schwetz (2000), Nucl. Phys. **572**, 211.
- Huber, M., and L. von Smekal (2013), JHEP **04**, 149.
- Huovinen, P., and P. Petreczky (2010), Nucl. Phys. A **837**, 26.
- Ilgenfritz, E.-M., M. Kalinowski, M. Muller-Preussker, B. Petersson, and A. Schreiber (2012), Phys. Rev. D **85**, 114504.
- Ilgenfritz, E.-M., B. Muller-Preussker, M. Petersson, and A. Schreiber (2014), Phys. Rev. D **89**, 054512.
- Inagaki, T., D. Kimura, and T. Murata (2004), Prog. Theor. Phys. **111**, 371.
- Johnson, K. (1975), Acta Phys. Pol. B **6**, 865.
- Kajantie, K., M. Laine, J. Peisa, K. Rummukainen, and M. Shaposhnikov (1998), Nuclear Phys. B **544**, 357.
- Kajantie, K., M. Laine, K. Rummukainen, and M. Shaposhnikov (1996), Phys. Rev. Lett. **77**, 2887.
- Kamikado, K., and T. Kanazawa (2014a), JHEP **03**, 009.
- Kamikado, K., and T. Kanazawa (2014b), arXiv:1410.6253 [hep-ph].
- Kamikado, K., N. Strodthoff, L. von Smekal, and J. Wambach (2012), Phys. Lett. B **718**, 1044.
- Karsch, F., E. Laermann, and A. Peikert (2001), Nucl. Phys. B **605**, 579.
- Karsch, F., K. Redlich, and A. Tawfik (2003), Eur. Phys. J. C **29**, 549.
- Kharzeev, D. E., L. D. McLerran, and H. J. Warringa (2008), Nucl. Phys. A **803**, 227.
- Klevansky, S. P. (1992), Rev. Mod. Phys. **64**, 649.
- Klevansky, S. P., and R. H. Lemmer (1989), Phys. Rev. D **39**, 3478.
- Klimenko, K. G. (1992a), Z. Phys. C **54**, 323.
- Klimenko, K. G. (1992b), Theor. Math. Phys. **89**, 1161.
- Klimenko, K. G. (1992c), Theor. Math. Phys. **90**, 3.
- Klimenko, K. G., and V. C. Zhukovsky (2008), Phys. Lett. B **665**, 352.
- Kojo, T., and N. Su (2013), Phys. Lett. B **720**, 192.
- Kondo, K. I. (2010), Phys. Rev. D **82**, 065024.
- Leinweber, D. B. e. a. (1999), Phys. Rev. D **60**, 094507.
- Leinweber, D. B. e. a. (2000), Erratum ibid. D **61**, 079901.
- Litim, D. (2001), Phys. Rev. D **64**, 105007.
- Loewe, M., and C. Villavicencio (2003), Phys. Rev. D **67**, 074034.
- Lourenco, O., M. Dutra, A. Delfino, and M. Malheiro (2011), Phys. Rev. D **84**, 125034.
- Menezes, D. P., M. B. Pinto, A. S. S., M. A. P., and C. Providência (2009), Phys. Rev. C **79**, 035807.
- Miransky, V. A., and I. A. Shovkovy (2002), Phys. Rev. D **66**, 045006.
- Mizher, A. J., M. N. Chernodub, and E. S. Fraga (2010), Phys. Rev. D **82**, 105016.
- Mueller, N., J. Bonnet, and C. S. Fischer (2014), Phys. Rev. D **89**, 094023.
- Nambu, Y., and G. Jona-Lasinio (1961a), Phys. Rev. **122**, 345.
- Nambu, Y., and G. Jona-Lasinio (1961b), Phys. Rev. **124**, 246.
- Nielsen, H. B., and S. Chadha (1976), Nucl. Phys. B **105**, 445.
- Nielsen, N. K., and P. Olesen (1978), Nucl. Phys. B **144**, 376.
- Noronha, J. L., and I. A. Shovkovy (2007), Phys. Rev. D **76**, 105030.
- Noronha, J. L., and I. A. Shovkovy (2012), Phys. Rev. D **86**, 049901.
- Orlovsky, V. D., and Y. A. Simonov (2014), Phys. Rev. D **89**, 054012.
- Ozaki, S. (2013), Phys. Rev. D **89**, 054022.
- Pisarski, R. D., and F. Wilczek (1984), Phys. Rev. D **29**, 338.
- Rajagopal, K., and F. Wilczek (2001), *At the frontier of particle physics, vol 3* (World Scientific, Singapore, p 2061).
- Ratti, C., S. Roessner, M. A. Thaler, and W. Weise (2007a), Eur. Phys. C **49**, 213.
- Ratti, C., S. Roessner, and W. Weise (2007b), Phys. Rev. D **75**, 034007.
- Ratti, C., M. A. Thaler, and W. Weise (2006), Phys. Rev. D **73**, 014019.
- Ritus, V. I. (1978), JETP **48**, 788.
- Ruggieri, M., M. Tachibana, and V. Greco (2013), JHEP **1307**, 165.
- Rummukainen, K., M. Tsypin, M. Laine, and M. Shaposhnikov (1998), Nucl. Phys. B **532**, 283.
- Sasaki, C., B. Friman, and K. Redlich (2007), Phys. Rev. D **75**, 074013.
- Scavenius, O., A. Mocsy, I. N. Mishustin, and D. H. Rischke (2001), Phys. Rev. C **64**, 045202.
- Schaefer, B.-J., J. M. Pawłowski, and J. Wambach (2007), Phys. Rev. D **76**, 074023.
- Schaefer, B.-J., M. Wagner, and J. Wambach (2010), Phys. Rev. D **81**, 074013.
- Schwinger, J. (1951), Phys. Rev. **82**, 664.
- Sher, M. (1989), Phys. Rept **179**, 273.
- Shovkovy, I. (2013), Lect. Notes Phys. **871**, 13.
- Shushpanov, I. A., and A. V. Smilga (1997), Phys. Lett. B **402**, 351.
- Skokov, V. (2012), Phys. Rev. D **85**, 034026.
- Skokov, V., B. Friman, E. Nakano, K. Redlich, and B.-J. Schaefer (2010), Phys. Rev. D **82**, 034029.
- Skokov, V., A. Y. Illarionov, and V. Toneev (2009), Int. J. Mod. Phys. A **24**, 5925.

- Son, D. T., and M. A. Stephanov (2001), Phys. Rev. Lett. **86**, 592.
- Stephanov, M. A. (2006), PoS LAT2006 , 024.
- Stokic, B., B. Friman, and K. Redlich (2010), J. Phys. C **67**, 425.
- Strickland, M., V. Dexheimer, and D. P. Menenez (2012), Phys. Rev. D **86**, 125032.
- Twafik, A. N., and N. Magdy (2014), Phys. Rev. C **90**, 015204.
- Watanabe, H., and H. Murayama (2014), Phys. Rev. X **4**, 031057.
- Watson, P., and H. Reinhardt (2014), Phys. Rev D **89**, 045008.
- Weinberg, S. (1979), Physica A **96**, 327.
- Werbos, E. (2008), Phys. Rev. C **77**, 065202.
- Wetterich, C. (1993), Phys. Lett. B **301**, 90.
- Yaffe, L. G., and B. Svetitsky (1982a), Phys. Rev. D **26**, 963.
- Yaffe, L. G., and B. Svetitsky (1982b), Nucl. Phys. B **210**, 423.
- Yu, L., H. Liu, and M. Huang (2014a), Phys.Rev. D **90**, 074009.
- Yu, L., J. Van Doorselaere, and M. Huang (2014b), arXiv:1411.7552 [hep-ph].
- Zhang, T., T. Brauner, and D. H. Rischke (2010), JHEP **06**, 064.